ISSN 1949-8470 (online)

World Journal of Radiology

World J Radiol 2010 August 28; 2(8): 289-338

A peer-reviewed, online, open-access journal of Radiology

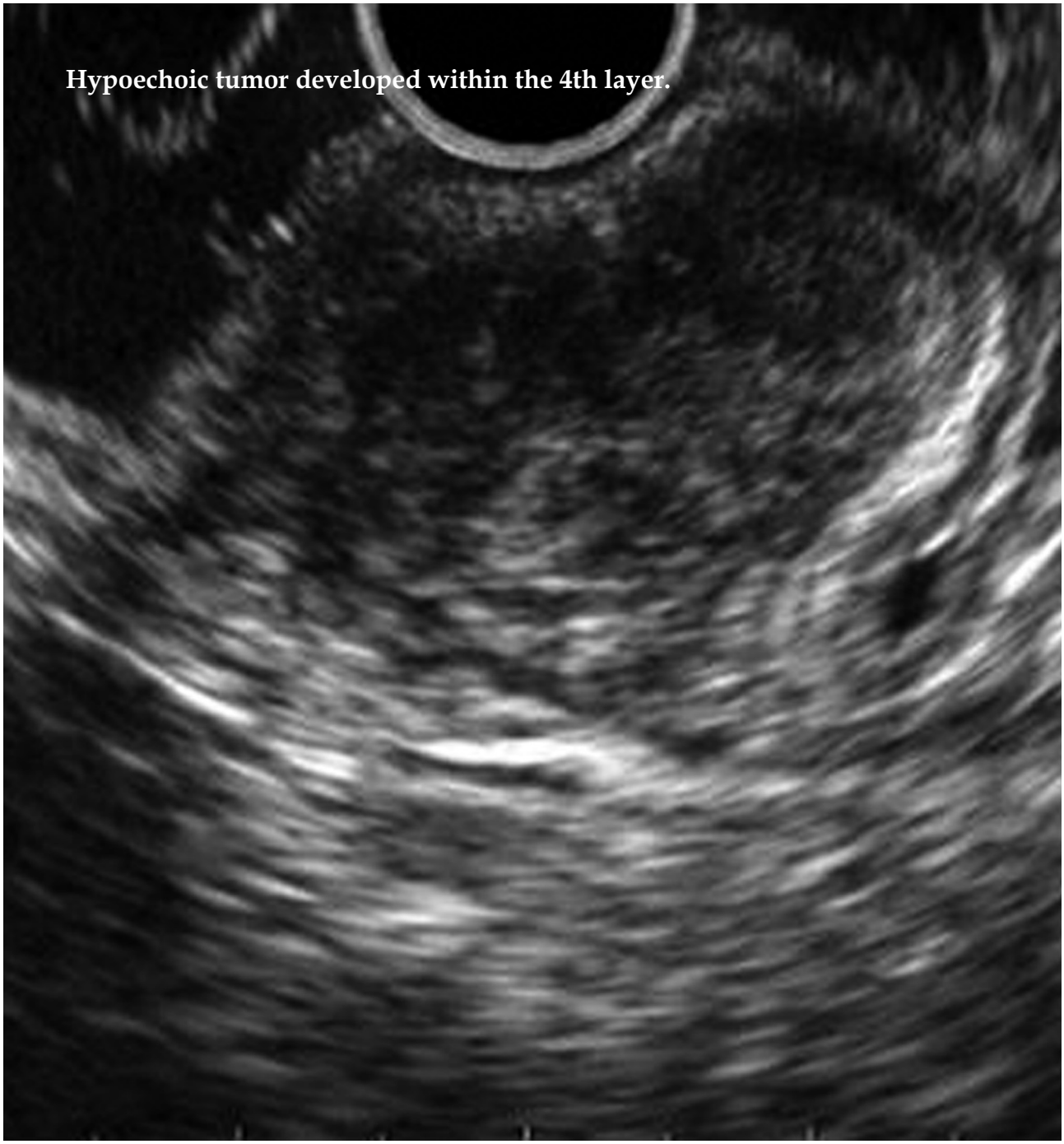

WJR World Journal of Radiology

A peer-reviewed, online, open-access journal of Radiology

Editorial Board

2009-2013

The *World Journal of Radiology* Editorial Board consists of 319 members, representing a team of worldwide experts in radiology. They are from 40 countries, including Australia (3), Austria (4), Belgium (5), Brazil (3), Canada (9), Chile (1), China (25), Czech (1), Denmark (1), Egypt (4), Estonia (1), Finland (1), France (6), Germany (17), Greece (8), Hungary (1), India (9), Iran (5), Ireland (1), Israel (4), Italy (28), Japan (14), Lebanon (1), Libya (1), Malaysia (2), Mexico (1), Netherlands (4), New Zealand (1), Norway (1), Saudi Arabia (3), Serbia (1), Singapore (2), Slovakia (1), South Korea (16), Spain (8), Switzerland (5), Thailand (1), Turkey (20), United Kingdom (16), and United States (82).

France

Alain Chapel, *Fontenay-Aux-Roses*
Nathalie Lassau, *Villejuif*
Youlia M Kirova, *Paris*
Géraldine Le Duc, *Grenoble Cedex*
Laurent Pierot, *Reims*
Frank Pilleul, *Lyon*
Pascal Pommier, *Lyon*

Germany

Ambros J Beer, *München*
Thomas Deserno, *Aachen*
Frederik L Giesel, *Heidelberg*
Ulf Jensen, *Kiel*
Markus Sebastian Juchems, *Ulm*
Kai U Juergens, *Bremen*
Melanie Kettering, *Jena*
Jennifer Linn, *Munich*
Christian Lohrmann, *Freiburg*
David Maintz, *Münster*
Henrik J Michaely, *Mannheim*
Oliver Micke, *Bielefeld*
Thoralf Niendorf, *Berlin-Buch*
Silvia Obenauer, *Duesseldorf*
Steffen Rickes, *Halberstadt*
Lars V Baron von Engelhardt, *Bochum*
Goetz H Welsch, *Erlangen*

Greece

Panagiotis Antoniou, *Alexandroupolis*
George C Kagadis, *Rion*
Dimitris Karacostas, *Thessaloniki*
George Panayiotakis, *Patras*
Alexander D Rapidis, *Athens*
C Triantopoulou, *Athens*
Ioannis Tsalafoutas, *Athens*
Virginia Tsapaki, *Anixi*
Ioannis Valais, *Athens*

Hungary

Peter Laszlo Lakatos, *Budapest*

India

Anil Kumar Anand, *New Delhi*
Surendra Babu, *Tamilnadu*
Sandip Basu, *Bombay*
Kundan Singh Chufal, *New Delhi*
Shivanand Gamanagatti, *New Delhi*
Vimoj J Nair, *Haryana*
R Prabhakar, *New Delhi*
Sanjeeb Kumar Sahoo, *Orissa*

Iran

Vahid Reza Dabbagh Kakhki, *Mashhad*
Mehran Karimi, *Shiraz*
Farideh Nejat, *Tehran*
Alireza Shirazi, *Tehran*
Hadi Rokni Yazdi, *Tehran*

Ireland

Joseph Simon Butler, *Dublin*

Israel

Amit Gefen, *Tel Aviv*
Eyal Sheiner, *Be'er-Sheva*
Jacob Sosna, *Jerusalem*
Simcha Yagel, *Jerusalem*

Italy

Mohssen Ansarin, *Milan*
Stefano Arcangeli, *Rome*
Tommaso Bartalena, *Imola*
Filippo Cademartiri, *Parma*
Sergio Casciaro, *Lecce*
Laura Crocetti, *Pisa*
Alberto Cuocolo, *Napoli*
Mirko D'Onofrio, *Verona*
Massimo Filippi, *Milan*
Claudio Fiorino, *Milano*
Alessandro Franchello, *Turin*
Roberto Grassi, *Naples*
Stefano Guerriero, *Cagliari*
Francesco Lassandro, *Napoli*
Nicola Limbucci, *L'Aquila*
Raffaele Lodi, *Bologna*
Francesca Maccioni, *Rome*
Laura Martincich, *Candiolo*
Mario Mascalchi, *Florence*
Roberto Miraglia, *Palermo*
Eugenio Picano, *Pisa*
Antonio Pinto, *Naples*
Stefania Romano, *Naples*
Luca Saba, *Cagliari*
Sergio Sartori, *Ferrara*
Mariano Scaglione, *Castel Volturno*
Lidia Strigari, *Rome*
Vincenzo Valentini, *Rome*

Japan

Shigeru Ehara, *Morioka*
Nobuyuki Hamada, *Chiba*
Takao Hiraki, *Okayama*
Akio Hiwatashi, *Fukuoka*
Masahiro Jinzaki, *Tokyo*
Hiroshi Matsuda, *Saitama*
Yasunori Minami, *Osaka*
Jun-Ichi Nishizawa, *Tokyo*
Tetsu Niwa, *Yokohama*
Kazushi Numata, *Kanagawa*
Kazuhiko Ogawa, *Okinawa*
Hitoshi Shibuya, *Tokyo*
Akira Uchino, *Saitama*
Haiquan Yang, *Kanagawa*

Lebanon

Aghiad Al-Kutoubi, *Beirut*

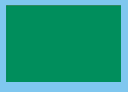

Libya

Anuj Mishra, *Tripoli*

Malaysia

R Logeswaran, *Cyberjaya*
Kwan-Hoong Ng, *Kuala Lumpur*

Mexico

Heriberto Medina-Franco, *Mexico City*

Netherlands

Jurgen J Fütterer, *Nijmegen*
Raffaella Rossin, *Eindhoven*
Paul E Sijens, *Groningen*
Willem Jan van Rooij, *Tilburg*

New Zealand

W Howell Round, *Hamilton*

Norway

Arne Sigmund Borthne, *Lørenskog*

Saudi Arabia

Mohammed Al-Omran, *Riyadh*
Ragab Hani Donkol, *Abha*
Volker Rudat, *Al Khobar*

Serbia

Djordjije Saranovic, *Belgrade*

Singapore

Uei Pua, *Singapore*
Lim CC Tchoyoson, *Singapore*

Slovakia

František Dubecký, *Bratislava*

South Korea

Bo-Young Choe, *Seoul*
Joon Koo Han, *Seoul*
Seung Jae Huh, *Seoul*
Chan Kyo Kim, *Seoul*
Myeong-Jin Kim, *Seoul*
Seung Hyup Kim, *Seoul*
Kyoung Ho Lee, *Gyeonggi-do*
Won-Jin Moon, *Seoul*
Wazir Muhammad, *Daegu*
Jai Soung Park, *Bucheon*
Noh Hyuck Park, *Kyunggi*
Sang-Hyun Park, *Daejeon*
Joon Beom Seo, *Seoul*
Ji-Hoon Shin, *Seoul*
Jin-Suck Suh, *Seoul*
Hong-Gyun Wu, *Seoul*

Spain

Eduardo J Aguilar, *Valencia*
Miguel Alcaraz, *Murcia*
Juan Luis Alcazar, *Pamplona*
Gorka Bastarrika, *Pamplona*
Rafael Martínez-Monge, *Pamplona*
Alberto Muñoz, *Madrid*
Joan C Vilanova, *Girona*

Switzerland

Nicolau Beckmann, *Basel*
Silke Grabherr, *Lausanne*
Karl-Olof Lövblad, *Geneva*
Tilo Niemann, *Basel*
Martin A Walter, *Basel*

Thailand

Sudsriluk Sampatchalit, *Bangkok*

Turkey

Olus Api, *Istanbul*
Kubilay Aydin, *İstanbul*
Işıl Bilgen, *Izmir*
Zulkif Bozgeyik, *Elazig*
Barbaros E Çil, *Ankara*
Gulgun Engin, *Istanbul*
M Fatih Evcimik, *Malatya*
Ahmet Kaan Gündüz, *Ankara*
Tayfun Hakan, *Istanbul*
Adnan Kabaalioglu, *Antalya*
Fehmi Kaçmaz, *Ankara*
Musturay Karcaaltincaba, *Ankara*
Osman Kizilkilic, *Istanbul*
Zafer Koc, *Adana*
Cem Onal, *Adana*
Yahya Paksoy, *Konya*
Bunyamin Sahin, *Samsun*
Ercument Unlu, *Edirne*
Ahmet Tuncay Turgut, *Ankara*
Ender Uysal, *Istanbul*

United Kingdom

K Faulkner, *Wallsend*
Peter Gaines, *Sheffield*
Balaji Ganeshan, *Brighton*
Nagy Habib, *London*
Alan Jackson, *Manchester*
Pradesh Kumar, *Portsmouth*
Tarik F Massoud, *Cambridge*
Igor Meglinski, *Bedfordshire*
Robert Morgan, *London*
Ian Negus, *Bristol*
Georgios A Plataniotis, *Aberdeen*
N J Raine-Fenning, *Nottingham*
Manuchehr Soleimani, *Bath*
MY Tseng, *Nottingham*
Edwin JR van Beek, *Edinburgh*
Feng Wu, *Oxford*

United States

Athanassios Argiris, *Pittsburgh*
Stephen R Baker, *Newark*
Lia Bartella, *New York*
Charles Bellows, *New Orleans*
Walter L Biffl, *Denver*
Homer S Black, *Houston*
Wessam Bou-Assaly, *Ann Arbor*
Owen Carmichael, *Davis*
Shelton D Caruthers, *St Louis*
Yuhchyau Chen, *Rochester*
Melvin E Clouse, *Boston*
Ezra Eddy Wyssam Cohen, *Chicago*
Aaron Cohen-Gadol, *Indianapolis*
Patrick M Colletti, *Los Angeles*
Kassa Darge, *Philadelphia*
Abhijit P Datir, *Miami*
Delia C DeBuc, *Miami*
Russell L Deter, *Houston*
Adam P Dicker, *Phil*
Khaled M Elsayes, *Ann Arbor*
Steven Feigenberg, *Baltimore*
Christopher G Filippi, *Burlington*
Victor Frenkel, *Bethesda*
Thomas J George Jr, *Gainesville*
Patrick K Ha, *Baltimore*
Robert I Haddad, *Boston*
Walter A Hall, *Syracuse*
Mary S Hammes, *Chicago*
John Hart Jr, *Dallas*
Randall T Higashida, *San Francisco*
Juebin Huang, *Jackson*
Andrei Iagaru, *Stanford*
Craig Johnson, *Milwaukee*
Ella F Jones, *San Francisco*
Csaba Juhasz, *Detroit*
Mannudeep K Kalra, *Boston*
Riyad Karmy-Jones, *Vancouver*
Daniel J Kelley, *Madison*
Amir Khan, *Longview*
Euishin Edmund Kim, *Houston*
Vikas Kundra, *Houston*
Kennith F Layton, *Dallas*
Rui Liao, *Princeton*
CM Charlie Ma, *Philadelphia*
Nina A Mayr, *Columbus*
Thomas J Meade, *Evanston*
Steven R Messé, *Philadelphia*
Nathan Olivier Mewton, *Baltimore*
Feroze B Mohamed, *Philadelphia*
Koenraad J Mortele, *Boston*
Mohan Natarajan, *San Antonio*
John L Nosher, *New Brunswick*
Chong-Xian Pan, *Sacramento*
Dipanjan Pan, *St Louis*
Martin R Prince, *New York*
Reza Rahbar, *Boston*
Carlos S Restrepo, *San Antonio*
Veronica Rooks, *Honolulu*
Maythem Saeed, *San Francisco*
Edgar A Samaniego, *Palo Alto*
Kohkan Shamsi, *Doylestown*
Jason P Sheehan, *Charlottesville*
William P Sheehan, *Willmar*
Charles Jeffrey Smith, *Columbia*
Monvadi B Srichai-Parsia, *New York*
Dan Stoianovici, *Baltimore*
Janio Szklaruk, *Houston*
Dian Wang, *Milwaukee*
Jian Z Wang, *Columbus*
Liang Wang, *New York*
Shougang Wang, *Santa Clara*
Wenbao Wang, *New York*
Aaron H Wolfson, *Miami*
Gayle E Woloschak, *Chicago*
Ying Xiao, *Philadelphia*
Juan Xu, *Pittsburgh*
Benjamin M Yeh, *San Francisco*
Terry T Yoshizumi, *Durham*
Jinxing Yu, *Richmond*
Jianhui Zhong, *Rochester*

WJR World Journal of Radiology

Contents

Monthly Volume 2 Number 8 August 28, 2010

World Journal of Radiology
Volume 2 Number 8 August 28, 2010

Contents

NAME OF JOURNAL
World Journal of Radiology

LAUNCH DATE
December 31, 2009

SPONSOR
Beijing Baishideng BioMed Scientific Co., Ltd.,
Room 903, Building D, Ocean International Center,
No. 62 Dongsihuan Zhonglu, Chaoyang District,
Beijing 100025, China
Telephone: 0086-10-8538-1892
Fax: 0086-10-8538-1893
E-mail: baishideng@wjgnet.com
http://www.wjgnet.com

EDITING
Editorial Board of *World Journal of Radiology*,
Room 903, Building D, Ocean International Center,
No. 62 Dongsihuan Zhonglu, Chaoyang District,
Beijing 100025, China
Telephone: 0086-10-8538-1892
Fax: 0086-10-8538-1893
E-mail: wjr@wjgnet.com
http://www.wjgnet.com

PUBLISHING
Baishideng Publishing Group Co., Limited,
Room 1701, 17/F, Henan Bulding,
No.90 Jaffe Road, Wanchai, Hong Kong, China
Fax: 00852-3115-8812
Telephone: 00852-5804-2046
E-mail: baishideng@wjgnet.com
http://www.wjgnet.com

SUBSCRIPTION
Beijing Baishideng BioMed Scientific Co., Ltd.,
Room 903, Building D, Ocean International Center,
No. 62 Dongsihuan Zhonglu, Chaoyang District,
Beijing 100025, China
Telephone: 0086-10-8538-1892
Fax: 0086-10-8538-1893
E-mail: baishideng@wjgnet.com
http://www.wjgnet.com

ONLINE SUBSCRIPTION
One-Year Price 216.00 USD

PUBLICATION DATE
August 28, 2010

CSSN
ISSN 1949-8470 (online)

EDITORIAL OFFICE
Na Ma, Director
World Journal of Radiology
Room 903, Building D, Ocean International Center,
No. 62 Dongsihuan Zhonglu, Chaoyang District,
Beijing 100025, China
Telephone: 0086-10-8538-1892
Fax: 0086-10-8538-1893
E-mail: wjr@wjgnet.com
http://www.wjgnet.com

INSTRUCTIONS TO AUTHORS
Full instructions are available online at http://www.wjgnet.com/1949-8470/g_info_20100316162358.htm. If you do not have web access please contact the editorial office.

ONLINE SUBMISSION
http://www.wjgnet.com/1949-8470office

World Journal of Radiology

Online Submissions: http://www.wjgnet.com/1949-8470office
wjr@wjgnet.com
doi:10.4329/wjr.v2.i8.289

World J Radiol 2010 August 28; 2(8): 289-297
ISSN 1949-8470 (online)

EDITORIAL

Diagnosis of subepithelial tumors in the upper gastrointestinal tract by endoscopic ultrasonography

Hiroki Sakamoto, Masayuki Kitano, Masatoshi Kudo

Hiroki Sakamoto, Masayuki Kitano, Masatoshi Kudo, Division of Gastroenterology and Hepatology, Department of Internal Medicine, Kinki University School of Medicine, Osaka-Sayama 589-8511, Japan
Author contributions: Sakamoto H wrote this manuscript; Kitano M and Kudo M revised the manuscript.
Supported by The Japan Society for Promotion of Science, Research and Development Committee Program of The Japan Society of Ultrasonics in Medicine, Japan Research Foundation for Clinical Pharmacology, and Japanese Foundation for Research and Promotion of Endoscopy
Correspondence to: Hiroki Sakamoto, MD, PhD, Division of Gastroenterology and Hepatology, Department of Internal Medicine, Kinki University School of Medicine, 377-2, Ohno-Higashi, Osaka-Sayama 589-8511, Japan. hiroki.sakamoto@nifty.com
Telephone: +81-72-3660221 Fax: +81-72-3672880
Received: June 11, 2010 Revised: July 29, 2010
Accepted: August 5, 2010
Published online: August 28, 2010

Abstract

Endoscopic ultrasonography (EUS) is the most accurate procedure for detecting and diagnosing subepithelial tumors, due to its higher sensitivity and specificity than other imaging modalities. EUS can characterize lesions by providing information on echogenic origin, size, borders, homogeneity, and the presence of echogenic or anechoic foci. Linear echoendoscopes, and recently also electronic radial echoendoscopes, can be used with color Doppler or power Doppler to assess the vascular signals from subepithelial masses, and thus permit the differentiation of vascular structures from cysts, as well as the assessment of the tumor blood supply. However, the diagnostic accuracy of EUS imaging alone has been shown to be low in subepithelial lesions with 3rd and 4th layers. It is also difficult to differentiate exactly between benign and malignant tumors and to gain an accurate picture of histology using EUS. On the other hands, EUS guided fine needle aspiration (EUS-FNA) can provide samples for cytologic or histologic analysis. Hypoechoic lesions of the 3rd and the 4th EUS layers, more than in 1 cm diameter are recommended, and histologic confirmation using endoscopic submucosal resection or EUS-FNA should be obtained when possible. Therefore, EUS-FNA plays an important role in the clinical management of subepithelial tumors. Furthermore improvements in endoscopic technology are expected to be more useful modalities in differential diagnosis and discrimination between benign and malignant subepithelial tumors.

Key words: Endoscopic ultrasonography; Submucosal tumor; Subepithelial tumor

Peer reviewers: Alain Chapel, PhD, Institut de Radioprotection et de S reté Nucléaire, DPHD, IRSN. B.P. no 17, F-92262 Fontenay-Aux-Roses, France; Antonio Pinto, MD, PhD, Department of Radiology, Cardarelli Hospital, Via Posillipo 168/D, I-80123, Naples, Italy

Sakamoto H, Kitano M, Kudo M. Diagnosis of subepithelial tumors in the upper gastrointestinal tract by endoscopic ultrasonography. *World J Radiol* 2010; 2(8): 289-297 Available from: URL: http://www.wjgnet.com/1949-8470/full/v2/i8/289.htm DOI: http://dx.doi.org/10.4329/wjr.v2.i8.289

INTRODUCTION

Submucosal masses or lesions often referred to as 'submucosal tumors', represent a growth underneath the mucosa of the gastrointestinal (GI) tract whose etiology cannot be determined by GI endoscopy or barium studies[1]. However, the term 'submucosal tumor' is inappropriate, because many of these lesions do not arise from the submucosa and many of them are not tumors[2-5]. Thus, 'subepithelial' is a more appropriate term than 'submucosal'. Hence, other authors call these abnormalities subepithelial lesions, because they are covered by normal mucosa[6]. These can

be caused by external compression by the neighboring organs or by intramural lesions. However, submucosal is still recognized and used.

The majority of subepithelial tumors do not cause symptoms and are discovered incidentally during endoscopic or radiologic examinations. The overlying mucosa usually appears smooth and normal at endoscopy. If symptoms do occur, they are nonspecific such as abdominal pain, obstruction, hemorrhage and intussusceptions[7,8]. Large submucosal neoplasms may outgrow their blood supply, ulcerate through the mucosa, and present as GI bleeding. Firm subepithelial tumors may also present with obstructive symptoms, especially if they are located near the cardia or the pylorus. Subepithelial tumors obstructing the major or minor papilla may cause jaundice or pancreatitis. Pain and weight loss, often associated with large submucosal GI stromal tumors (GISTs), are symptoms that suggest malignancy[7,9].

Endoscopic ultrasonography (EUS) is the most sensitive imaging procedure for the characterization of subepithelial tumors and it can also diagnose them, especially small ones[10-14]. Linear echoendoscopes and electronic radial echoendoscopes can be used with color Doppler or power Doppler to assess the vascular signals from subepithelial masses, and thus permit the differentiation of vascular structures from cysts, as well as the assessment of the tumor blood supply[11,12,15]. Furthermore, Catheter US (miniprobes), if available, may be particularly useful for evaluating subepithelial tumors because they permit sonographic examination of the tumor while the patient is having a diagnostic endoscopy[16,17]. In addition to being convenient, catheter-type US probes are particularly useful for imaging small subepithelial tumors that are difficult to identify with dedicated echoendoscopes. They are also useful in imaging subepithelial tumors in the colon[7], however, miniprobes are not useful if the subepithelial lesions are over 2 cm in diameter because of the limited penetrating depths. Therefore, EUS is performed as the second intervention following standard endoscopy[14]. On the other hand, it is difficult to differentiate exactly between benign and malignant tumors and to gain an accurate picture of histology using EUS. EUS guided fine needle aspiration (EUS-FNA) can be used to provide samples for cytologic or histologic analysis. Therefore, EUS-FNA plays an important role in the clinical management of subepithelial tumors. This review will focus on EUS appearances of common subepithelial GI tract tumors, the diagnostic accuracy of EUS-FNA, and surveillance by EUS, highlighting their relative advantages and their complementary roles in clinical practice.

EUS IMAGING

Optimal imaging of subepithelial lesions requires submersion under water, which sometimes requires repositioning of the patient after the GI lumen has been filled with water. Endosonographically, the wall of the GI tract consists of 5 layers of alternating echogenicity (Figure 1). The 1st layer is hyperechoic and represents the superficial layer of the mucosa. The 2nd layer is hypoechoic and constitutes of the deep layer of the mucosa, including the muscularis mucosa. The 3rd, hyperechoic layer is the submucosa, the 4th hypoechoic the muscularis propria and the 5th hyperechoic is the serosa/adventitia[18]. For subepithelial tumors that are intrinsic to the GI wall, it is important to characterize the layer(s) of origin or involvement, the echogenicity of the tumor, the smoothness of the border and any internal feature (Table 1). Inflation of the balloon covering the transducer with water may improve the ultrasonic contact. However, this may compress the GI tract wall and distort the EUS image. This is the reason why the esophagus and duodenum are sometimes visualized with only three layers, with the first hyperechoic layer corresponding to the balloon-mucosa-submucosa together with the submucosa-muscularis-propria interface.

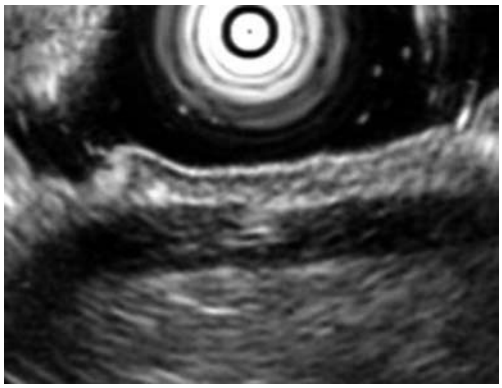

Figure 1 Normal structure of the gastric wall with five endoscopic ultrasonography layers present.

Extrinsic compressions

An enlarged left atrium, left hepatic lobe, and spleen may commonly masquerade as a subepithelial tumor of the esophagus and stomach during endoscopy[19-21]. A recent international multicenter study reported that the sensitivity and the specificity of extramural compression with endoscopy alone were 87% and 29%, respectively[2]. The EUS characterization of these organs is useful in the evaluation of extraluminal organs which compress the GI tract lumen, 100% accurate for the differential diagnosis and superior to transabdominal ultrasound or CT scans (Figure 2). Pancreatic pseudocysts or tumors can also be identified when assessing subepithelial tumors by EUS.

Varices

Occasionally, large gastric varices may be polypoid[3-5,22]. EUS imaging of gastric varices demonstrates characteristic anechoic serpiginous structures in the third hyperechoic layer. Flow within the varix can be demonstrated by Doppler examination.

Lipomas

Lipomas are generally soft, exhibiting a pillow sign when

Table 1 Endoscopic ultrasonography feature of subepithelial tumors

	EUS layer	Organ	EUS appearance
Varices	3rd	Fundus	Anechoic
Lipomas	3rd	Stomach, duodenum, rectum	Hyperechoic, smooth margins
Ectopic pancreas	3rd, 4th (2nd, 5th)	Antrum	Hypoechoic, heterogeneous (possible ductal structure)
Cysts	3rd	Esophagus, stomach, duodenum	Anechoic, compressible, round or oval (3rd or 5th layer are suggestive of duplication cyst)
Inflammatory fibroid polyp	2nd	Antrum, duodenum	Polypoid, hypoechoic, covered by a thin mucosa
Granular cell tumor	2nd, 3rd, 4th	Esophagus	Hypoechoic, oval, heterogeneous,
Leiomyoma	4th (2nd)	Esophagus, cardia	Hypoechoic, round or oval, well demarcated
Schwannoma	4th (3rd)	Stomach	Hypoechoic, round or oval, well demarcated
Gastrointestinal stromal tumor	4th (2nd, 3rd, 5th)	Stomach, small intestine	Hypoechoic, round (large tumors > 4 cm, homogeneous, irregular border, cystic areas of echogenic foci: borderline or malignant)
Leiomyosarcoma	2nd, 4th	Esophagus, stomach	Hypoechoic, heterogeneous, irregular extraluminal border or invasiveness of the neighbouring organs
Carcinod	2nd, 3rd	Fundus, rectum	Hypoechoic
Lymphoma	2nd, 3rd, 4th	Stomach	Hypoechoic
Metastases	1st-5th or all	All	Hypoechoic, heterogeneous, irregular margin

EUS: Endoscopic ultrasonography.

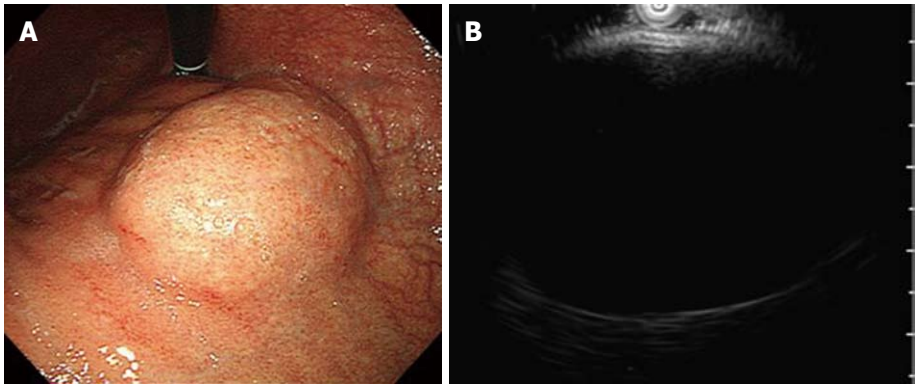

Figure 2 Endoscopic and endoscopic ultrasonography finding of extrinsic compression. A: Endoscopic view of subepithelial lesion of the gastric angle; B: Endoscopic ultrasonography shows an extramural compression by a liver cyst.

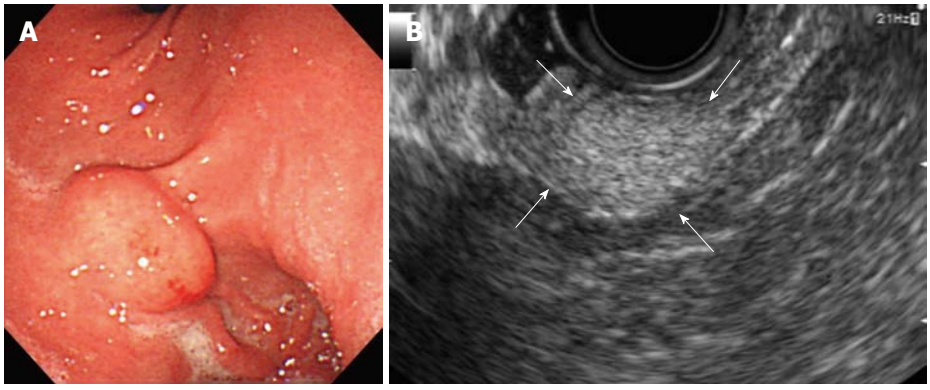

Figure 3 Endoscopic and endoscopic ultrasonography finding of lipomas. A: Endoscopic view of 1.5 cm subepithelial lesion of the anterior part of the gastric angle; B: Endoscopic ultrasonography shows an typical aspect of an 1.6 cm lipoma of the gastric angle (arrows).

probed, and have a yellowish hue. EUS demonstrates lipomas as hyperechoic, homogeneous, well-circumscribed ovoid masses in the 3rd layer (Figure 3)[3-5].

Cysts/duplication cyst

Cysts typically appear as round or ovoid, smooth anechoic compressible structures located within the 3rd layer. The wall of the duplication cyst may appear as a three or a five layer structure[23,24].

Ectopic pancreas

Ectopic pancreas, also called heterotopic or aberrant pan-

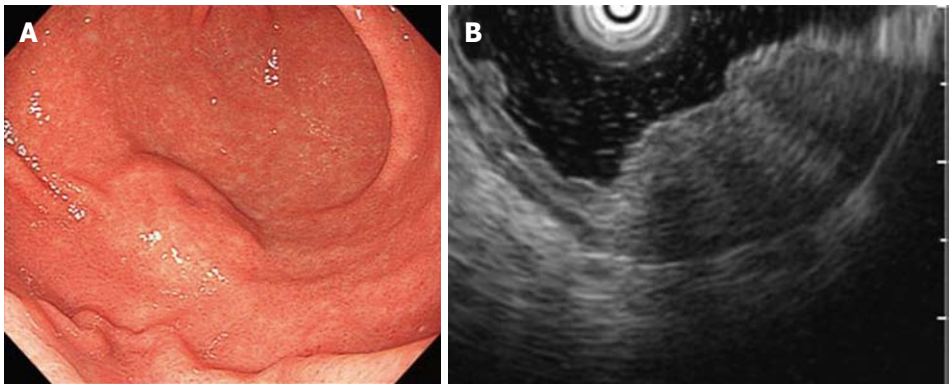

Figure 4 Endoscopic and endoscopic ultrasonography finding of ectopic pancreas. A: Endoscopic view of a subepithelial lesion of the greater curvature of the gastric antrum, covered with normal mucosa, with a central depression; B: Endoscopic ultrasonography shows indistinct margin, hypoechoic tumor developed within the 4th layer.

creas, is defined as pancreatic tissue lying outside its normal location and lacking anatomic or vascular connection with the pancreas. Ectopic pancreas, which usually does not cause symptoms, is found incidentally in the stomach, duodenum, and small intestine. Gastric lesions are discovered in the antrum in 85%-90%, either on the posterior or anterior wall, being more common along the greater curvature. The frequency of ectopic pancreas has been estimated as 1 case per 500 explorations of the upper abdomen or 0.6% to 13.7% of autopsies. The endoscopic appearance of a pancreatic rest is usually that of a firm, slightly irregular nodule in the stomach or elsewhere in the GI tract (Figure 4A). The mucosa over the nodule may have a central depression or dimpling, and ducts may empty into the lumen at this site. Usually, the characteristic EUS demonstrates an indistinct margin, hypoechoic or mixed echogenicity, a heterogeneous lesion, and most locations are within either the 3rd or 4th layers or only in the 3rd layer (Figure 4B)[3-5].

Granular cell tumor

Granular cell tumors are benign neoplasms. Typically they are located in the distal part of the esophagus with a yellowish appearance; EUS demonstrates a heterogeneous mass with smooth borders located in the 3rd layer[25,26].

Submucosa cancer/metastases

Subepithelial primary carcinoma, lymphoma or metastases may rarely involve the submucosa. EUS show a hypoechoic, heterogeneous lesion in any or all of the EUS layers[1,7]. The most frequent primary tumors that result in GI metastases are breast cancer, melanoma and lung cancer[18].

Gastric inflammatory fibroid polyp

Inflammatory fibroid polyp (IFP) appears as a 2 cm almost-pedunculated polyp on the antrum when analysed using endoscopy. The polyp is covered mostly by normal mucosa, with whitish exudates. The appearance of IFPs on EUS is characterized by an indistinct margin, hypoechoic homogeneous lesion and location within the 2nd and/or 3rd layer with an intact 4th layer[27].

Mesenchymal tumor

Mesenchymal tumors of the GI tract are classified in three type tumors, GIST, leiomyoma, and schwannoma. Pathologically, most of these tumors are completely or partly composed of spindle cells and have a light microscopic appearance suggestive of smooth muscle or nerve sheath differentiation. These tumors therefore have been presumed to be of smooth muscle origin and often labeled as leiomyomatous or Schwann cell tumors[28,29]. In recent years, with the advance of immunohistochemical[30,31] and ultrastructural[32] studies, it has been shown that most gastric and small intestinal mesenchymal tumors are neither leiomyoma nor schwannoma but GIST derived from the interstitial cells of Caja. GISTs are the most common GI mesenchymal tumors, now defined as KIT-positive mesenchymal tumors. Leiomyoma tumors demonstrate α-smooth muscle actin, desmin protein on immunohistochemistry, but not KIT expression. Schwannoma tumors demonstrate S100 protein on immunohistochemistry, but not KIT expression[30-32].

Leiomyoma

Leiomyomas are benign tumors without malignant potential which arise from the muscularis mucosa or the muscularis propria. They are found in the esophagus, but are rare in the stomach and small intestine. EUS demonstrates a hypoechoic, well-circumscribed, homogeneous lesion, developed in the 2nd or 4th layer (Figure 5A).

Schwannoma

The GI schwannoma to GISTs (the most frequent GI SMTs) ratio is approximately 1:50-100[33]. Therefore, GI schwannomas are rare. The schwannoma appearance is similar to that of leiomyoma or GISTs (Figure 5B)[34-36].

GIST

GISTs occur most frequently in the stomach (65%) and in the small bowel (25%), rarely in the rectum and the colon. They are exceptional in the esophagus (1%)[1,7,33-36]. Approximately 10%-30% of GISTs are clinically malignant, although the fact that all GISTs are considered to have some degree of malignant potential should be kept

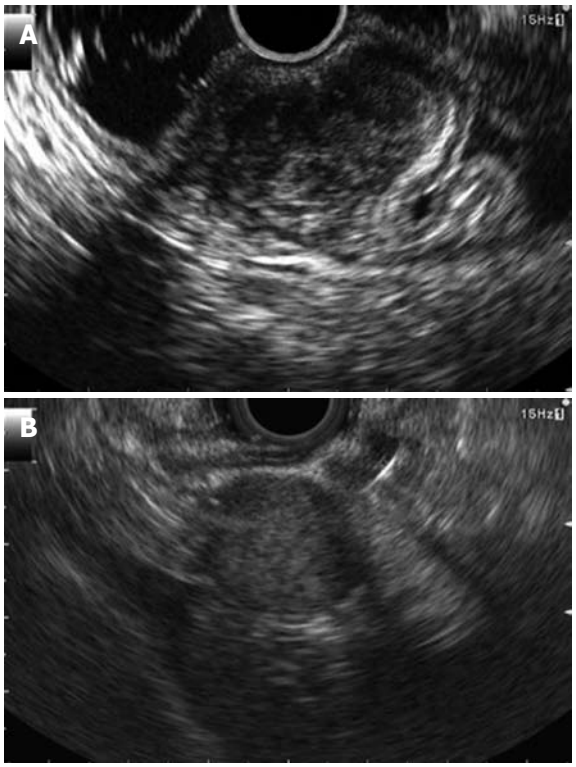

Figure 5 Hypoechoic tumor developed within the 4th layer. A: Leiomyoma of the esophagus (30 mm); B: Schwannoma of the stomach (22 mm).

in mind. GISTs in the small intestine are more aggressive that those located in the stomach[37]. EUS demonstrates a hypoechoic tumor contiguous with the 4th layer and well-delineated lesion (Figure 6). However recent reports also indicate the presence of GISTs in the 3rd layer[1-7,34] contiguous with the muscularis mucosa[38-41].

Differentiation between leiomyomas, schwannomas and GISTs is extremely difficult by imaging modalities, even EUS. Recently, Okai *et al*[42] tried to differentiate between 19 GISTs, 3 leiomyomas, and 2 schwannomas by EUS. A complete or incomplete marginal hypoechoic halo was found in more than half of the patients with GISTs and schwannomas, whereas a distinct marginal halo was not seen in leiomyomas. It was also demonstrated that the echogenicities of GISTs were generally low but slightly higher than that of the normal surrounding proper muscle layer, whereas the level of leiomyomas was nearly equal to that of the surrounding normal proper muscle layer and that of schwannoma was extremely low. Accordingly, the difference in echogenicities among the three mesenchymal tumors might reflect the pathologic differences of cellularity and structural components of the tumor. Although the number of patients enrolled in their study was too small to make a comparison, these EUS findings may be helpful for differentiation between these gastric mesenchymal tumors.

DIFFERENTIAL DIAGNOSIS

We have described the EUS appearance of each subepithelial tumor. Determination of the histologic layer and the echotexture of the lesion can significantly narrow the

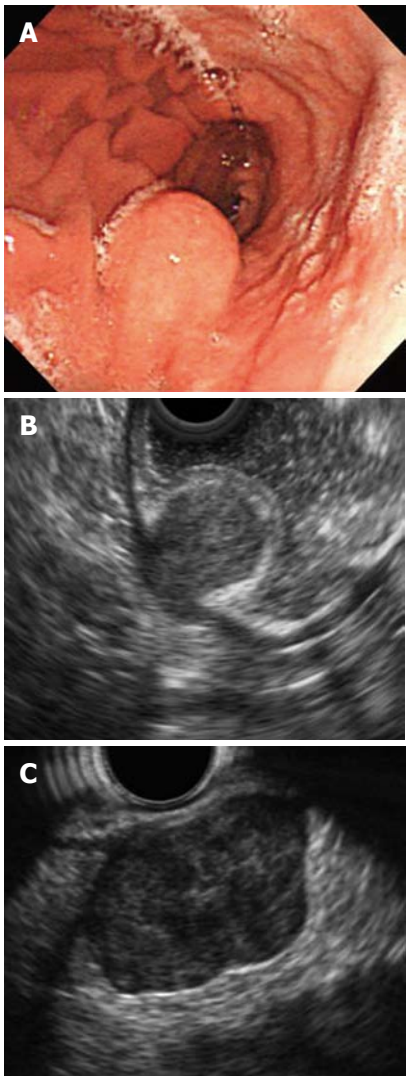

Figure 6 Endoscopic and endoscopic ultrasonography finding of gastrointestinal stromal tumor. A: Endoscopic view of subepithelial lesion of the posterior side of the greater curvature of the gastric body; B: Endoscopic ultrasonography shows hypoechoic, homogeneous 2 cm tumor developed within the 4th layer (low risk gastrointestinal stromal tumor of the stomach); C: 35 mm hypoechoic, heterogeneous, lobulated submucosal lesion with exogastric growth developed within the 4th layer (high risk gastrointestinal stromal tumor of the stomach).

differential diagnosis. However, the differential diagnosis of a hypoechoic 4th layer lesion is broad and includes benign, premalignant, and malignant lesions[43]. EUS performs better than other modalities in evaluating GI subepithelial lesion, but the diagnostic accuracy of EUS imaging alone has been shown to be as low as 43% in subepithelial lesions with 3rd and 4th layers[2]. Hwang *et al*[2] prospectively evaluated the performance characteristics of EUS in the diagnosis of GI subepithelial masses. Most incorrect EUS diagnoses occurred with hypoechoic 3rd and 4th layer masses with two of the cases demonstrating malignancies. One case was an invasive squamous cell carcinoma invading the esophagus that on EUS coincided with the 4th EUS layers and was hypoechoic with internal hyperechoic foci, and had an irregular appearing margin. The 2nd case was a gastric adenocarcinoma with EUS demonstrating the lesion coincided with the 3rd EUS layers and was

hypoechoic with internal hyperechoic foci, with smooth margins. Therefore, hypoechoic lesions of the 3rd and the 4th EUS layer were considered. Histologic confirmation by using endoscopic submucosal resection or EUS-FNA should be obtained when possible.

DIFFERENTIAL DIAGNOSIS BETWEEN BENIGN AND MALIGNANT TUMORS

In 1992, Rösch *et al*[10] compared the EUS features of benign with malignant tumors in SMT of the upper GI tract, and concluded there was no single reliable criterion that would enable a differential diagnosis. However, they proposed larger, echo-inhomogeneous masses with irregular outer borders are suggestive of malignancy whereas smaller (< 3 cm) echo-homogeneous subepithelial tumors with a smooth margin are likely to be benign. Chak *et al*[16] found that features predictive of malignant subepithelial tumors were diameter > 4 cm, irregular extraluminal border, echogenic foci, and cystic space. When the presence of at least two of the following three features were used as malignancy determinants, sensitivity ranged from 80% to 100%, depending on the endosonographer. Recently, it has been considered that subepithelial tumors are mostly gastric GISTs, and there are some reports that assess EUS characteristics for predicting the malignant potential of GISTs[44]. Tumor size (more than 3 to 5 cm depending on the study) was the most the important. The predictive value of other features, such as irregular borders, echogenic foci, cystic spaces, ulcerated mucosae, lymph nodes and exogastric growths with malignant pattern, is unclear (Figure 6C)[1,7,34-36,42]. However, those studies are retrospective and included small numbers of tumor samples, thus somewhat conflicting results that have not been validated in prospective series have been obtained. Therefore, larger study numbers and prospective multicenter studies are needed.

With the use of EUS, subepithelial lesions can be further characterized by demonstrating the location of the mass, size, and echogenicity[8,20,21]. Furthermore, if a lesion is intramural, EUS can demonstrate the histologic layer of origin within the GI wall. Determination of the histologic layer and the echotexture of the lesions can significantly narrow the differential diagnosis and may be diagnostic in some cases.

In addition, studies have shown interobserver agreement to be poor, and the diagnostic accuracy to depend heavily on the experience of the endosonographer[45].

EUS-FNA

EUS-FNA is a safe and effective technique for obtaining samples for cytologic or histologic examinations either as a primary procedure or in cases where biopsy techniques have failed (Figure 7). Williams *et al*[46] reported that the overall sensitivity, specificity and accuracy of EUS-FNA for the diagnosis of malignancy were 85%, 100% and 89%, respectively, for lymph nodes; 82%, 100%, and 85%, respectively, for pancreatic lesions; 88%, 100%, and 90%, respectively, for perirectal masses; and 50%, 25%, and 38%, respectively, for intramural lesions. They suggested that when providing accurate diagnosis of pancreatic and perirectal malignancies, the technique is less useful for intramural lesions. Similarly, Wiersema *et al*[47] reported that EUS-FNA sensitivity, specificity, and accuracy were 92%, 93%, and 92%, respectively, for lymph nodes, 88%, 95%, and 90%, respectively, for extraluminal masses, and 61%, 79%, and 67%, respectively, for GI wall lesions. Therefore, from those previous reports, EUS-FNA for subepithelial tumors has not had high reliability and sufficient diagnostic accuracy. Recently, there are some reports that the diagnostic yield of EUS-FNA depends on site, size and characteristics of the tumor as well as technical and procedural factors (type of needle, biopsy technique and material processing). Other weighting factors include expertise, training and interaction between the endosonographer and cytopathologist[41,44]. Another factor that appears to affect the accuracy of EUS-FNA is the presence of an on-site pathologist since, in most studies that reported high levels of EUS-FNA diagnostic accuracy, a cytopathologist was present during the procedure to ensure that adequate cytological specimens were obtained[48,49]. When a cytopathologist is present during EUS-FNA, it appears that the diagnostic yield increases by 10%[50,51]. Vander Noot *et al*[52] reported that the sensitivity, specificity, and diagnostic accuracy of EUS-FNA on-site cytological evaluation during FNA procedure in diagnosing GI tract neoplastic lesions were 89%, 88%, and 89%, respectively. When specimens with suspicious cytologic diagnoses were classified as being positive for malignancy the sensitivity and specificity became 96% and 81%, respectively, and the diagnostic accuracy improved to 92%. It is noteworthy that the results of this study were better than those reported in the literature. They suggested that one possible explanation is a cytopathologist is always present on site to assess specimen adequacy and to determine whether additional material should be obtained for ancillary studies, such as flow cytometric and immunocytochemical analyses. Klapman *et al*[53] observed that an EUS center with on-site cytologic

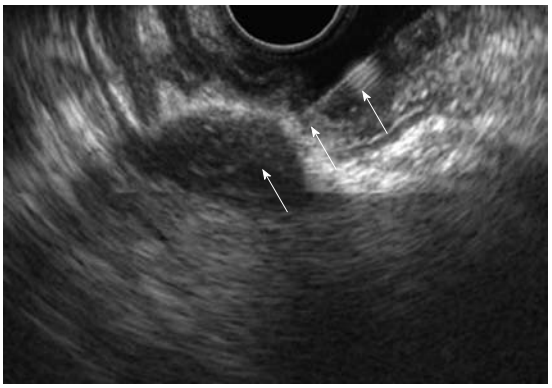

Figure 7 Endoscopic ultrasonography-guided fine needle aspiration of a 20 mm hypoechoic subepithelial tumor of the stomach, using a 25-gauge (arrows).

interpretation had significantly lower rates of unsatisfactory specimens and a higher rate of positive or negative cytologic diagnoses for malignancy compared with an EUS center without on-site cytologic interpretation. False-positive diagnosis of malignancy in EUS-guided biopsy is also rare. Jenssen *et al*[54] reported that the high prognostic and therapeutic relevance of the cytopathological diagnoses resulting from EUS-guided biopsy calls for a shared responsibility of an endosonographer and a cytologist.

For EUS-guided biopsy predictors of malignancy GIST, several factors have been studied in an effort to provide preoperative cytologic risk assessment. Ando *et al*[55] reported that the presence of mitoses in specimens collected by fine-needle aspiration was associated with malignant GISTs. However, mitoses are seldom seen on smears. The same study also found that a high Ki-67 labeling index, a protein marker of cell proliferation, was significantly associated with malignant lesion. Okubo *et al*[56] reported that the presence of an MIB-1 labeling index of more than 5% indicated a high-grade malignancy, with a diagnostic accuracy of 85.7%. KIT and PDGFRA mutation analysis has been proven possible using EUS-guided cell block specimens[57-59]. As KIT mutation analysis has prognostic importance and can be predictive of response to treatment[60-63], its preoperative determination may help to guide the approach to treatment in locally advanced and metastatic disease. The clinical role of such testing is currently being investigated.

EUS-FNA is a safe and precise non-invasive procedure for the diagnosis of subepithelial upper GI tract tumors. Furthermore, utilization of sampling material by EUS-FNA has been expected to improve treatment and management in clinical practice. However, recently, two cases of tumor seeding after percutaneous biopsy for malignant GIST were reported[48,49]. Although there have been no reports of seeding after EUS-FNA for malignant subepithelial tumors, obtaining samples by EUS-FNA from small tumors and from tumors with exogastric growth may result in high peritoneal seeding risk because the FNA needle may easily penetrate not only the tumor but also the whole gastric wall, reaching the peritoneal side and seeding tumor cells along the way. Therefore, during sampling by EUS-FNA in such cases we must play attention to the needle in order not to penetrate the tumor.

SURVEILLANCE BY EUS

For management of subepithelial tumors, EUS is recommended for subepithelial tumors more than 1 cm in diameter, and histologic evaluation, such as EUS-FNA, is recommended for hypoechoic subepithelial tumors less than 3 cm in diameter. Surgery is recommended for subepithelial tumors more than 3 cm in diameter[64]. Although these procedures are helpful in a categorizing a lesion, they cannot absolutely determine the type of lesion or determine if a lesion is benign or malignant[7]. The American Gastroenterological Association recommends periodic endoscopic or endosonographic follow-up or surgical resection for small (less than 3 cm), hypoechoic, 3rd and 4th layer masses, which are most likely GISTs[22]. GISTs are most commonly identified intramural subepithelial tumors in the upper GI tract[7]. Small GISTs (less than 2 cm) have very low malignant potential according to the classification system proposed by the National Institutes of Health Consensus Conference[65]. The recommended duration of follow-up is very variable. Hwang *et al*[43] suggested a 1 year follow-up interval and suggested that the interval between surveillance examinations be extended if the lesion remained unchanged for 2 consecutive follow-up EUS. Guidelines in Japan recommended endoscopic examination once or twice per year for subepithelial lesions less than 2 cm in diameter[66].

CONCLUSION

EUS imaging is essential for the evaluation of subepithelial tumors, because EUS performs better than other modalities in evaluating GI subepithelial lesions. However, the diagnostic accuracy of EUS imaging alone has been shown to be low in subepithelial lesions with a 3rd and 4th layer. In the case of hypoechoic lesions of the 3rd and the 4th EUS layers that are more than in 1 cm diameter, histologic confirmation by using EUS-FNA should be obtained when possible. Although EUS-FNA is a safer and more accurate non-invasive method than other methods of getting samples of the subepithelial tumor, even EUS-FNA is not always accurate enough to determine malignancy, especially determination of malignant GISTs. Furthermore improvements in endoscopic technology are expected to be more useful modalities in differential diagnosis and discrimination between benign and malignant subepithelial tumors.

REFERENCES

1 **Chak A**. EUS and natural orifice transluminal endoscopic surgery. *Gastrointest Endosc* 2009; **69**: S210-S211
2 **Hwang JH**, Saunders MD, Rulyak SJ, Shaw S, Nietsch H, Kimmey MB. A prospective study comparing endoscopy and EUS in the evaluation of GI subepithelial masses. *Gastrointest Endosc* 2005; **62**: 202-208
3 **Polkowski M**, Butruk E. Submucosal lesions. *Gastrointest Endosc Clin N Am* 2005; **15**: 33-54, viii
4 **Nickl N**. Endoscopic approach to gastrointestinal stromal tumors. *Gastrointest Endosc Clin N Am* 2005; **15**: 455-466, viii
5 **Polkowski M**. Endoscopic ultrasound and endoscopic ultrasound-guided fine-needle biopsy for the diagnosis of malignant submucosal tumors. *Endoscopy* 2005; **37**: 635-645
6 **Landi B**, Palazzo L. The role of endosonography in submucosal tumours. *Best Pract Res Clin Gastroenterol* 2009; **23**: 679-701
7 **Chak A**. EUS in submucosal tumors. *Gastrointest Endosc* 2002; **56**: S43-S48
8 **Caletti G**, Zani L, Bolondi L, Brocchi E, Rollo V, Barbara L. Endoscopic ultrasonography in the diagnosis of gastric submucosal tumor. *Gastrointest Endosc* 1989; **35**: 413-418
9 **Hsu CC**, Chen JJ, Changchien CS. Endoscopic features of metastatic tumors in the upper gastrointestinal tract. *Endoscopy* 1996; **28**: 249-253
10 **Rösch T**, Lorenz R, Dancygier H, von Wickert A, Classen M. Endosonographic diagnosis of submucosal upper gastrointestinal tract tumors. *Scand J Gastroenterol* 1992; **27**: 1-8

11 **Shim CS**, Jung IS. Endoscopic removal of submucosal tumors: preprocedure diagnosis, technical options, and results. *Endoscopy* 2005; **37**: 646-654
12 **Hizawa K**, Matsumoto T, Kouzuki T, Suekane H, Esaki M, Fujishima M. Cystic submucosal tumors in the gastrointestinal tract: endosonographic findings and endoscopic removal. *Endoscopy* 2000; **32**: 712-714
13 **Hünerbein M**, Dohmoto M, Haensch W, Schlag PM. Endosonography-guided biopsy of mediastinal and pancreatic tumors. *Endoscopy* 1998; **30**: 32-36
14 **Frank N**, Grieshammer B, Zimmermann W. A new miniature ultrasonic probe for gastrointestinal scanning: feasibility and preliminary results. *Endoscopy* 1994; **26**: 603-608
15 **Fockens P**. Current endosonographic possibilities in the upper gastrointestinal tract. *Baillieres Clin Gastroenterol* 1994; **8**: 603-619
16 **Chak A**, Canto M, Stevens PD, Lightdale CJ, Van de Mierop F, Cooper G, Pollack BJ, Sivak MV Jr. Clinical applications of a new through-the-scope ultrasound probe: prospective comparison with an ultrasound endoscope. *Gastrointest Endosc* 1997; **45**: 291-295
17 **Buscarini E**, Stasi MD, Rossi S, Silva M, Giangregorio F, Adriano Z, Buscarini L. Endosonographic diagnosis of submucosal upper gastrointestinal tract lesions and large fold gastropathies by catheter ultrasound probe. *Gastrointest Endosc* 1999; **49**: 184-191
18 **Wiech T**, Walch A, Werner M. Histopathological classification of nonneoplastic and neoplastic gastrointestinal submucosal lesions. *Endoscopy* 2005; **37**: 630-634
19 **Boyce GA**, Sivak MV Jr, Rösch T, Classen M, Fleischer DE, Boyce HW Jr, Lightdale CJ, Botet JF, Hawes RH, Lehman GA. Evaluation of submucosal upper gastrointestinal tract lesions by endoscopic ultrasound. *Gastrointest Endosc* 1991; **37**: 449-454
20 **Yasuda K**, Nakajima M, Yoshida S, Kiyota K, Kawai K. The diagnosis of submucosal tumors of the stomach by endoscopic ultrasonography. *Gastrointest Endosc* 1989; **35**: 10-15
21 **Motoo Y**, Okai T, Ohta H, Satomura Y, Watanabe H, Yamakawa O, Yamaguchi Y, Mouri I, Sawabu N. Endoscopic ultrasonography in the diagnosis of extraluminal compressions mimicking gastric submucosal tumors. *Endoscopy* 1994; **26**: 239-242
22 **Hwang JH**, Rulyak SD, Kimmey MB. American Gastroenterological Association Institute technical review on the management of gastric subepithelial masses. *Gastroenterology* 2006; **130**: 2217-2228
23 **Seidal T**, Edvardsson H. Expression of c-kit (CD117) and Ki67 provides information about the possible cell of origin and clinical course of gastrointestinal stromal tumours. *Histopathology* 1999; **34**: 416-424
24 **Franquemont DW**. Differentiation and risk assessment of gastrointestinal stromal tumors. *Am J Clin Pathol* 1995; **103**: 41-47
25 **Palazzo L**, Landi B, Cellier C, Roseau G, Chaussade S, Couturier D, Barbier J. Endosonographic features of esophageal granular cell tumors. *Endoscopy* 1997; **29**: 850-853
26 **Tada S**, Iida M, Yao T, Miyagahara T, Hasuda S, Fujishima M. Granular cell tumor of the esophagus: endoscopic ultrasonographic demonstration and endoscopic removal. *Am J Gastroenterol* 1990; **85**: 1507-1511
27 **Matsushita M**, Hajiro K, Okazaki K, Takakuwa H. Gastric inflammatory fibroid polyps: endoscopic ultrasonographic analysis in comparison with the histology. *Gastrointest Endosc* 1997; **46**: 53-57
28 **Pidhorecky I**, Cheney RT, Kraybill WG, Gibbs JF. Gastrointestinal stromal tumors: current diagnosis, biologic behavior, and management. *Ann Surg Oncol* 2000; **7**: 705-712
29 **Miettinen M**, Sarlomo-Rikala M, Lasota J. Gastrointestinal stromal tumors: recent advances in understanding of their biology. *Hum Pathol* 1999; **30**: 1213-1220
30 **Sarlomo-Rikala M**, Kovatich AJ, Barusevicius A, Miettinen M. CD117: a sensitive marker for gastrointestinal stromal tumors that is more specific than CD34. *Mod Pathol* 1998; **11**: 728-734
31 **Miettinen M**, Sobin LH, Sarlomo-Rikala M. Immunohistochemical spectrum of GISTs at different sites and their differential diagnosis with a reference to CD117 (KIT). *Mod Pathol* 2000; **13**: 1134-1142
32 **Kindblom LG**, Remotti HE, Aldenborg F, Meis-Kindblom JM. Gastrointestinal pacemaker cell tumor (GIPACT): gastrointestinal stromal tumors show phenotypic characteristics of the interstitial cells of Cajal. *Am J Pathol* 1998; **152**: 1259-1269
33 **Miettinen M**, Lasota J. Gastrointestinal stromal tumors--definition, clinical, histological, immunohistochemical, and molecular genetic features and differential diagnosis. *Virchows Arch* 2001; **438**: 1-12
34 **Shen EF**, Arnott ID, Plevris J, Penman ID. Endoscopic ultrasonography in the diagnosis and management of suspected upper gastrointestinal submucosal tumours. *Br J Surg* 2002; **89**: 231-235
35 **Caletti G**, Fusaroli P, Bocus P. Endoscopic ultrasonography. *Endoscopy* 1998; **30**: 198-221
36 **Lambert R**, Caletti G, Cho E, Chang KJ, Fusaroli P, Feussner H, Fockens P, Hawes RH, Inui K, Kida M, Lightdale CJ, Matos C, Napoleon B, Palazzo L, Rösch T, Van Dam J. International Workshop on the clinical impact of endoscopic ultrasound in gastroenterology. *Endoscopy* 2000; **32**: 549-584
37 **Miettinen M**, Lasota J. Gastrointestinal stromal tumors: review on morphology, molecular pathology, prognosis, and differential diagnosis. *Arch Pathol Lab Med* 2006; **130**: 1466-1478
38 **Kawamoto K**, Yamada Y, Furukawa N, Utsunomiya T, Haraguchi Y, Mizuguchi M, Oiwa T, Takano H, Masuda K. Endoscopic submucosal tumorectomy for gastrointestinal submucosal tumors restricted to the submucosa: a new form of endoscopic minimal surgery. *Gastrointest Endosc* 1997; **46**: 311-317
39 **Kameyama H**, Niwa Y, Arisawa T, Goto H, Hayakawa T. Endoscopic ultrasonography in the diagnosis of submucosal lesions of the large intestine. *Gastrointest Endosc* 1997; **46**: 406-411
40 **Kojima T**, Takahashi H, Parra-Blanco A, Kohsen K, Fujita R. Diagnosis of submucosal tumor of the upper GI tract by endoscopic resection. *Gastrointest Endosc* 1999; **50**: 516-522
41 **Waxman I**, Saitoh Y, Raju GS, Watari J, Yokota K, Reeves AL, Kohgo Y. High-frequency probe EUS-assisted endoscopic mucosal resection: a therapeutic strategy for submucosal tumors of the GI tract. *Gastrointest Endosc* 2002; **55**: 44-49
42 **Okai T**, Minamoto T, Ohtsubo K, Minato H, Kurumaya H, Oda Y, Mai M, Sawabu N. Endosonographic evaluation of c-kit-positive gastrointestinal stromal tumor. *Abdom Imaging* 2003; **28**: 301-307
43 **Hwang JH**, Kimmey MB. The incidental upper gastrointestinal subepithelial mass. *Gastroenterology* 2004; **126**: 301-307
44 **Săftoiu A**, Vilmann P, Ciurea T. Utility of endoscopic ultrasound for the diagnosis and treatment of submucosal tumors of the upper gastrointestinal tract. *Rom J Gastroenterol* 2003; **12**: 215-229
45 **Gress F**, Schmitt C, Savides T, Faigel DO, Catalano M, Wassef W, Roubein L, Nickl N, Ciaccia D, Bhutani M, Hoffman B, Affronti J. Interobserver agreement for EUS in the evaluation and diagnosis of submucosal masses. *Gastrointest Endosc* 2001; **53**: 71-76
46 **Williams DB**, Sahai AV, Aabakken L, Penman ID, van Velse A, Webb J, Wilson M, Hoffman BJ, Hawes RH. Endoscopic ultrasound guided fine needle aspiration biopsy: a large single centre experience. *Gut* 1999; **44**: 720-726
47 **Wiersema MJ**, Vilmann P, Giovannini M, Chang KJ, Wiersema LM. Endosonography-guided fine-needle aspiration biopsy: diagnostic accuracy and complication assessment. *Gastroenterology* 1997; **112**: 1087-1095
48 **Erickson RA**, Sayage-Rabie L, Beissner RS. Factors predicting the number of EUS-guided fine-needle passes for diagnosis of pancreatic malignancies. *Gastrointest Endosc* 2000; **51**: 184-190

49 **Chang KJ**, Katz KD, Durbin TE, Erickson RA, Butler JA, Lin F, Wuerker RB. Endoscopic ultrasound-guided fine-needle aspiration. *Gastrointest Endosc* 1994; **40**: 694-699

50 **Mertz H**, Gautam S. The learning curve for EUS-guided FNA of pancreatic cancer. *Gastrointest Endosc* 2004; **59**: 33-37

51 **Eisen GM**, Dominitz JA, Faigel DO, Goldstein JA, Petersen BT, Raddawi HM, Ryan ME, Vargo JJ 2nd, Young HS, Wheeler-Harbaugh J, Hawes RH, Brugge WR, Carrougher JG, Chak A, Faigel DO, Kochman ML, Savides TJ, Wallace MB, Wiersema MJ, Erickson RA. Guidelines for credentialing and granting privileges for endoscopic ultrasound. *Gastrointest Endosc* 2001; **54**: 811-814

52 **Vander Noot MR 3rd**, Eloubeidi MA, Chen VK, Eltoum I, Jhala D, Jhala N, Syed S, Chhieng DC. Diagnosis of gastrointestinal tract lesions by endoscopic ultrasound-guided fine-needle aspiration biopsy. *Cancer* 2004; **102**: 157-163

53 **Klapman JB**, Logrono R, Dye CE, Waxman I. Clinical impact of on-site cytopathology interpretation on endoscopic ultrasound-guided fine needle aspiration. *Am J Gastroenterol* 2003; **98**: 1289-1294

54 **Jenssen C**, Dietrich CF. Endoscopic ultrasound-guided fine-needle aspiration biopsy and trucut biopsy in gastroenterology - An overview. *Best Pract Res Clin Gastroenterol* 2009; **23**: 743-759

55 **Ando N**, Goto H, Niwa Y, Hirooka Y, Ohmiya N, Nagasaka T, Hayakawa T. The diagnosis of GI stromal tumors with EUS-guided fine needle aspiration with immunohistochemical analysis. *Gastrointest Endosc* 2002; **55**: 37-43

56 **Okubo K**, Yamao K, Nakamura T, Tajika M, Sawaki A, Hara K, Kawai H, Yamamura Y, Mochizuki Y, Koshikawa T, Inada K. Endoscopic ultrasound-guided fine-needle aspiration biopsy for the diagnosis of gastrointestinal stromal tumors in the stomach. *J Gastroenterol* 2004; **39**: 747-753

57 **Gomes AL**, Bardales RH, Milanezi F, Reis RM, Schmitt F. Molecular analysis of c-Kit and PDGFRA in GISTs diagnosed by EUS. *Am J Clin Pathol* 2007; **127**: 89-96

58 **Rader AE**, Avery A, Wait CL, McGreevey LS, Faigel D, Heinrich MC. Fine-needle aspiration biopsy diagnosis of gastrointestinal stromal tumors using morphology, immunocytochemistry, and mutational analysis of c-kit. *Cancer* 2001; **93**: 269-275

59 **Willmore-Payne C**, Layfield LJ, Holden JA. c-KIT mutation analysis for diagnosis of gastrointestinal stromal tumors in fine needle aspiration specimens. *Cancer* 2005; **105**: 165-170

60 **Debiec-Rychter M**, Sciot R, Le Cesne A, Schlemmer M, Hohenberger P, van Oosterom AT, Blay JY, Leyvraz S, Stul M, Casali PG, Zalcberg J, Verweij J, Van Glabbeke M, Hagemeijer A, Judson I. KIT mutations and dose selection for imatinib in patients with advanced gastrointestinal stromal tumours. *Eur J Cancer* 2006; **42**: 1093-1103

61 **Heinrich MC**, Corless CL, Blanke CD, Demetri GD, Joensuu H, Roberts PJ, Eisenberg BL, von Mehren M, Fletcher CD, Sandau K, McDougall K, Ou WB, Chen CJ, Fletcher JA. Molecular correlates of imatinib resistance in gastrointestinal stromal tumors. *J Clin Oncol* 2006; **24**: 4764-4774

62 **Heinrich MC**, Corless CL, Demetri GD, Blanke CD, von Mehren M, Joensuu H, McGreevey LS, Chen CJ, Van den Abbeele AD, Druker BJ, Kiese B, Eisenberg B, Roberts PJ, Singer S, Fletcher CD, Silberman S, Dimitrijevic S, Fletcher JA. Kinase mutations and imatinib response in patients with metastatic gastrointestinal stromal tumor. *J Clin Oncol* 2003; **21**: 4342-4349

63 **Singer S**, Rubin BP, Lux ML, Chen CJ, Demetri GD, Fletcher CD, Fletcher JA. Prognostic value of KIT mutation type, mitotic activity, and histologic subtype in gastrointestinal stromal tumors. *J Clin Oncol* 2002; **20**: 3898-3905

64 **Eckardt AJ**, Wassef W. Diagnosis of subepithelial tumors in the GI tract. Endoscopy, EUS, and histology: bronze, silver, and gold standard? *Gastrointest Endosc* 2005; **62**: 209-212

65 **Fletcher CD**, Berman JJ, Corless C, Gorstein F, Lasota J, Longley BJ, Miettinen M, O'Leary TJ, Remotti H, Rubin BP, Shmookler B, Sobin LH, Weiss SW. Diagnosis of gastrointestinal stromal tumors: A consensus approach. *Hum Pathol* 2002; **33**: 459-465

66 **Nishida T**, Hirota S, Yanagisawa A, Sugino Y, Minami M, Yamamura Y, Otani Y, Shimada Y, Takahashi F, Kubota T. Clinical practice guidelines for gastrointestinal stromal tumor (GIST) in Japan: English version. *Int J Clin Oncol* 2008; **13**: 416-430

S- Editor Cheng JX **L- Editor** O'Neill M **E- Editor** Zheng XM

World Journal of Radiology

Online Submissions: http://www.wjgnet.com/1949-8470office
wjr@wjgnet.com
doi:10.4329/wjr.v2.i8.298

World J Radiol 2010 August 28; 2(8): 298-308
ISSN 1949-8470 (online)

EDITORIAL

Magnetic resonance imaging for acute pancreatitis

Bo Xiao, Xiao-Ming Zhang

Bo Xiao, Xiao-Ming Zhang, Sichuan Key Laboratory of Medical Imaging, Department of Radiology, Affiliated Hospital of North Sichuan Medical College, Nanchong 637000, Sichuan Province, China
Author contributions: Xiao B and Zhang XM designed the research and wrote the paper; Xiao B performed the research and analyzed the data.
Supported by Grant No. 206126, Key project of Science and Technology Research, and NCET-06-0820, Ministry of Education, China
Correspondence to: Xiao-Ming Zhang, MD, PhD, Professor, Head of Sichuan Key Laboratory of Medical Imaging, Department of Radiology, Affiliated Hospital of North Sichuan Medical College, Nanchong 637000, Sichuan Province, China. cjr.zhxm@vip.163.com
Telephone: +86-817-2262218 Fax: +86-817-2222856
Received: May 31, 2010 Revised: July 29, 2010
Accepted: August 5, 2010
Published online: August 28, 2010

Abstract

Acute pancreatitis is characterized by acute chemical injury of the pancreatic parenchyma and peripancreatic tissue. The increased frequency of death in acute pancreatitis is directly correlated with the degree and progress of pancreatic necrosis. Moreover, the occurrence of some local complications in acute pancreatitis, such as pancreatic hemorrhage, peripancreatic abscess or large pseudocyst, and pseudoaneurysm, could influence the choice of treatment for these patients. Magnetic resonance imaging (MRI) can be used to help evaluate the presence and degree of pancreatic necrosis, and is crucial for identifying complications of acute pancreatitis and predicting prognosis. The purpose of this article is to describe MRI techniques for acute pancreatitis, to review the spectrum of pancreatic and peripancreatic patterns, as well as to survey various complications secondary to acute pancreatitis on MRI. The role of MRI in the initial evaluation and staging of acute pancreatitis is emphasized.

Key words: Magnetic resonance imaging; Acute pancreatitis; Pancreatic necrosis; Pancreatic pseudocyst; Complications

Peer reviewer: Charikleia Triantopoulou, MD, PhD, Head of Radiology Department, Konstantopouleio general Hospital, 3-5, Agias Olgas street, 14233 N. Ionia, Athens, Greece

Xiao B, Zhang XM. Magnetic resonance imaging for acute pancreatitis. *World J Radiol* 2010; 2(8): 298-308 Available from: URL: http://www.wjgnet.com/1949-8470/full/v2/i8/298.htm
DOI: http://dx.doi.org/10.4329/wjr.v2.i8.298

INTRODUCTION

Acute pancreatitis is caused by acute chemical injury of the pancreas, and the leakage of activated pancreatic enzymes leads to autodigestion of the pancreatic parenchyma and peripancreatic tissues[1-3]. Alcoholism and choledocholithiasis are the most common etiological factors for this disease[2-6]. The clinical variety of mild acute pancreatitis (70%-80% of patients), also called edematous interstitial pancreatitis, exhibits a self-limiting disease with no or minimal organ dysfunction, without complications, and with a favorable prognosis[1]. Severe acute pancreatitis (20%-30%), also called hemorrhagic necrotizing pancreatitis, is characterized by conspicuous organ dysfunction, a high incidence of local complications and a dramatic increase in mortality rate (10%-23% in necrotizing pancreatitis)[4,7].

Increased levels of serum and/or urinary pancreatic amylase and lipase have been detected in most individuals with acute pancreatitis after the onset of symptoms. However, these pancreatic enzymes have no role in the assessment of disease severity[8]. Imaging for acute pancreatitis has a significant role in confirming the diagnosis of this disease, which helps to detect pancreatic necrosis and diagnose local complications[9]. Furthermore, imaging is useful in the early assessment of disease severity[5,10,11].

Ultrasonography (US), a convenient and inexpensive imaging technique, can help evaluate the presence of gall-

bladder and/or common duct stones in acute pancreatitis. However, visualization of the pancreas is often disturbed by overlying gastrointestinal gas, which is an important limitation for US applications in this disease[8].

Contrast-enhanced computerized tomography (CT) is often used to aid the diagnosis of pancreatic necrosis and help evaluate the presence and development of local complications in acute pancreatitis[12]. CT severity index (CTSI), a very good imaging grading system for disease severity, has shown excellent correlation with the incidence of death in patients with acute pancreatitis[4,8]. However, CT has the potential aggravation of pancreatic injury that results from the use of iodinated contrast media and an increased radiation burden that can result from follow-up scans[13].

As with the development of high-field-strength magnetic resonance imaging (MRI), it has been established that several techniques such as abdominal rapid gradient-echo breath-hold, magnetic resonance cholangiopancreatography (MRCP) and three-dimensional dynamic contrast-enhanced sequences are performed to depict satisfactorily the normal pancreas and pancreatic disorders[14,15].

Advantages for using MRI in patients with acute pancreatitis are as follows: (1) it is a diagnostic imaging method without radiation hazard; (2) it is particularly useful in patients who cannot receive iodinated contrast material owing to allergic reactions or other contraindications; (3) MRCP has the unique capability of providing noninvasive images of pancreatic parenchyma and pancreatic duct integrity, and it has the advantage of demonstrating possible communication of a pancreatic pseudocyst with pancreatic ducts[8,15]; (4) MRI has a potential advantage over CT in detecting bile duct lithiasis and pancreatic hemorrhage of pseudocysts or pseudoaneurysm, which can help plan surgery; (5) non-enhanced MRI seems to be more accurate and reliable for the early assessment of severity and prognosis of acute pancreatitis than is contrast-enhanced CT[12,16,17]; and (6) non-enhanced MRI is superior to CT for depiction and confirmation of mild forms of acute pancreatitis[18].

Nevertheless, there are several limitations for using MRI in this disease. (1) It requires patient cooperation and breath holding, otherwise, there can be motion artifacts that affect the visualization of the pancreas and its adjacent structures[7,8]. In our clinical practice, this requirement is difficult for patients with severe pancreatitis, who are too old or too weak to hold their breath for long enough; (2) On MRCP, pancreatic duct visibility can be decreased by the overlap of fluid-containing organs (e.g. stomach and duodenum); (3) MRI is time-consuming and relatively expensive with comparison to US or CT; and (4) MR contrast media (e.g. gadolinium) have a potential risk of developing nephrogenic systemic fibrosis in patients with severe acute pancreatitis associated with renal insufficiency after performing MR enhancement[19].

MRI TECHNIQUE

For a comprehensive assessment of acute pancreatitis, it is necessary to evaluate the pancreatic parenchyma, the peripancreatic tissues and vasculature[7]. MRI for acute pancreatitis requires the combined use of T1-weighted imaging (e.g. fast spin-echo imaging with multiple breath-hold acquisitions or single-breath-hold gradient echo imaging); T2-weighted imaging [e.g. fast recovery fast spin-echo or single-shot fast spin-echo (SSFSE) imaging]; and MRCP (e.g. a thick-slab, SSFSE T2-weighted sequence). The characteristics of these are as follows. (1) T1-weighted imaging with fat suppression improves the delineation of pancreatic borders and the pancreas itself, and it additionally has important value in evaluation of pancreatic hemorrhage and hemorrhagic complications of acute pancreatitis[7,8]; (2) T2-weighted imaging has significant advantage in demonstrating fluid-filled lesions in or around the pancreas and the pancreatic ducts. Fat-suppressed T2-weighted imaging is additionally helpful for evaluating the mild forms of acute pancreatitis[18,20]; and (3) MRCP has an excellent capability of allowing noninvasive evaluation of pancreatic ducts, side-branches and the whole extrahepatic biliary tract, and it provides few respiratory artifacts or susceptibility effects[7].

Furthermore, after the intravenous administration of contrast agent, the dynamic contrast-enhanced MRI (e.g. T1-weighted imaging performed with liver acquisition with volume acceleration is utilized, and magnetic resonance angiography (MRA) is performed to provide information for better visualization of the pancreatic vascular network.

MRI FINDINGS OF ACUTE PANCREATITIS

In acute pancreatitis, the patterns of pancreas and peripancreatic tissue involvement can be depicted very well on MRI.

Pancreatic patterns

Morphology of the pancreas: MR T1-weighted with fat-suppression images are particularly useful for defining diffuse or a focal enlarged pancreatic gland. Lace-like contours of the pancreas can disappear and pancreatic boundaries are blurred (Figure 1). However, it should be emphasized that a few patients with edematous pancreatitis have no morphological changes of the pancreas[8,21]. In such circumstances, the objective assessment of this disease should be based on clinical manifestations and several laboratory markers.

Signal intensity of pancreatic parenchyma: Due to inflammation and edema of the pancreas in acute pancreatitis, the signal intensity of the pancreatic parenchyma might be hypointense relative to the liver on T1-weighted images, and hyperintense on T2-weighted images (Figure 2). However, signal changes between the pancreas and liver have been reported in a minority of patients with acute interstitial edematous pancreatitis[22].

Pancreatic interlobular septa: Acute pancreatitis can re-

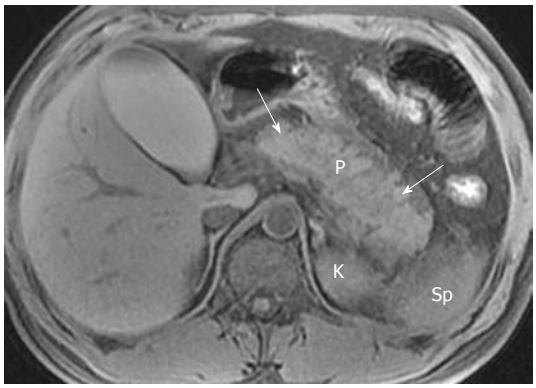

Figure 1 Acute pancreatitis in a 37-year-old man. Axial non-enhanced magnetic resonance T1-weighted with fat-suppression image obtained at the time of hospital admission shows an edematous, homogeneously enlarged pancreas (arrows). Pancreatic boundaries are blurred due to peripancreatic fluid exudations. K: Kidney; P: Pancreas; Sp: Spleen.

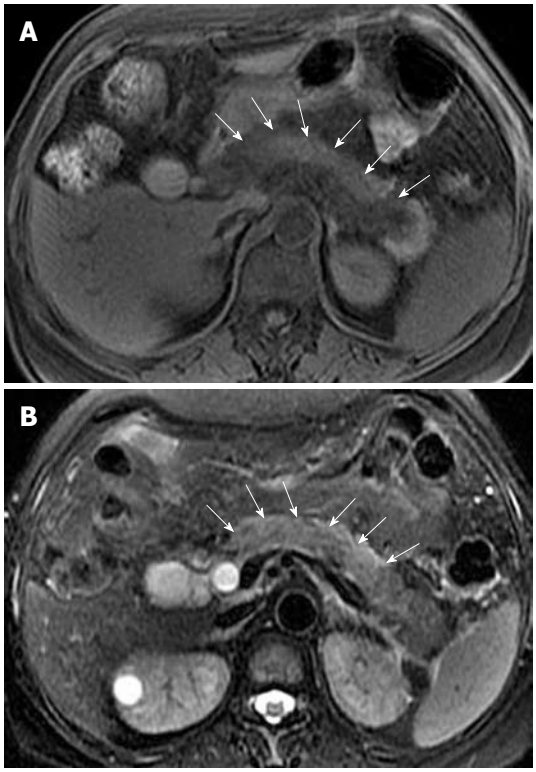

Figure 2 Acute edematous pancreatitis in a 29-year-old man. Axial non-enhanced magnetic resonance T1-weighted with fat-suppression image (A) and axial T2-weighted with fat-suppression image (B) show that the parenchyma of the pancreatic head, body and part of the tail is hypointense (arrows in A) and hyperintense (arrows in B) relative to the liver.

sult in pancreatic interlobular septal inflammation, edema, and fluid collections[7,23]. MR T2-weighted with fat-suppression images can accurately depict subtle interlobular septal abnormalities, such as threadlike hyperintense structures (Figure 3).

Pancreatic necrosis: Pancreatic necrosis refers to a pathological collection of devitalized tissue in the pancreas, and it can be focal or diffuse, or superficial or deep in the pancreatic gland[1,4,8]. Patients with pancreatic necrosis are routinely monitored in the intensive care unit because the increased mortality has been shown to correlate directly with the presence and degree of pancreatic necrosis[4]. Thus, the early detection of pancreatic necrosis is a prognostic indicator in these patients[5]. However, recognition of pancreatic necrosis by means of clinical examination is unreliable, therefore, the importance of diagnostic imaging for that purpose is clinically emphasized.

Figure 3 Acute pancreatitis in a 42-year-old man. Axial magnetic resonance T2-weighted with fat-suppression image shows intrapancreatic threadlike hyperintense structures consistent with interlobular septal inflammation (arrows).

Accepted criteria for the diagnosis of pancreatic necrosis, similar to contrast-enhanced CT, have been defined as areas of diminished or non-enhanced pancreatic parenchyma depicted on dynamic contrast-enhanced MRI[11,13,21]. Furthermore, intravenous administration of contrast material is essential to enable differentiation of real pancreatic necrosis from transient pancreatic ischemia. The visualization of non-enhanced pancreatic parenchyma during the entire processes, including the arterial, venous and delayed phases, supports the diagnosis of the real pancreatic necrosis[8]. The diagnosis of pancreatic necrosis can be made in the course of 2-3 d after onset of acute pancreatitis[24].

Focal pancreatic necrosis is characterized by spotted, patchy non-enhanced areas (like "pepper") on contrast-enhanced MR images (Figure 4). The large, diffuse, non-enhanced zones of the pancreas (like "black pancreas") on enhanced MR images reflect pancreatic diffuse necrosis (Figure 5). A special type of the diffuse necrosis is gland-liquefied necrosis. In this setting, the edge of the pancreas becomes discontinuous or the pancreatic head is not consistent with the body and/or tail, which exhibits "rupture of the pancreas" (Figure 6).

The extent of necrosis can be further quantified to less than 30% (mild), 30%-50% (moderate), and > 50% (severe) of the pancreatic gland, which is based on Balthazar's criteria and grade points[8]. MR severity index (MRSI) derived from CTSI, which combines a consideration of both Balthazar grading scores and scores of the extent of pancreatic necrosis, can also be tested. It has been reported that MRSI is significantly correlated with CTSI, Ranson score, C-reactive protein levels, appearance of systemic complications, duration of hospitalization, and

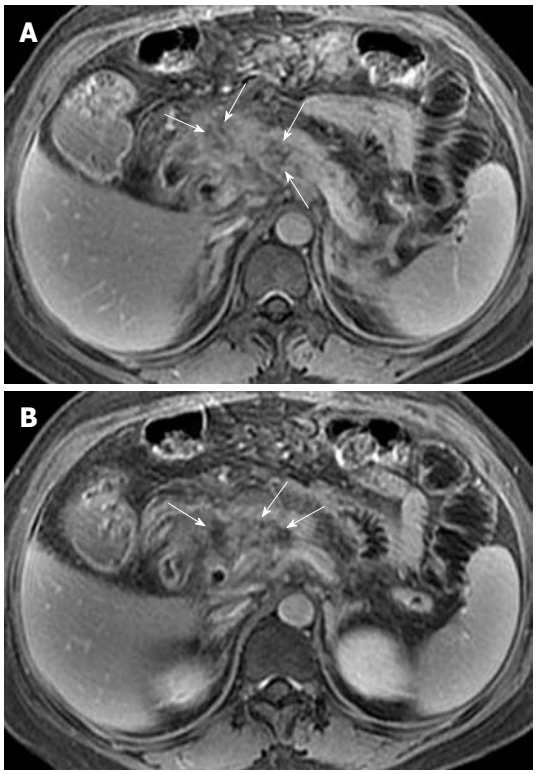

Figure 4 Pancreatic focal necrosis in a 43-year-old woman after an episode of acute pancreatitis. A, B: Axial magnetic resonance T1-weighted images obtained after intravenous contrast material reveal the spotted, patchy necrosis (like "pepper") (arrows) in the head and body of the pancreas. The extent of necrosis is < 30% of the pancreatic gland.

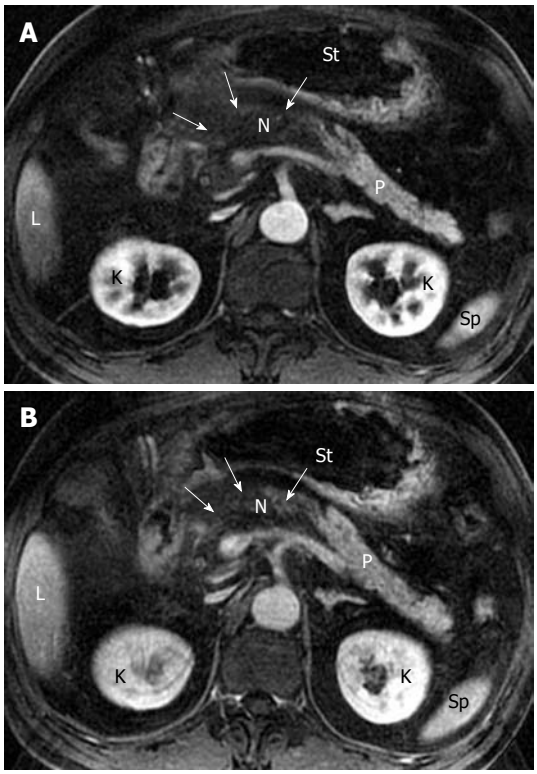

Figure 5 Pancreatic diffuse necrosis in a 65-year-old man after an episode of acute pancreatitis. A, B: Axial magnetic resonance T1-weighted images obtained in late arterial phase and venous phase reveal large necrotic areas (arrows) ("black pancreas") in the pancreatic head, neck and part of the body. The extent of necrosis is up to 30-50% of the pancreatic gland. N: Necrosis; K: Kidney; L: Liver; P: Pancreas; Sp: Spleen; St: Stomach.

clinical outcome[12,25]. Moreover, there is an additional and inevitable problem that infection cannot be excluded in areas of gland necrosis (mentioned below).

Pancreatic hemorrhage: Pancreatic hemorrhage, also called hemorrhagic pancreatitis, is seen in 2%-5% of patients with acute pancreatitis and commonly occurs in the setting of severe forms of pancreatitis[8-10,23]. With conversion of hemoglobin to methemalbumin in the hemorrhagic zones, MRI shows the spotted or patchy (like "salt") (Figure 7) or threadlike or girdle-shaped hyperintensity (Figure 8) on T1-weighted images with fat suppression. To the best of our knowledge, MRI is better than CT for detecting hemorrhagic pancreatitis. This is because the signal intensity changes of hemorrhage on MRI can be sustained for a long time, and have different MR features of hemorrhage at various times (e.g. serum methemalbumin with hyperintensity on T1-weighted images with fat suppression, and hemosiderin with hypointensity on T2-weighted images)[10,13,21]. Other complications of acute pancreatitis, such as pancreatic pseudocyst or pseudoaneurysm, also can show hemorrhage (mentioned below).

Peripancreatic changes

Pancreatic capsule: The pancreas is surrounded by the formation of a capsule, which is actually loose connective tissue[7,8]. In normal individuals, the pancreatic capsule is not seen on CT and MR images, whereas, in patients with acute pancreatitis, abnormalities of the covering of the pancreas, such as edematous thickening of the pancreatic capsule and subcapsular fluid collections, can be accurately depicted on MR T2-weighted with fat-suppression images[22] (Figure 9). In our clinical practice, these pancreatic capsule changes might be the most common findings in patients with edematous or interstitial pancreatitis, and MRI is more helpful than CT to depict them.

Peripancreatic and retroperitoneal fat changes: The pancreatic capsule almost forms no barrier to inflammatory extension of acute pancreatitis, because of the previously mentioned anatomical characteristics. Extravasation of activated pancreatic enzymes (such as pancreatic lipase) after an episode of acute pancreatitis can induce the development of peripancreatic fat edema and necrosis to variable degrees; a common phenomenon that occurs in patients with or without parenchymal necrosis[2,8,13]. However, it is difficult to differentiate pathological changes of peripancreatic fat edema from peripancreatic fat necrosis because they are combined with each other and have similar findings on MR images. Some patients with severe pancreatitis have shown extensive fat edema and necrosis located in omental and mesenteric zones and the extrapancreatic retroperitoneal fatty tissue regions (Figure 10). The inflammatory involvement of retroperitoneal fat edema and necrosis is often consistent with an anterior pararenal

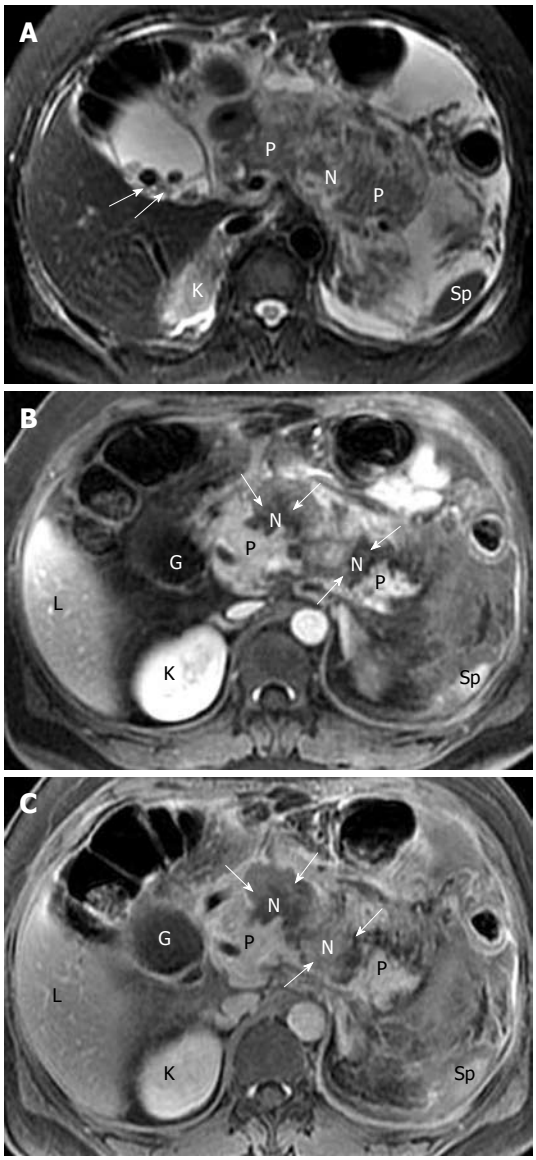

Figure 6 Gallstones, acute pancreatitis, and gland liquefied necrosis in a 33-year-old woman. Axial magnetic resonance T2-weighted with fat-suppression image (A) shows hypointense gallstones (arrows), and axial T1-weighted images obtained in late arterial phase (B) and venous phase (C) reveal two zones (arrows) of pancreatic liquefied necrosis in the neck and body of the gland (like "rupture of the pancreas"). The extent of necrosis is > 50% of the pancreatic gland. The head and the tail of the pancreas are still enhancing (P). N: Liquefied gland necrosis; G: Gallbladder; K: Kidney; L: Liver; P: Pancreas; Sp: Spleen.

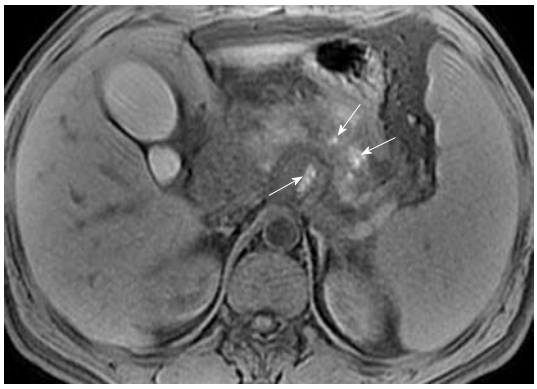

Figure 7 Acute pancreatitis in a 30-year-old man. Axial non-enhanced magnetic resonance T1-weighted with fat-suppression image obtained at the time of hospital admission shows multiple patchy hemorrhagic foci (like "salt") (arrows) in the pancreas and in the fatty tissue behind the pancreas.

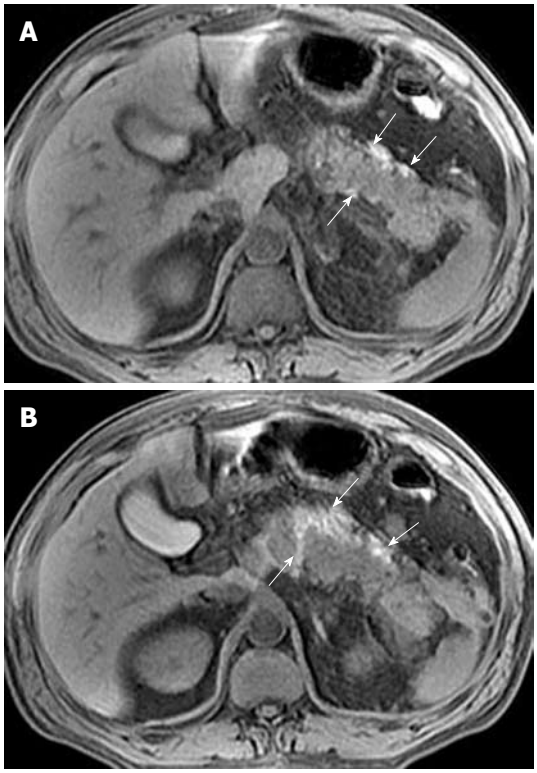

Figure 8 Acute pancreatitis in a 50-year-old man. Axial non-enhanced magnetic resonance T1-weighted with fat-suppression images (A, B) reveal areas of pancreatic and peripancreatic hemorrhage. Hemorrhage involvement adjacent to the pancreas exhibits threadlike, girdle-shaped hyperintense areas (arrows).

space of the left kidney, the right kidney, or both. Cross-sectional T2-weighted imaging and fat-suppressed T1-weighted imaging combined with MRCP might be helpful for comprehensively assessing the range of peripancreatic and retroperitoneal fat changes in acute pancreatitis, which also has an advantage over transverse CT examinations.

Peripancreatic and retroperitoneal fluid collections: As previously mentioned, extravasation of activated pancreatic enzymes results in extrapancreatic chemical injury and multiple areas of fat edema and tissue necrosis, which favor secondary peripancreatic and retroperitoneal fat tissue liquefaction and further develop fluid collections[8,21]. MRI, particularly fat-suppressed T2-weighted imaging, can accurately depict simple or complex fluid collections. The latter one includes: (1) areas of hemorrhage in fluid collections; or (2) pancreatic and/or fat tissue necrosis pieces or fragments in fluid collections (Figure 11). The sequelae of fluid collections might: (1) be absorbed completely; (2) progress to pseudocysts; or (3) be concomitant with infection to form pancreatic cellulitis or abscesses (mentioned below).

Peritoneal and fascial changes: Acute pancreatitis can

Figure 9 Acute pancreatitis and inflammatory extension to pancreatic capsule in a 42-year-old man. Axial magnetic resonance T2-weighted with fat-suppression image shows thickening of pancreatic capsule co-existing with subcapsular fluid collections with threadlike or strip-line hyperintense (arrows).

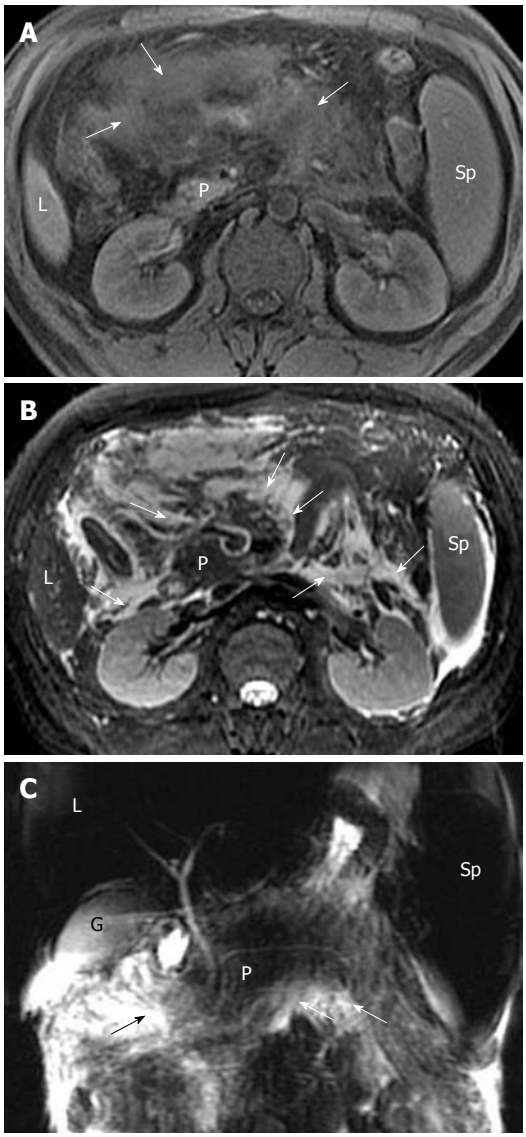

Figure 10 Acute pancreatitis in a 34-year-old man. Axial magnetic resonance (MR) T1-weighted with fat-suppression (A) and T2-weighted with fat-suppression (B) images reveal peripancreatic inflammation extension co-existing with fat necrosis (arrows) in mesenteric fat tissue regions and anterior pararenal space of both kidneys. Extravasated fluid (arrows) is also present around the gland on MR cholangiopancreatography (C). L: Liver; P: Pancreas; Sp: Spleen; G: Gallbladder.

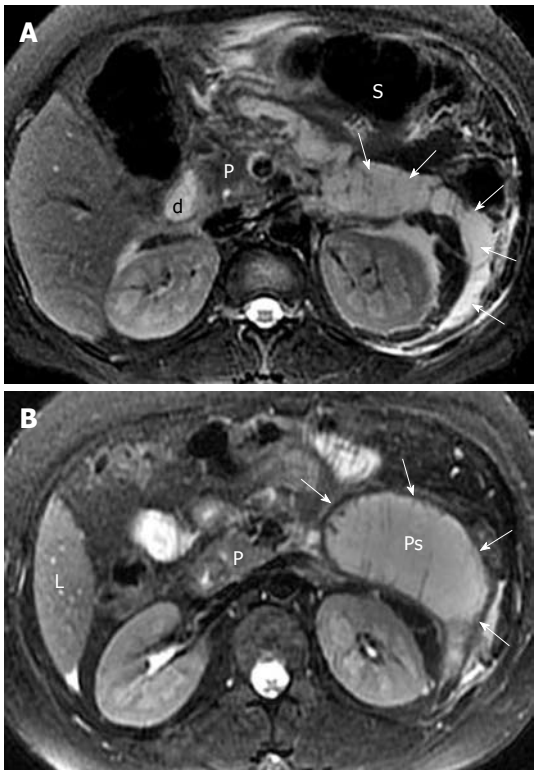

Figure 11 Acute pancreatitis and peripancreatic and retroperitoneal fluid collections in a 42-year-old man. A: Axial magnetic resonance T2-weighted with fat-suppression image obtained at the time of hospital admission shows large heterogeneous fluid collections (arrows) associated with areas of tissue liquified necrosis in the pararenal space of the left kidney; B: Follow-up axial T2-weighted with fat-suppression image reveals an encapsulated fluid collection (arrows) in the process of the development of a pseudocyst. L: Liver; P: Pancreas; S: Stomach; d: Duodenal bulb; Ps: Pseudocyst.

exhibit peritoneal and fascial abnormalities. Both of them are secondary to extrapancreatic inflammatory extension and occur simultaneously in most patients with this disease[7,8]. Anterior fascia of the kidney is the most common one that is invaded by peripancreatic inflammatory extension, due to its proximity to the pancreas. The inflammatory extravasation also can involve one or several structures of the peritoneum such as omentum, mesentery, and colic mesentery[1,8]. With the development and progress of this disease, these peritoneal structures develop edema or swelling with/without fat necrosis or fluid collections. Contrast-enhanced MRI can show the irregular thickening and heterogeneous enhancement of the intestinal wall, and MRCP can manifest the range of edematous mesentery and fluid collections with hyperintensity (Figure 12).

MRI FINDINGS OF COMPLICATIONS IN ACUTE PANCREATITIS

Pseudocyst

Pancreatic pseudocyst is a very common type of local complications of acute pancreatitis, and it develops in most patients who are already suffering from post-necrotic pancreatitis[7,8,26]. It is defined as a localized collection of pancreatic juices by a fibrous membrane without an

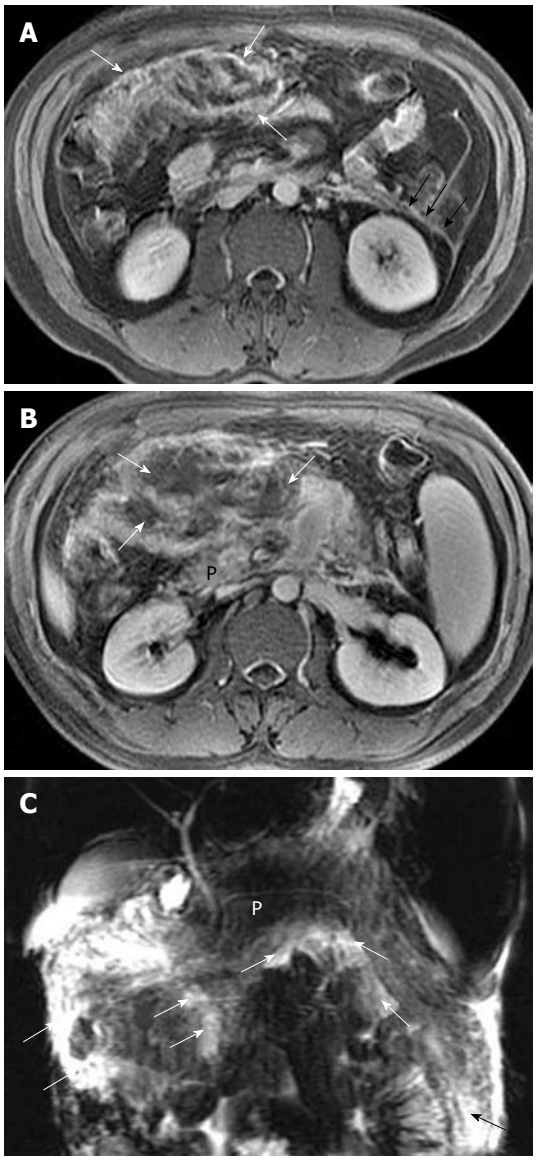

Figure 12 Pancreatic focal necrosis in a 35-year-old man after an episode of acute pancreatitis. A, B: Enhanced axial T1-weighted images reveal the irregular thickening and heterogeneous enhancement of the intestinal wall (white arrows in A), anterior fascia of the left kidney (black arrows in A), and mesenteric edema associated with fat necrosis (arrows in B); C: Magnetic resonance cholangiopancreatography reveals multiple edema and small fluid collections (arrows) adjacent to small intestine and colon. P: Pancreas.

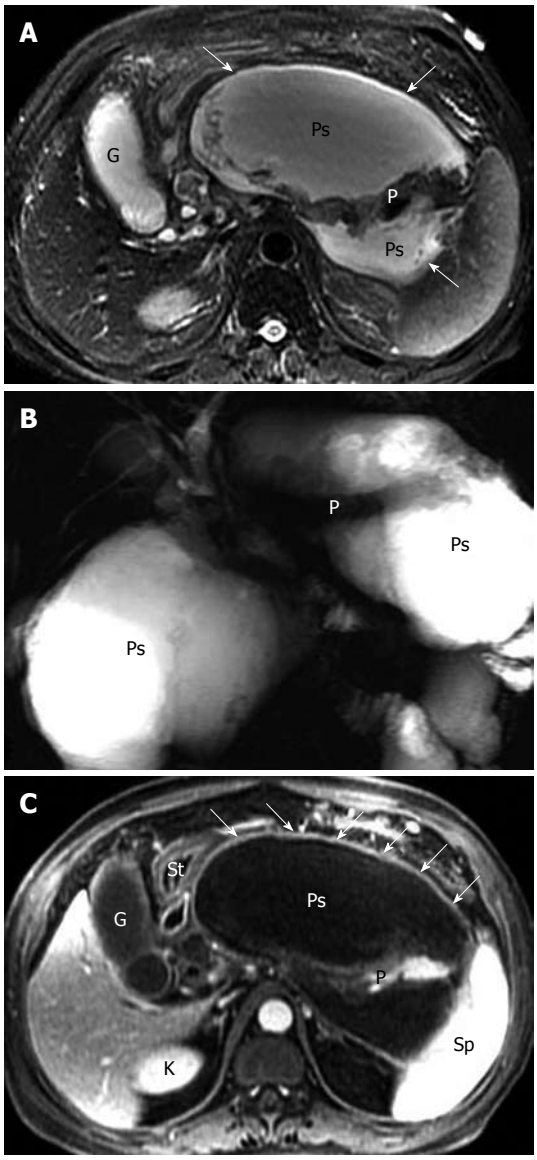

Figure 13 A large peripancreatic pseudocyst in a 41-year-old man who present as abdominal distension after acute post-necrotic pancreatitis. Axial magnetic resonance (MR) T2-weighted with fat-suppression image (A) and MR cholangiopancreatography (B) show a large pseudocyst (arrows) with homogeneous hypersignal intensity around the pancreas. Axial T1-weighted image obtained with intravenous contrast material (C) reveals the enhancement of the thick wall (arrows) of the pseudocyst. The extrusion and displacement of the stomach (St) is seen due to the tension of the pseudocyst. G: Gallbladder; P: Pancreas; Ps: Pseudocyst; K: Kidney; Sp: Spleen; St: Stomach.

epithelium, and occurs approximately 4-6 wk after a first episode of acute pancreatitis[27,28]. According to spatial locations, pancreatic pseudocysts are classified as intraparenchymal (within the pancreatic tissue) or extrapancreatic (surrounding the pancreas), or both. The intraparenchymal pseudocyst might be communicating with pancreatic ducts and associated with partial pancreatic ductal obstruction, whereas the extrapancreatic pseudocyst might be related to the development of peripancreatic fluid collections[7,27,28]. The other classification is based on whether the pseudocyst is accompanied by mucus, protein and hemorrhage. The simple pseudocyst is present as a round or oval fluid collection surrounded by a thin or thick wall and homogeneous water-like signal intensity (Figure 13), and the complex pseudocyst is present as a round or oval heterogeneous lesion dominated by hyperintensity on T1-weighted images with fat suppression (Figure 14). In our experience, when one or several pseudocysts are suspected of bleeding, MRI is more favorable than CT (previously mentioned in pancreatic hemorrhage).

Infections

In acute pancreatitis, secondary bacterial contamination can occur in the setting of: (1) pancreatic necrosis; (2) peripancreatic fat necrosis; (3) retroperitoneal fat necrosis; (4) peripancreatic fluid collections; or (5) pseudocysts. It has

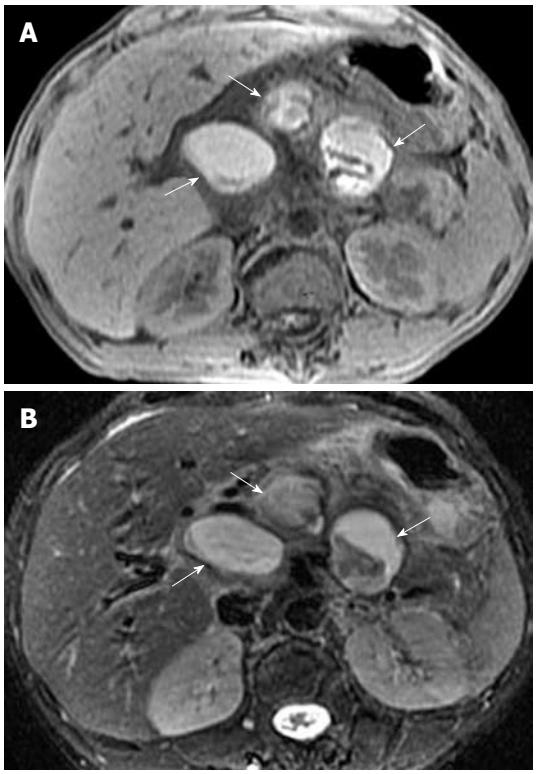

Figure 14 Multiple pseudocysts complicated hemorrhage in a 36-year-old man who had previously suffered from acute pancreatitis. Axial non-enhanced magnetic resonance T1-weighted with fat-suppression (A) and axial T2-weighted with fat-suppression (B) images reveal multiple hemorrhagic pseudocysts (arrows) with heterogeneous signal intensity.

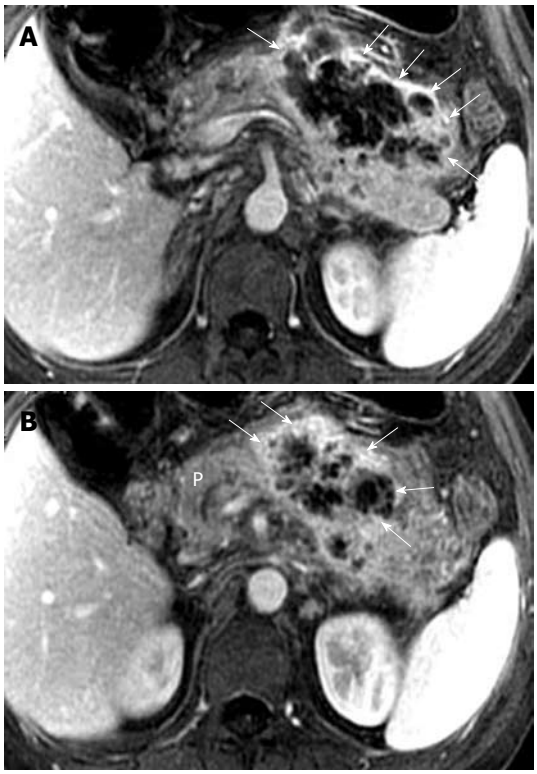

Figure 15 Acute necrotic pancreatitis and peripancreatic cellulitis in a 39-year-old man. A, B: Axial magnetic resonance T1-weighted images obtained with intravenous contrast material reveal an ill-defined, multilocular, inflammatory mass (arrows) with ring-like and separated enhancement adjacent to the body and tail of the pancreas. P: Pancreas.

been noted that 40%-70% of patients with pancreatic necrosis have secondary necrosis or severe bacterial contamination[8,29]. Pancreatic liquefied necrosis with or without multiple areas of fat necrosis might progress to pancreatic cellulitis, whereas peripancreatic fluid collections or pseudocysts might become infected to develop abscesses. Once the infectious complications occur, whether pancreatic cellulitis or abscesses, they constitute a major mortality risk for patients with acute pancreatitis.

Pancreatic cellulitis, with an incidence that varies from 8.3% to 10.6%, is clinically difficult to differentiate from pancreatic abscess[30]. It is an inflammatory entity that is situated at the intraparenchymal region of the pancreas and is associated with peripancreatic zones, as a result of pathological pancreatic swelling and necrosis, inflammatory cell infiltration and peripancreatic fat tissue necrosis[29,30]. After administration of contrast material, an ill-defined multilocular mass (like "hornets' nest") exhibits ring-like and separated enhanced areas with fragments of post-necrotic gland and fat tissue, and non-enhanced tissue liquefaction (Figure 15).

Pancreatic abscess, with an incidence that varies from 1% to 9% and a high mortality, occurs in the course of 2-5 wk after the onset of acute pancreatitis[31]. Unfortunately, in our clinical practice, it is not easy to differentiate pancreatic abscesses from pseudocysts due to the similar MR findings. Thus, confirmed diagnosis often depends on fine-needle aspiration biopsy of a lesion[28,31]. The

Figure 16 Extrapancreatic abscess confirmed by a surgical operation in a 33-year-old man after acute post-necrotic pancreatitis. Axial magnetic resonance T1-weighted image with fat suppression obtained with intravenous contrast material shows an encapsulated liquid collection (arrows) with a well-defined, thickened and enhancing wall.

bubble or gas attenuation within a lesion could indicate pancreatic abscess on non-enhanced CT images, however, in our experience, bubble or gas in an abscess cannot be easily identified on MR images. Therefore, we emphasize that the pancreatic abscess should be suspected to occur when patients have suffered from acute pancreatitis and develop fever, tachycardia, abdominal distention or an encapsulated liquid collection with an enhancing wall on MRI (Figure 16).

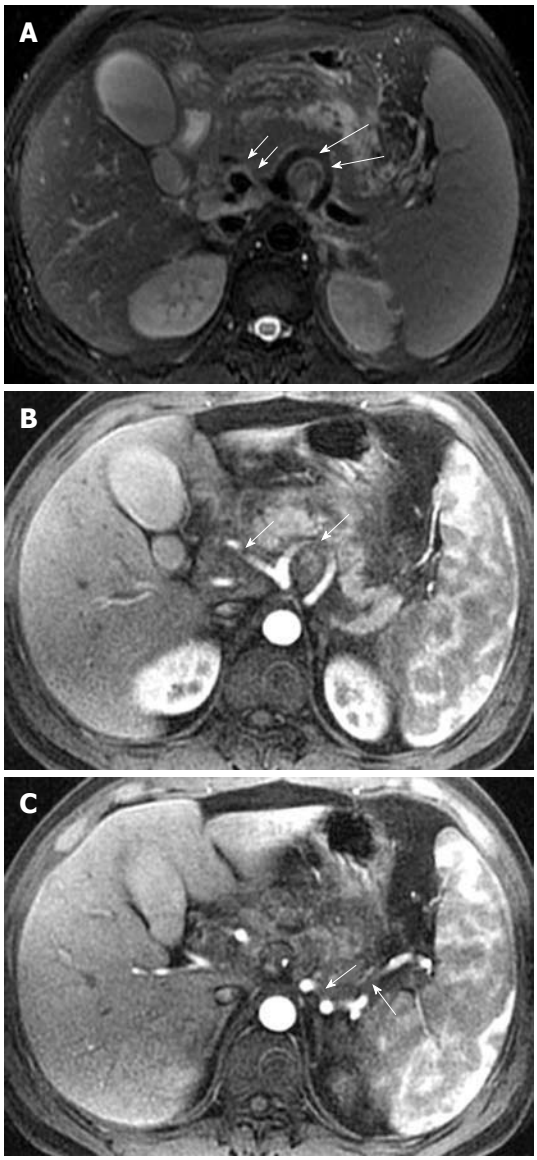

Figure 17 Artery involvement and vasculitis in a 30-year-old man after an episode of acute pancreatitis. A: Axial magnetic resonance T2-weighted with fat-suppression image shows the loss of vascular flow voiding effect of the involved parts of the common hepatic artery (small arrows) and splenic artery (large arrows); B, C: Axial contrast-enhanced T1-weighted images obtained in arterial phase reveal the poor enhancement of the involved parts of these arteries (arrows) associated with the obscure and rough edges.

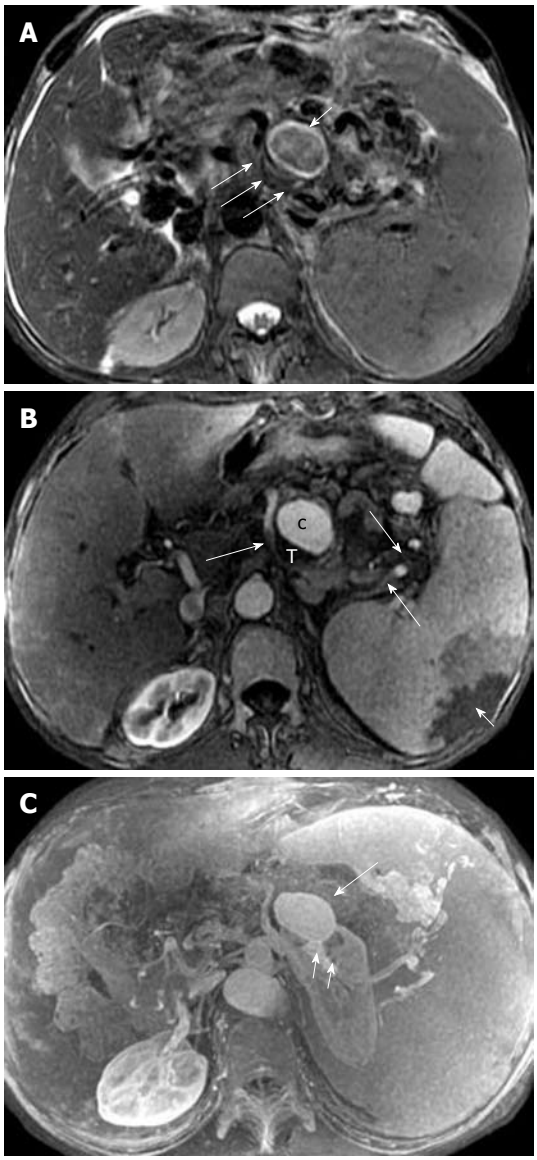

Figure 18 Splenic artery pseudoaneurysm in a 36-year-old man with a history of acute pancreatitis. A: Axial magnetic resonance (MR) T2-weighted with fat-suppression image shows the involved part of the splenic artery (large arrows) and aneurysmal dilatation (small arrows); B: Axial T1-weighted image obtained with intravenous contrast material reveals enhancement of the pseudoaneurysm cavity (c) and a filling defect present as mural thrombosis (T), and wedge-shape zones of infarction of the spleen (small arrows) due to the involved parts of the splenic artery (large arrows); C: MR angiography further depicts the visualization of the relationship between this pseudoaneurysm (large arrow) and the involved splenic artery (small arrows). c: Cavity of the pseudoaneurysm; T: Mural thrombosis in the pseudoaneurysm.

Vascular involvement

Vascular involvement is a common but ignorable local complication of acute pancreatitis[2,7,15,21]. Intraparenchymal and peripancreatic extravasation of activated digestive enzymes is responsible for damage to the pancreatic vascular network, including feeding arteries and draining veins. A spectrum of vascular abnormalities includes: (1) vasculitis; (2) artery bleeding or pseudoaneurysm; (3) phlebothrombosis or vein occlusion; (4) pancreatic regional portal hypertension; and (5) combination of these. MRA can be performed to supplement the information for visualization of vascular complications, besides common axial contrast-enhanced MRI.

The splenic, gastroduodenal and pancreaticoduodenal arteries are more frequently involved than other peripancreatic arteries[23,32]. The arterial invasion exhibits the loss of the vascular flow voiding effect ("black blood") on T2-weighted images, and poor or no enhancement on MR images during the contrast-enhanced arterial phase. The obscure and rough edges of the involved arterial wall are indicative of vasculitis (Figure 17). Vasculitis associated with incomplete arterial occlusion might favor secondary abdominal organ infarction, for example, of the spleen (mentioned below).

Pseudoaneurysm, a relatively uncommon and delayed

Figure 19 Acute pancreatitis with splenic venous thrombosis in a 30-year-old man. Axial magnetic resonance T1-weighted image obtained with intravenous contrast material during the venous phase reveals the involved parts of splenic vein with intravenous filling defects (arrows).

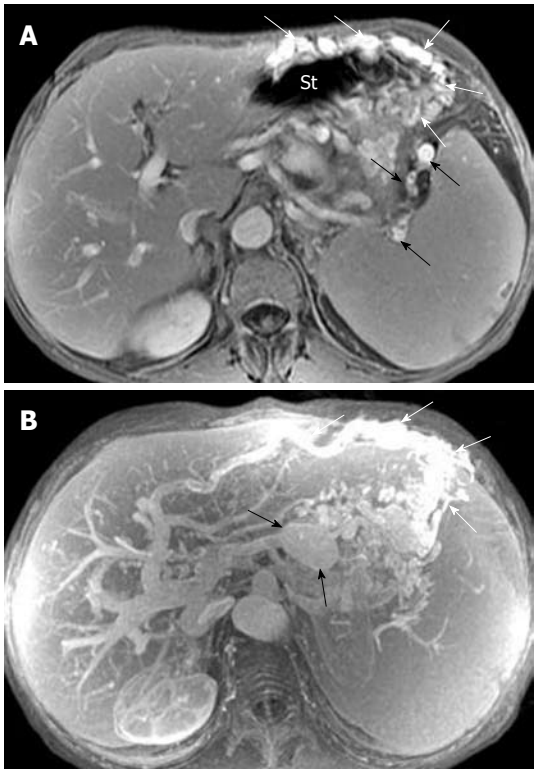

Figure 20 Pancreatic regional portal hypertension in a 36-year-old man with a history of acute pancreatitis. A: Axial T1-weighted image obtained with intravenous contrast material reveals enhancement of numerous and circuitous veins (white arrows) around the gastric fundus, and splenic veins (black arrows) adjacent to the splenic hilum; B: Magnetic resonance angiography depicts the establishment of numerous and conspicuous collateral vessels due to gastric fundic varices (white arrows) and a pseudoaneurysm (black arrows). St: Stomach.

complication of acute pancreatitis, can be a life-threatening emergency if rupture occurs[23]. The cavity of pseudoaneurysm communicates with the involved artery and can show marked enhancement on MR images after the administration of contrast material, whereas the non-enhanced zones reflect the mural thrombosis in the pseudoaneurysm (like the Chinese "Yin-Yang" sign)[33] (Figure 18).

The splenic vein is the most common of the veins that are involved, by inflammatory extension due to its proximity to the pancreas[23,32]. The involved vein might be complicated by local thrombosis and occlusion. MRI shows the loss of the vascular flow voiding effect on T2-weighted images. After administration of contrast agent, an intravenous asymmetrical filling defect can be seen on venous phase images (Figure 19).

Additionally, venous thrombosis and occlusion, particularly of the splenic vein, can result in pancreatogenic regional portal hypertension[34,35]. It shows the establishment of multiple, conspicuous collateral circulation, which usually involves gastric short veins around the fundus of the stomach, gastroepiploic veins close to the greater curvature of stomach, and splenic veins adjacent to the spleen hilum. Contrast-enhanced MRI shows numerous and circuitous blood vessels with abnormal enhancement, and splenomegaly with or without splenic infarction (Figure 20).

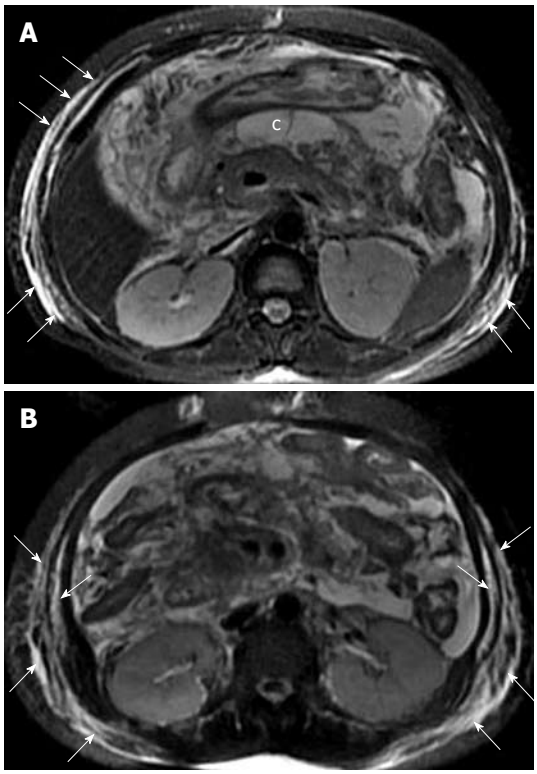

Figure 21 Subcutaneous and intermuscular involvement in a 38-year-old woman after an episode of acute pancreatitis. A, B: Axial magnetic resonance T2-weighted with fat-suppression images obtained at the time of hospital admission show oval fluid collections (c) in the omental bursa, and bilateral subcutaneous and intermuscular fat edema with hyperintensity (arrows). c: Fluid collections.

Subcutaneous and intermuscular involvement

Pancreatic inflammatory extravasation in some patients with severe pancreatitis can result in extrapancreatic multiple injury, and even present as subcutaneous and intermuscular soft tissue involvement such as fat edema, swelling, necrosis, and small fluid collections (Figure 21).

CONCLUSION

The comprehensive assessment of acute pancreatitis is

based on clinical, laboratory and imaging evaluation. MRI is an excellent noninvasive modality of choice to help stage the severity of inflammatory processes, and detect the presence and extent of pancreatic necrosis. The presence and development of complications of acute pancreatitis such as hemorrhage, fluid collections, pseudocysts, abscesses, pseudoaneurysm, and venous thrombosis are well-demonstrated by MRI.

REFERENCES

1 **Scaglione M**, Casciani E, Pinto A, Andreoli C, De Vargas M, Gualdi GF. Imaging assessment of acute pancreatitis: a review. *Semin Ultrasound CT MR* 2008; **29**: 322-340
2 **Balthazar EJ**, Freeny PC, vanSonnenberg E. Imaging and intervention in acute pancreatitis. *Radiology* 1994; **193**: 297-306
3 **Lenhart DK**, Balthazar EJ. MDCT of acute mild (nonnecrotizing) pancreatitis: abdominal complications and fate of fluid collections. *AJR Am J Roentgenol* 2008; **190**: 643-649
4 **Larvin M**. Management of infected pancreatic necrosis. *Curr Gastroenterol Rep* 2008; **10**: 107-114
5 **Sandrasegaran K**, Tann M, Jennings SG, Maglinte DD, Peter SD, Sherman S, Howard TJ. Disconnection of the pancreatic duct: an important but overlooked complication of severe acute pancreatitis. *Radiographics* 2007; **27**: 1389-1400
6 **Kwak SW**, Kim S, Lee JW, Lee NK, Kim CW, Yi MS, Kim GH, Kang DH. Evaluation of unusual causes of pancreatitis: role of cross-sectional imaging. *Eur J Radiol* 2009; **71**: 296-312
7 **Matos C**, Cappeliez O, Winant C, Coppens E, Devière J, Metens T. MR imaging of the pancreas: a pictorial tour. *Radiographics* 2002; **22**: e2
8 **Balthazar EJ**. Acute pancreatitis: assessment of severity with clinical and CT evaluation. *Radiology* 2002; **223**: 603-613
9 **Saokar A**, Rabinowitz CB, Sahani DV. Cross-sectional imaging in acute pancreatitis. *Radiol Clin North Am* 2007; **45**: 447-460, viii
10 **Balci NC**, Bieneman BK, Bilgin M, Akduman IE, Fattahi R, Burton FR. Magnetic resonance imaging in pancreatitis. *Top Magn Reson Imaging* 2009; **20**: 25-30
11 **Bollen TL**, van Santvoort HC, Besselink MG, van Es WH, Gooszen HG, van Leeuwen MS. Update on acute pancreatitis: ultrasound, computed tomography, and magnetic resonance imaging features. *Semin Ultrasound CT MR* 2007; **28**: 371-383
12 **Stimac D**, Miletić D, Radić M, Krznarić I, Mazur-Grbac M, Perković D, Milić S, Golubović V. The role of nonenhanced magnetic resonance imaging in the early assessment of acute pancreatitis. *Am J Gastroenterol* 2007; **102**: 997-1004
13 **Robinson PJ**, Sheridan MB. Pancreatitis: computed tomography and magnetic resonance imaging. *Eur Radiol* 2000; **10**: 401-408
14 **Tkacz JN**, Anderson SA, Soto J. MR imaging in gastrointestinal emergencies. *Radiographics* 2009; **29**: 1767-1780
15 **Kim DH**, Pickhardt PJ. Radiologic assessment of acute and chronic pancreatitis. *Surg Clin North Am* 2007; **87**: 1341-1358, viii
16 **Kim YK**, Kim CS, Han YM. Role of fat-suppressed t1-weighted magnetic resonance imaging in predicting severity and prognosis of acute pancreatitis: an intraindividual comparison with multidetector computed tomography. *J Comput Assist Tomogr* 2009; **33**: 651-656
17 **Viremouneix L**, Monneuse O, Gautier G, Gruner L, Giorgi R, Allaouchiche B, Pilleul F. Prospective evaluation of nonenhanced MR imaging in acute pancreatitis. *J Magn Reson Imaging* 2007; **26**: 331-338
18 **Amano Y**, Oishi T, Takahashi M, Kumazaki T. Nonenhanced magnetic resonance imaging of mild acute pancreatitis. *Abdom Imaging* 2001; **26**: 59-63
19 **Jain R**, Levine M. Correction to the relative risk calculation for gadolinium-enhanced MR imaging and nephrogenic systemic fibrosis. *Radiology* 2010; **255**: 307-308; author reply 308
20 **Kim YK**, Ko SW, Kim CS, Hwang SB. Effectiveness of MR imaging for diagnosing the mild forms of acute pancreatitis: comparison with MDCT. *J Magn Reson Imaging* 2006; **24**: 1342-1349
21 **Arvanitakis M**, Delhaye M, De Maertelaere V, Bali M, Winant C, Coppens E, Jeanmart J, Zalcman M, Van Gansbeke D, Devière J, Matos C. Computed tomography and magnetic resonance imaging in the assessment of acute pancreatitis. *Gastroenterology* 2004; **126**: 715-723
22 **Zhang XM**, Feng ZS, Zhao QH, Xiao CM, Mitchell DG, Shu J, Zeng NL, Xu XX, Lei JY, Tian XB. Acute interstitial edematous pancreatitis: Findings on non-enhanced MR imaging. *World J Gastroenterol* 2006; **12**: 5859-5865
23 **Miller FH**, Keppke AL, Dalal K, Ly JN, Kamler VA, Sica GT. MRI of pancreatitis and its complications: part 1, acute pancreatitis. *AJR Am J Roentgenol* 2004; **183**: 1637-1644
24 **Hirota M**, Kimura Y, Ishiko T, Beppu T, Yamashita Y, Ogawa M. Visualization of the heterogeneous internal structure of so-called "pancreatic necrosis" by magnetic resonance imaging in acute necrotizing pancreatitis. *Pancreas* 2002; **25**: 63-67
25 **Arvanitakis M**, Koustiani G, Gantzarou A, Grollios G, Tsitouridis I, Haritandi-Kouridou A, Dimitriadis A, Arvanitakis C. Staging of severity and prognosis of acute pancreatitis by computed tomography and magnetic resonance imaging-a comparative study. *Dig Liver Dis* 2007; **39**: 473-482
26 **Degen L**, Wiesner W, Beglinger C. Cystic and solid lesions of the pancreas. *Best Pract Res Clin Gastroenterol* 2008; **22**: 91-103
27 **Kim YH**, Saini S, Sahani D, Hahn PF, Mueller PR, Auh YH. Imaging diagnosis of cystic pancreatic lesions: pseudocyst versus nonpseudocyst. *Radiographics* 2005; **25**: 671-685
28 **Andrén-Sandberg A**, Dervenis C. Pancreatic pseudocysts in the 21st century. Part I: classification, pathophysiology, anatomic considerations and treatment. *JOP* 2004; **5**: 8-24
29 **Maroun Marun C**, Uscanga L, Lara F, Passareli L, Quiroz-Ferrari F, Robles-Díaz G, Campuzano-Fernández M. [Pancreatic phlegmon: a potentially fatal form of acute pancreatitis] *Rev Invest Clin* 1992; **44**: 507-512
30 **Fan ST**, Choi TK, Chan FL, Lai EC, Wong J. Pancreatic phlegmon: what is it? *Am J Surg* 1989; **157**: 544-547
31 **Hill MC**, Dach JL, Barkin J, Isikoff MB, Morse B. The role of percutaneous aspiration in the diagnosis of pancreatic abscess. *AJR Am J Roentgenol* 1983; **141**: 1035-1038
32 **Mortelé KJ**, Mergo PJ, Taylor HM, Wiesner W, Cantisani V, Ernst MD, Kalantari BN, Ros PR. Peripancreatic vascular abnormalities complicating acute pancreatitis: contrast-enhanced helical CT findings. *Eur J Radiol* 2004; **52**: 67-72
33 **Lupattelli T**. The yin-yang sign. *Radiology* 2006; **238**: 1070-1071
34 **Wang CX**, Li R, Cai XJ, Peng Z, Liang FQ. [Diagnosis and treatment of pancreatogenic portal hypertension: analysis of 26 cases] *Zhonghua Yixue Zazhi* 2008; **88**: 395-397
35 **Liu QD**, Zhou NX, Zhang WZ, Wang MQ. Diagnosis and management of regional portal hypertension. *Chin J Dig Dis* 2005; **6**: 87-92

S- Editor Cheng JX **L- Editor** Kerr C **E- Editor** Zheng XM

World Journal of Radiology

Online Submissions: http://www.wjgnet.com/1949-8470office
wjr@wjgnet.com
doi:10.4329/wjr.v2.i8.309

World J Radiol 2010 August 28; 2(8): 309-322
ISSN 1949-8470 (online)

REVIEW

Magnetic resonance imaging: Review of imaging techniques and overview of liver imaging

Santhi Maniam, Janio Szklaruk

Santhi Maniam, Janio Szklaruk, Department of Diagnostic Radiology, University of Texas M. D. Anderson Cancer Center, Houston, TX 77030, United States
Author contributions: Both authors contribute the research, text, organization, editing, and revision of the manuscript.
Correspondence to: Janio Szklaruk, MD, PhD, Department of Diagnostic Radiology, University of Texas M. D. Anderson Cancer Center, 1515 Holcombe, Box 368, Houston, TX 77030, United States. jszklaru@mdanderson.org
Telephone: +1-713-7451453 Fax: +1-713-7451302
Received: May 20, 2010 Revised: June 24, 2010
Accepted: July 15, 2010
Published online: August 28, 2010

Abstract

Magnetic resonance imaging (MRI) of the liver is slowly transitioning from a problem solving imaging modality to a first line imaging modality for many diseases of the liver. The well established advantages of MRI over other cross sectional imaging modalities may be the basis for this transition. Technological advancements in MRI that focus on producing high quality images and fast imaging, increasing diagnostic accuracy and developing newer function-specific contrast agents are essential in ensuring that MRI succeeds as a first line imaging modality. Newer imaging techniques, such as parallel imaging, are widely utilized to shorten scanning time. Diffusion weighted echo planar imaging, an adaptation from neuroimaging, is fast becoming a routine part of the MRI liver protocol to improve lesion detection and characterization of focal liver lesions. Contrast enhanced dynamic T1 weighted imaging is crucial in complete evaluation of diseases and the merit of this dynamic imaging relies heavily on the appropriate timing of the contrast injection. Newer techniques that include fluoro-triggered contrast enhanced MRI, an adaptation from 3D MRA imaging, are utilized to achieve good bolus timing that will allow for optimum scanning. For accurate interpretation of liver diseases, good understanding of the newer imaging techniques and familiarity with typical imaging features of liver diseases are essential. In this review, MR sequences for a time efficient liver MRI protocol utilizing newer imaging techniques are discussed and an overview of imaging features of selected common focal and diffuse liver diseases are presented.

Key words: Magnetic resonance imaging; Liver; Oncology; Contrast agents

Peer reviewers: Rajasvaran Logeswaran, PhD, Associate Professor, Faculty of Engineering, Multimedia University, 63100 Cyberjaya, Malaysia; Kenneth Coenegrachts, MD, PhD, Department of Radiology, AZ St.-Jan AV, Ruddershove 10, B-8000 Bruges, Belgium

Maniam S, Szklaruk J. Magnetic resonance imaging: Review of imaging techniques and overview of liver imaging. *World J Radiol* 2010; 2(8): 309-322 Available from: URL: http://www.wjgnet.com/1949-8470/full/v2/i8/309.htm DOI: http://dx.doi.org/10.4329/wjr.v2.i8.309

INTRODUCTION

Magnetic resonance imaging (MRI) of the abdomen has been routinely performed to further characterize indeterminate lesions seen on other cross sectional imaging, such as ultrasound (US) and computed tomography (CT). However, MRI is increasingly used as the principal diagnostic modality, especially for staging and restaging of oncologic patients. With advancement of technology and development of newer imaging techniques, MRI of the abdomen allows for near optimal evaluation of, not only the liver, but also most of the other organs in the abdomen, retroperitoneal structures and even the peritoneum[1].

One of the obstacles to optimal MRI of the abdomen is periodic motion associated with respiratory movement and the historic long examinations. To overcome this limitation, novel imaging techniques, such as parallel imag-

ing (PI), have allowed for shorter breath hold sequences without significant loss in the signal to noise ratio (SNR)[2-4]. Although to a lesser degree than on CT or US, a limitation of liver MRI has been the overlap of imaging features of various disease processes that render them as indeterminate findings. Incorporation of newer imaging techniques (such as PI) and new contrast agents (such as hepatocyte agents) have improved the diagnostic accuracy of MRI, for example, the utilization of diffusion weighted echo planar imaging (EPI), which had been standard practice in neuroimaging. The enhancement pattern at different phases after contrast administration can be crucial for the detection and characterization of liver pathology. The addition of the hepatocyte phase after contrast administration has permitted increased discrimination between liver and non-hepatocyte containing lesions. In this review, we discuss the design of a time-efficient MR protocol and the justification for various sequences and techniques for optimum liver imaging. We present the specific imaging features of selected common focal and diffuse liver diseases utilizing this model MR protocol technique[1].

MRI TECHNIQUES

Axial T1 weighted spoiled gradient echo in-phase and opposed-phase

Historically, T1 weighted imaging (T1WI) of the liver have been obtained with a spin-echo technique. Although this technique provided exquisite SNR and minimum artifacts, the scan time could be considered as prohibitive. Currently, routine T1WI evaluation is obtained with spoiled gradient echo (SPGR) techniques (GE Medical Systems, Milwaukee, WI; fast low-angle shot sequences, Siemens Medical Systems, Erlangen, Germany). The imaging parameters for this sequence with a 1.5T magnet were TE = 4.2 ms and 2.1 ms with TR = 100 ms. For the 3T magnets, a TE of 2.1 ms and 4.2 ms correspond to in-phase (IP) and out-of-phase (OP) imaging, respectively. The slice thickness was 5 mm/0 mm gap. Utilizing a double echo technique, IP and OP images were obtained in one TR. At 1.5T, an echo time of 4.2 ms resulted in a predominantly IP image (water and fat signal are added), with a 2.1 ms echo time, water and fat signal cancel each other resulting in out of phase image. The addition of PI (see discussion on PI below) to the image acquisition parameters resulted in a scan time of 14-18 s, which was short enough for a breath hold in most patients, to cover the entire abdomen[5].

The normal signal of the liver on T1WI is slightly hyperintense to muscle and kidneys. The signal was variable depending on the fat and iron content of the liver. In a fatty liver, the signal of the liver in the IP T1WI is slightly hyperintense. In a liver with high iron content, the signal on the IP T1WI is slightly hypointense.

Axial T2 weighted imaging

The use of fast spin echo (FSE) techniques with a multiple echo train has significantly shortened scan times[6]. However, scan time reduction comes at the expense of the contrast to noise ratio (CNR) and SNR[7]. To minimize mis-registration, a respiratory triggered FSE (RT-FSE) T2 weighted imaging (T2WI) sequence is preferred[8]. A respiratory triggered technique with an echo train length (ETL) of 16-20 provides excellent T2WI. Longer ETL (> 20) may result in loss of CNR between the lesion and liver. A TE of 80-90 ms results in high quality images with an optimal combination of high SNR and CNR[7]. Modification of the echo time to longer TE (150-250 ms) has been used to discriminate between cysts (long T2 relaxation masses) and solid lesions (relatively shorter T2 relaxation masses[9,10].

The T2WI can also be obtained with breath hold techniques. The fast recovery FSE techniques (FRFSE, GE Medical Systems) can provide good breath hold T2WI contrast with improved scan times[8]. This pulse sequence includes recovery of the compulsory longitudinal magnetization. The T2WI (RT-FSE or FRFSE) are obtained with fat-saturation. The fat suppression is achieved with frequency selective techniques.

The imaging parameters for T2 weighted RT-FSE comprise TR = 4000-6000 ms and TE = 85 ms. The number of excitations is 3-4. The slice thickness/gap is 6 mm/0 mm. The imaging parameters for FRFSE were comprised of TE = 85 ms and TR = 2000 ms.

The normal signal of the liver on T2WI is hypointense to the spleen, kidneys, and pancreas. In contrast, most of the liver pathology is hyperintense to the liver parenchyma. This has been very useful since the early days of liver MR.

Diffusion weighted imaging

Neuroimaging has used diffusion weighted imaging (DWI) in the detection and characterization of brain lesions. This has been successfully applied to the evaluation of the liver. The principle is to apply two identical diffusion-sensitizing gradient pulses separated by a 180° refocusing pulse to a T2 weighted sequence. Stationary protons are unaffected by the gradient pulses because the phase shift acquired on the first pulse is reversed by the second pulse with an end result of no phase shift, which means no signal is lost. On the contrary, moving protons acquire a phase shift from the first gradient, which is not completely reversed by the second gradient pulse, which results in signal loss. Diffusion of protons thus is visually perceived as signal attenuation on the diffusion weighted images. EPI is used to obtain the T2WI for DWI. The EPI can be obtained with a breath hold, free-breathing, or respiratory triggered techniques. The respiratory triggered EPI is preferred over breath-hold EPI for SNR reasons. The diffusion gradients are best obtained in three orthogonal planes but, in the liver, adequate images can be obtained with only one axis (z-axis) gradient. DWI of at least two b-values are performed (b = 0 or 500 s/mm^2). The higher b-value image will result in the reduction of signal from moving protons in the bile ducts, cysts, vessels, and fluid in the bowel. This will result in an increased contrast between the lesion and liver. Visual assessment is of value to distin-

guish cystic from solid lesions, however, to distinguish benign and malignant solid lesions is often difficult. Another confounding factor in visual tumor assessment is that the signal intensity of a lesion is dependent on both water proton diffusion and the T2-relaxation time. Thus a lesion may have a high signal on DWI, suggesting diffusion restriction, when in fact it is due to the tissue's intrinsic long T2 relaxation time; a phenomenon called T2 shine-through effect. Since DWI is originally a T2 weighted sequence, the DWI imaging should be interpreted, along with other standard sequences and especially the standard T2 weighted sequences, to avoid this potential error[11-13]. DWI at low b-value (50 s/mm^2) (yes) results in black blood images of the liver that facilitates identification of small focal liver lesions (< 10 mm) from the dark intrahepatic vessels[14].

The imaging parameters for the DWI EPI using a breath hold technique and PI with multi-channel phased array coil are: TR/TE (1200-1800 s/50-60 s); FOV (38-44 cm); matrix (200 × 160); number of excitations (NEX-6); slice thickness (7 mm/0 mm); two acquisitions obtained for b-values of 0 and 500 s/mm^2 with a scan time of 21 s.

The normal signal of the liver on DWI is the same as on other T2WI. The liver is hypointense to the kidneys and pancreas.

Parallel imaging

PI is an accelerated imaging technique that combines available MRI methods and newly developed multi-channel phased array coils to significantly reduce scanning time. In PI techniques, under sampled k-space, data in the phase encoding direction are acquired to shorten scanning time. These incomplete data are supplemented by the spatial information encoded by the multi-channeled phase array surface coils to complete the MRI. Theoretically, the maximum acceleration factor is limited by the number of coil elements. Practically, the acceleration factor is currently limited by a factor of 2 to 4, which results in high quality images[14].

Different parallel reconstruction algorithms, such as ASSET (GEMS), SENSE (Phillips), and SMASH (Siemens), are used to generate unaliased final images[5,15]. The PI technique improves breath hold imaging by eliminating periodic respiratory motion artifacts due to fast imaging with subsequent increased spatial resolution. Acceleration factors of 2 to 3 are commonly used. The important limiting factor of PI is loss of SNR with improving resolution[16].

Dynamic axial T1 weighted FSPGR LAVA contrast enhanced imaging

Dynamic contrast enhanced (DCE)-MRI of the liver is a vital part of the liver imaging protocol due to its greater diagnostic accuracy. Given the distinctive liver physiology and its dual blood supply, dynamic enhancement patterns for a particular disease on the different phases of liver enhancement can narrow the differential diagnosis.

Images are acquired in three phases following contrast administration: a predominant arterial (or late arterial) phase, portal phase, and a delayed (equilibrium) phase. The first phase is the most time sensitive phase. The timing for the portal venous and delayed phases is less critical. To optimize the capture of this first phase of enhancement, novel techniques have been developed.

For example, a less preferred method uses a standard delay of 20 s following the administration of contrast. This method does not compensate for cardiac output or other physiologic delays. A second method is to do a timing bolus. This is performed with a small amount (1-2 mL) that is injected while a single slice of the abdomen is monitored during the entire injection to determine the appropriate delay time for the contrast to arrive to the liver. The main limitations are longer scans and the introduction of contrast prior to the complete exam. A third method is to obtain two consecutive arterial phases following contrast administration after a preset short delay[17]. This requires a decrease in spatial resolution to shorten the scan time[18]. Finally, fluoro-triggered images provide an alternative method to visualize the contrast injection and set a short delay after the visualization of contrast in the aorta or pulmonary arteries.

To calculate the optimum delay in these methods, it is important to have knowledge of the k-space filling method of the MR software. A platform with the first echo at the center of k-space will be at a different stage of enhancement compared to a method where the center of k-space is obtained in the middle of the acquisition[18,19]. The image contrast relies mainly on data acquired near the center of the k-space, while the image edge sharpness depends on data from the periphery of the k-space. The development of a new method of imaging, such as the key-hole method, allows for merging of high frequency k-space data from a reference image acquired with a reduced matrix. This data merging method combines the spatial resolution of full matrix images and the temporal resolution of a set of rapidly acquired, reduced matrix images. The key-hole method thus yields images with high temporal resolution without significantly compromised spatial resolution[20-22].

DCE-MRI of the liver is performed using a 3D axial T1 weighted fast SPGR LAVA (GEMS) sequence with the following parameters: TE > 1.5 ms; FOV (34-44 cm), matrix [320 × (160-192)], slice thickness (4-5 mm), Zerofill interpolation processing 2 breath-hold technique with PI used during triphasic acquisition of the entire abdomen after contrast infusion at late arterial, portal venous, and delayed phase of contrast administration.

Hepatocyte specific gadolinium based contrast agent (Gd-EOB-DTPA)

Gd-EOB-DTPA (known as Eovist, Primovist and EOB-Primovist, Bayer Pharmaceuticals) is a paramagnetic, highly water soluble, hydrophilic compound that has a lipophilic moiety, called an ethoxybenzyl group, covalently linked to the Gd-DTPA to form Gd-EOB-DTPA. Gd-EOB-DTPA is selectively taken up by hepatocytes *via* an anionic transporter protein, which makes it the first tissue specific gadolinium based contrast agent (GBCA). It is eliminated unchanged *via* two routes in equal quantities: one route

is *via* biliary excretion of contrast selectively taken up by hepatocytes and the other route is *via* urinary excretion of contrast after glomerular filtration in the kidney[23]. The recommended dose of Gd-EOB-DTPA is 0.025 mmol/kg of body weight, which is about one quarter of the standard dose of nonspecific GBCA. The relaxivity of Gd-EOB-DTPA is comparable to most nonspecific GBCA due to non covalent weak transient binding with serum albumin[3,22,23].

Gd-EOB-DTPA combines both features of extracellular contrast agent and hepatocyte specific contrast, which allows for DCE imaging due to its extracellular function and delayed static hepatobiliary imaging due to its hepatocyte specific function[20]. Therefore, in addition to tumor characterization based on perfusion in the dynamic phase, Gd-EOB-DTPA offers concurrent assessment during the hepatocyte phase for the presence of intralesional functioning hepatocytes[24]. The selective uptake by hepatocytes increases lesion to liver contrast particularly in the hepatocyte phase, which is not attainable with nonspecific GBCA. The peak liver enhancement using Gd-EOB-DTPA is best observed after 20 min[23]. A time delay of 20 min for the hepatocyte phase is a widely accepted duration and has been part of liver imaging protocols using Gd-EOB-DTPA. To shorten the overall examination time, a new suggestion of a shorter delay of 10 min for the hepatocyte phase with sufficient liver enhancement has been made in patients with normal liver function[20]. In patients with chronic liver disease, where suppressed and delayed liver enhancement in the hepatocyte phase is routinely observed, a 20 min delay for hepatocyte imaging is compulsory[20,23]. Another recommendation to reduce the total examination time is to acquire T2 weighted sequences (FSE, FRFSE, and DWI) after contrast administration[23].

COMMON FOCAL LIVER LESIONS

Simple liver cysts

Simple liver cysts are common benign livers lesions that are developmental in origin. They are usually incidental findings that do not require further workup[10]. At MR imaging, liver cysts are hypointense on T1WI and hyperintense on T2WI. They do not show enhancement at dynamic imaging or uptake of contrast in the hepatocyte phase. Most liver cysts, including sub centimeter cysts, usually can be diagnosed based on typical MRI features (Figure 1). However, when contraindicated, further characterization with non-contrast MRI is still possible. On T2WI, cysts tend to remain hyperintense or become more hyperintense than surrounding liver parenchyma at longer TE > 250 ms[10]. At DWI, cysts usually have high signal at b = 0 with signal attenuation at higher b-values. Unfortunately, due to the T2 shine through effect, cysts can remain hyperintense at higher b-values[25]. In this setting, an apparent diffusion coefficient (ADC) map will be very useful. For a simple cyst, an ADC of $2.61 \times 10^{-3}/mm^2$ per second will suggest a cyst *vs* a mean ADC of $1.31 \times 10^{-3}/mm^2$ per second for hepatomas[12,26]. Even though the use of ADC values has been proven to be useful, there still is significant overlap between different types of focal liver lesions.

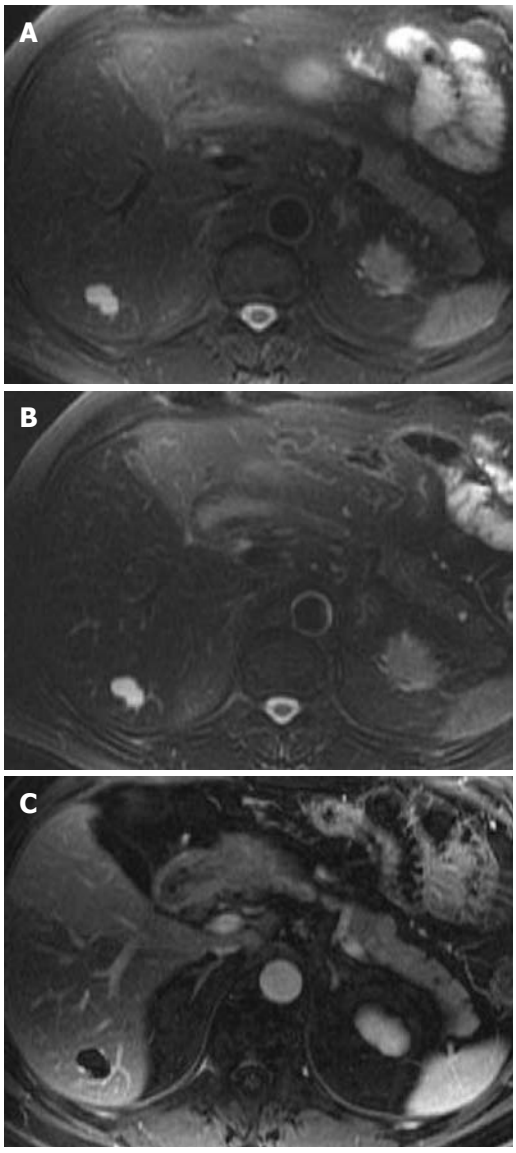

Figure 1 A 51-year-old male with colorectal cancer and liver cysts. A, B: The short (A, TE = 85 ms) and long (B, TE = 160 ms) respiratory triggered fast spin echo T2 weighted imaging demonstrates a stable contrast to noise ratio of lesion to liver; C: The post-gadolinium image shows no enhancement.

Hemangiomas

Hemangiomas are the most common solid benign liver lesions and are typically asymptomatic. At MR imaging, hemangiomas are classically hypointense on TIWI and hyperintense on T2WI. On T2WI with a longer echo time (TE = 140 ms), hemangiomas, like cysts, will remain hyperintense relative to the liver[27]. The CNR will not suffer as much with cysts and hemangiomas compared to other masses (Figure 2). On DWI, similar to cysts, hemangiomas will have high signal at b = 0 with a lesser degree of signal attenuation at higher b-values in the absence of the T2 shine through effect[27]. For hemangiomas, the mean ADC of $1.84 \times 10^{-3}/mm^2$ per second is between that of cysts and the ADC for hepatomas[12,26]. There is some

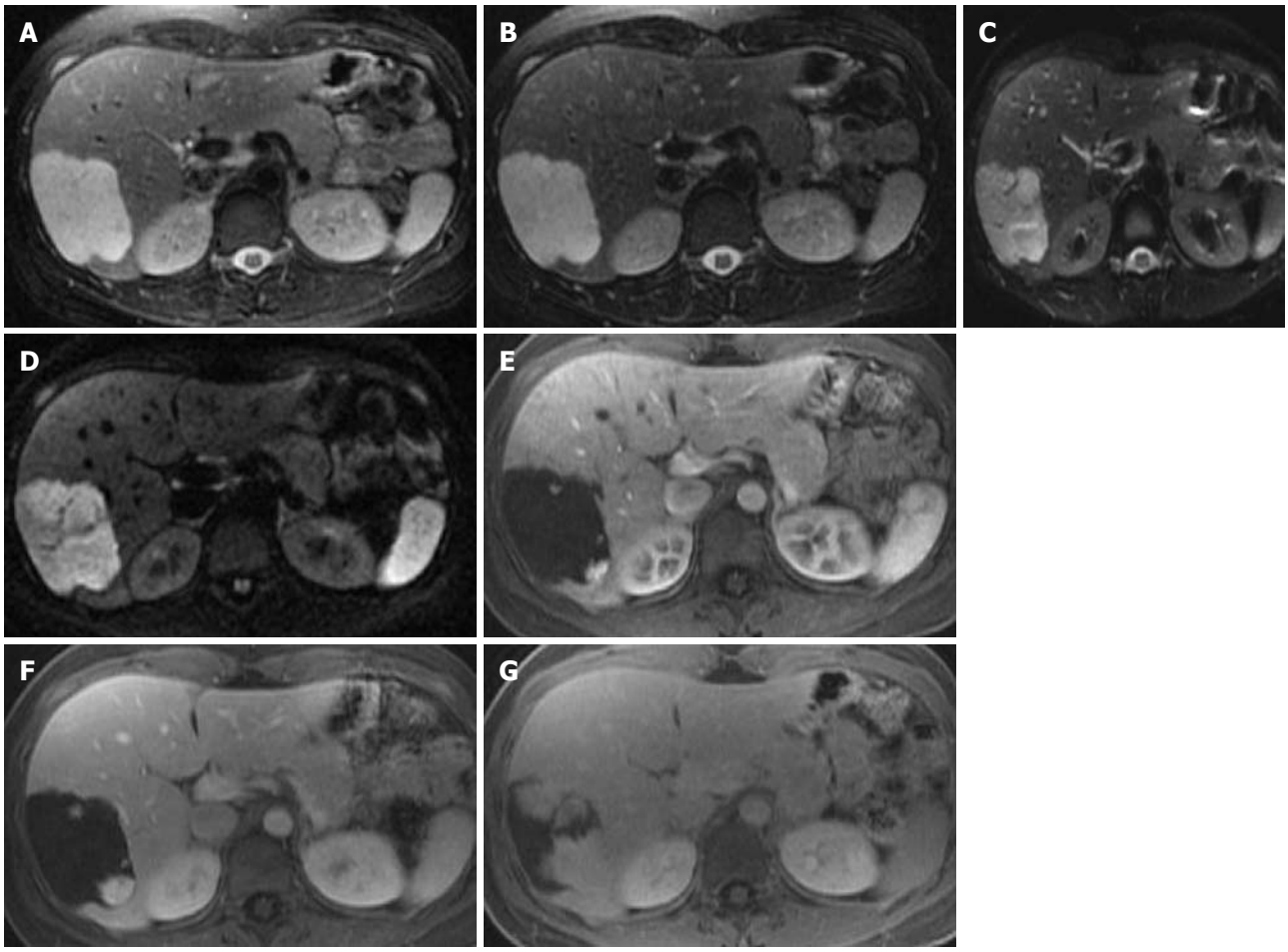

Figure 2 A 21-year-old female with right upper quadrant pain with a hemangioma. A, B: The short (A, TE = 85 ms) and long (B, TE = 160 ms) respiratory triggered fast spin echo T2 weighted imaging demonstrates a stable contrast to noise ratio of lesion to liver; C, D: The diffusion weighted imaging (C, b = 0, and D, b = 500) demonstrates high signal intensity of the hemangioma; E-G: The multiphasic post-Gd images demonstrate peripheral interrupted nodular enhancement with delayed fill-in, in the late arterial (E), portal venous (F), and excretory phase (G) of post-Gd images.

overlap between the ADC value of malignant lesions and hemangiomas[12,26].

Post-Gd imaging features of hemangiomas on DCE-MRI depend on their size. Three distinct dynamic enhancement patterns have been described. Pattern 1 is seen in small capillary hemangiomas < 1.5 cm and is typified by homogenous enhancement in early arterial enhancement with persistent enhancement on subsequent phases. Pattern 2 is seen in hemangiomas > 1.5 cm and is typified by classic peripheral nodular discontinuous enhancement in the arterial and portal phases with persistent enhancement peripherally with possible complete fill in on the delayed images (Figure 2). The second pattern is the most common and classic enhancement pattern of hemangiomas. Pattern 3 is seen in giant hemangiomas > 6 cm and is typified by peripheral nodular interrupted enhancement with gradual partial filling in on the arterial and portal phases but with a persistent hypointense center on delayed images. At the hepatocyte phase, no contrast is taken up by hemangiomas[27]. This can be challenging in the setting of hemangiomas and liver metastases, where both lesions will appear hypointense on the hepatocyte phase of contrast administration.

Focal nodular hyperplasia

Focal nodular hyperplasia (FNH) is the second most common benign liver lesion after hemangioma. They are thought to be a hyperplastic reaction to a congenital or acquired vascular malformation. On histopathology, they contain normal hepatocytes with malformed biliary tracts. They tend to be hypervascular lesions that often are incidental findings and are asymptomatic. FNH are grouped into two subtypes based on histology-classic (80%) and nonclassic (20%). At MR imaging, the classic imaging features on standard sequences are isointense on T1WI and T2WI with well formed central scars that are hyperintense on T2WI and are hypointense T1WI[4,28]. At DWI, they have variable signal intensity[29]. At DCE-MRI, they show intense enhancement in the arterial phase that returns to isointense to surrounding liver parenchyma in subsequent phases. The central scar has characteristic enhancement on the delayed images (Figure 3). The nonclassic type tends to lack the central scar, therefore, these FNH are isointense on T1WI and T2WI and show intense arterial enhancement on DCE-MRI that become isointense to background liver on subsequent phases[5,28]. One of the most common indications of liver MRI is to characterize

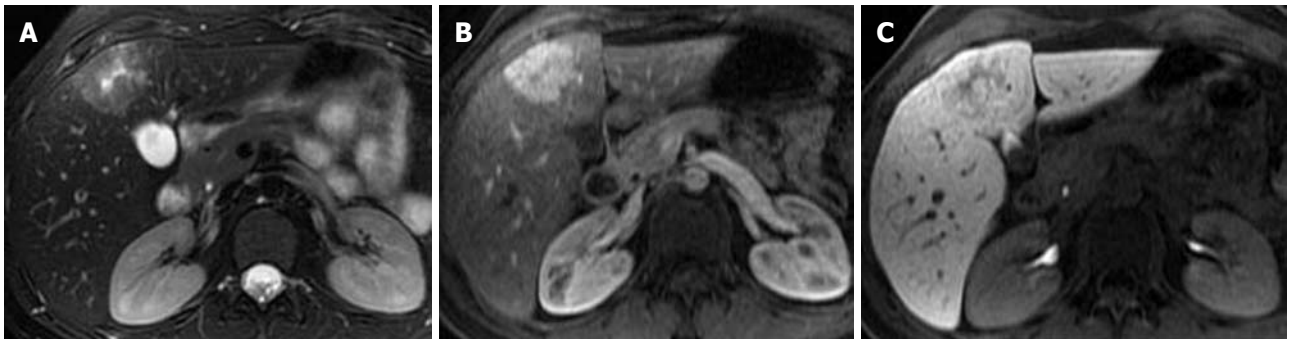

Figure 3 A 22-year-old female with an focal nodular hyperplasia in the liver. A: Respiratory triggered fast spin echo T2 weighted imaging at TE = 85 ms. This demonstrates a high signal in the center of the lesion; B: The late arterial phase of contrast administration shows hyperintense enhancement; C: The hepatocyte phase of contrast administration shows hepatocyte contrast uptake.

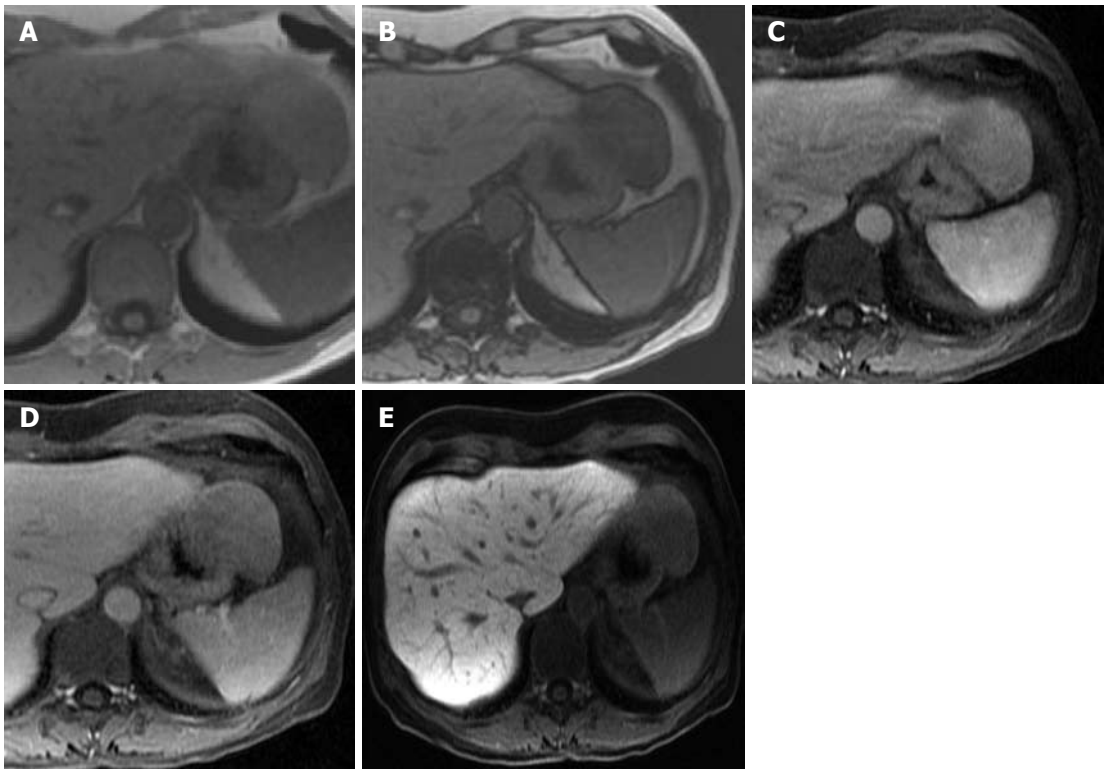

Figure 4 A 58-year-old female with a hepatic adenoma. A, B: In phase (A) and out-of-phase (B) T1 weighted imaging shows a signal drop in the adenoma on the out-of-phase image; C, D: Late arterial and delayed phase imaging demonstrates early enhancement (C) and delayed washout (D); E: The hepatocyte phase of contrast administration does not show uptake.

hypervascular lesions on CT or MRI that may represent an FNH. Hepatocyte agents are useful in this application of liver imaging. Given its hepatocellular origin, most FNH will appear isointense to hyperintense relative to surrounding liver at the hepatocyte phase (Figure 3). This is due to retention of contrast in dysfunctional bile ducts with poor drainage within the FNH[19].

Adenoma

Adenomas are rare benign liver neoplasms that occur commonly in women who are on oral contraceptives and with increased incidence in glycogen storage disease and with anabolic steroid use. Adenomas are usually symptomatic, however, they can be complicated by intralesional hemorrhage, rupture and rarely malignant transformation. Histopathologically, adenoma consists of hepatocytes arranged in plates that are separated by dilated sinusoids. A fibrous capsule or pseudocapsule consisting of compressed liver parenchyma is usually present. Portal triad and bile ducts are absent with minimal to complete absence of Kupffer cells. They contain variable amounts of glycogen and lipids[28]. At MR imaging, adenomas demonstrate variable signal intensity depending on lipid content and presence of hemorrhage. At T1WI, adenomas can be isointense to hyperintense due to lipid content or hemorrhage. High signals from lipid content drop out at T1WI OP imaging (Figure 4), while high signals from hemorrhage persist. They have variable signal intensity at T2WI and DWI. At

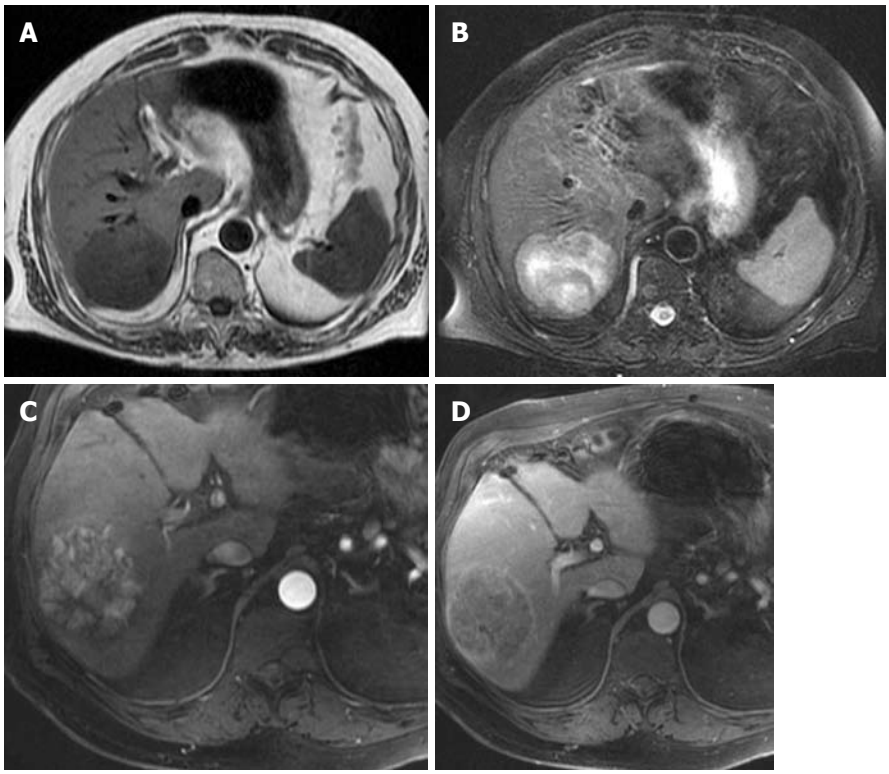

Figure 5 A 65-year-old male with hepatocellular carcinoma. A: T1 weighted imaging in phase image shows a hypointense mass in the right lobe of the liver; B: T2 weighted imaging (TE = 85 ms) shows a hyperintense mass in the right lobe of the liver; C, D: Late arterial (C) and excretory phase (D) shows a hypervascular mass in the liver that demonstrates an enhancing capsule on the delayed images.

DCE-MRI, they can have heterogeneous early enhancement during the arterial phase with variable degrees of washout on the venous and delayed phases (Figure 4). A peripheral delayed enhancement of the pseudocapsule can be seen. At the hepatocyte phase, even though an adenoma takes up minimal to moderate amounts of contrast relative to the surrounding liver, the adenoma will commonly appear hypointense due to the absence of biliary ducts resulting in no contrast being excreted or accumulated prior to drainage[19].

Hepatocellular carcinoma

Hepatocellular carcinoma (HCC) is the most common primary liver malignancy. HCC most commonly develops in the background of chronic liver disease, ending in cirrhosis due to various etiologies including viral hepatitis, alcohol, hematochromatosis and Wilson's disease. HCC typically develops in a stepwise manner that begins with regenerative nodules (RN) (non-premalignant), to dysplastic nodules (DN, pre-malignant), to DN with HCC, to HCC. HCCs can be solitary (50%), multifocal (40%) or diffuse (less than 10%)[30]. MRI plays an important role in differentiating these non malignant nodules from HCC[31-33]. At MR imaging, HCCs have variable appearances but usually they are hypointense on T1WI and mild to moderately hyperintense on T2WI. Smaller HCCs (< 2.0 cm) are frequently isointense on both T1WI and T2WI[30,34]. At DCE-MRI, HCCs demonstrate classic intense early arterial enhancement that washes out in the equilibrium phase (Figure 5). The majority of HCCs have a capsule consisting of compressed liver parenchyma that usually enhances on the delayed images. Some DN can mimic HCCs with intense early arterial enhancement, however, they do not show the typical washout in the equilibrium phase or increased signal on T2WI. The hepatocyte phase has been evaluated in the setting of HCC. Most hepatomas are hypointense to liver in this phase of contrast administration. This is a function of organic anion transport function rather than stage of tumor differentiation[30,34,35].

Intrahepatic cholangiocarcinoma

Intrahepatic cholangiocarcinoma (IHCC) is the second most common primary liver malignancy, after HCC. IHCCs are part of a spectrum of cholangiocarcinoma tumors of the biliary epithelium. Cholangiocarcinoma tumors are classified based on the site of origin: intrahepatic, gallbladder, or extrahepatic biliary cancers. At MR imaging, IHCC is iso- to hypointense on T1WI and mild to marked hyperintense on T2WI (Figure 6). Appearance on T2WI and DWI can vary depending on its content: amount of fibrous content (predominant central hypointensity) and mucin content (hyperintense). On the DWI, IHCC that exhibits restrictive diffusion will have no signal drop on high b-value imaging. At DCE-MRI, IHCC demonstrates incomplete arterial enhancement (Figure 6). On delayed images, mild progressive enhancement is usually observed[3,30,36]. During the hepatocyte phase of contrast administration, IHCCs are hypointense to liver (Figure 7).

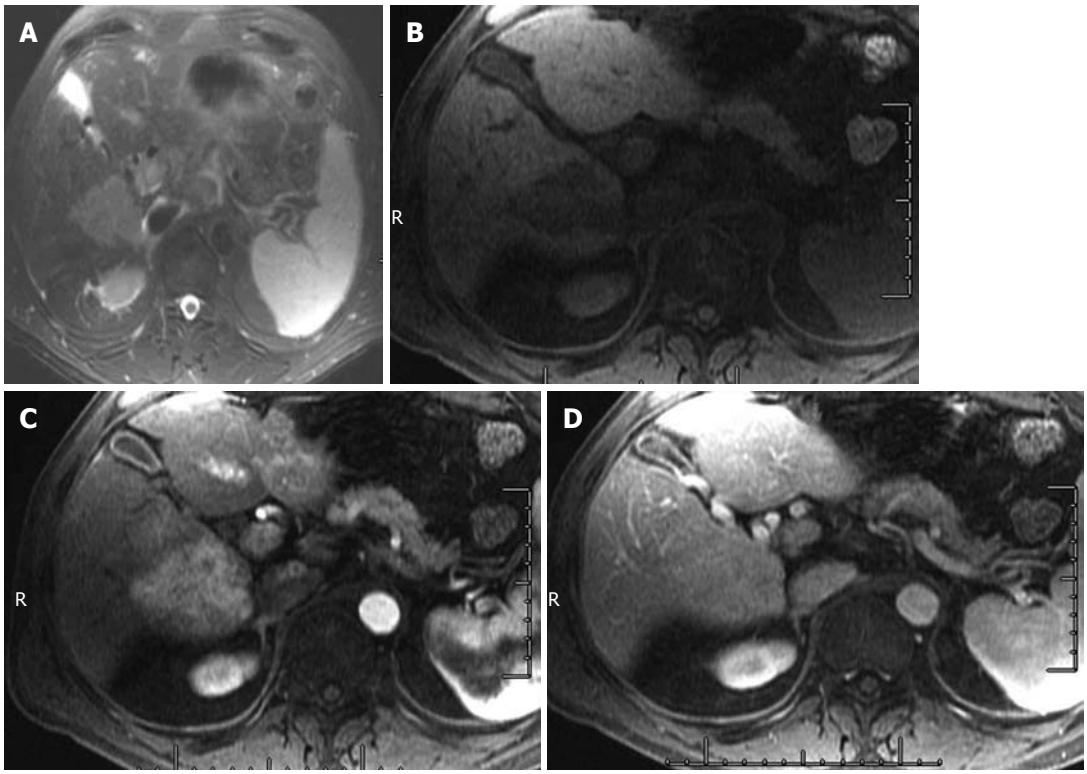

Figure 6 A 62-year-old male with intrahepatic cholangiocarcinoma. A: Short TE (85 ms) T2 weighted imaging shows a hyperintense mass in the right lobe of the liver; B-D: Pre-contrast (B) late arterial (C), and 5 min delayed images (D) of the abdomen shows delayed enhancement.

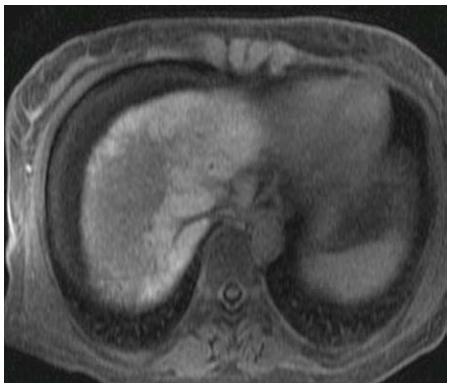

Figure 7 A 54-year-old female with intrahepatic cholangiocarcinoma. The hepatocyte phase of contrast administration shows no uptake of contrast.

Liver metastases

Metastases are the most common malignant liver lesions, with colorectal cancer as the most common primary malignancy. All metastatic liver lesions, with the exception of highly cystic or necrotic lesions, have variable degrees of vascularity and can be classified into hypovascular and hypervascular metastases. This refers to the vascularity of the lesions relative to the vascularity of surrounding liver parenchyma[24,27].

Hypervascular liver metastases

Metastases that are considered hypervascular typically arise from thyroid carcinoma, carcinoid tumor, neuroendocrine tumor, renal cell carcinoma, choriocarcinoma, melanoma and sarcomas. At MR imaging, these metastases generally have variable appearances on both T1WI and T2WI. On T1WI, metastases are usually mildly to moderately hypointense relative to liver parenchyma. Some intralesional substances such as hemorrhage, melanin, fat and protein can cause shortening of T1 relaxation times resulting in hyperintense metastatic lesions on T1WI. On T2WI, liver metastases are hyperintense relative to liver but generally less hyperintense than cysts and hemangioma. The difference in CNR between the metastases and these benign lesions can be highlighted on longer TE where signal attenuation is observed with metastases and hyperintensity accentuation is observed with cysts and hemangioma. However, a subset of metastases that include neuroendocrine tumors, sarcomas and melanoma can appear cystic and markedly hyperintense on T2WI without signal attenuation at longer TE, thus mimicking simple cysts and hemangioma[27,37]. At DWI, these cystic metastases are usually hyperintense on low b-values with variable degrees of signal attenuation at high b-values. On the contrary, solid metastatic lesions will remain hyperintense at high b-values due to restrictive diffusion (Figure 8)[38,39]. Dynamic enhancement patterns also play a critical role in distinguishing these lesions.

Variable early arterial enhancement at the DCE-MRI has been observed that includes peripheral ring and homogenous and heterogeneous enhancement. The peripheral ring pattern is the most commonly described enhancement pattern. Homogenous arterial enhancement is usually seen in smaller hypervascular metastases (< 1.5 cm). Heterogeneous enhancement can be seen in lesions larger than

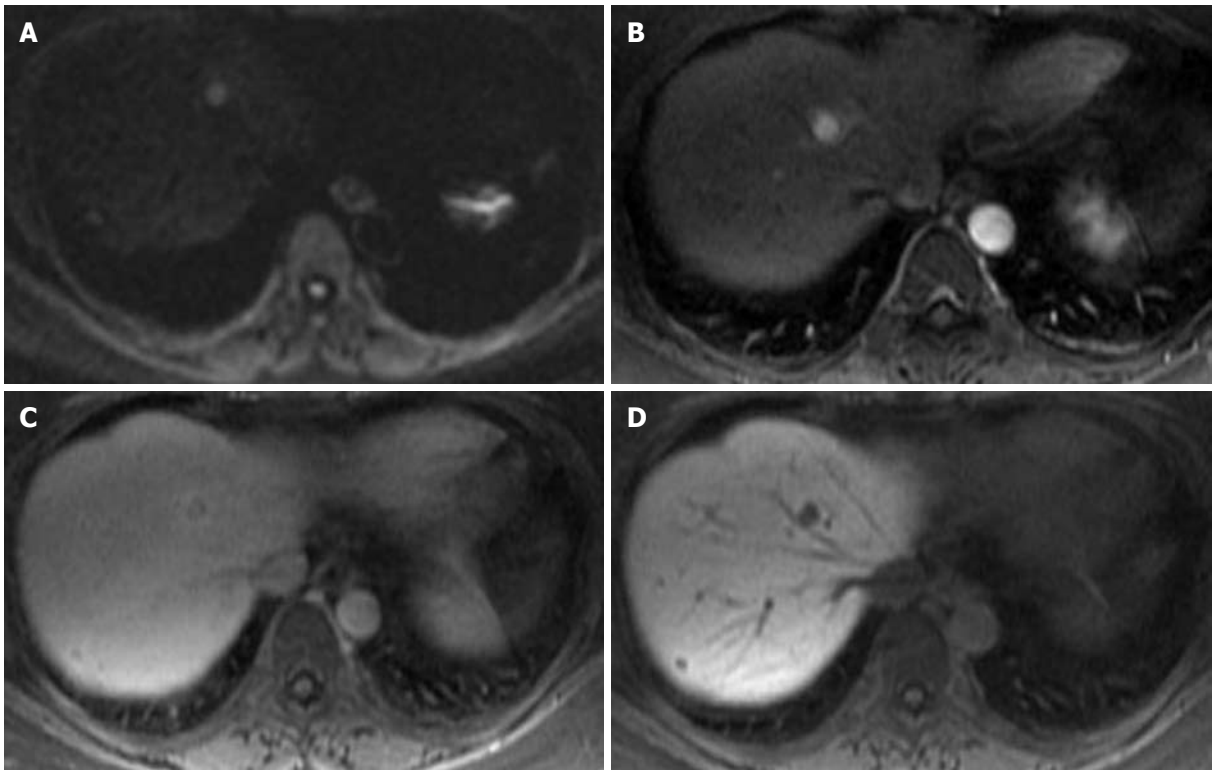

Figure 8 A 51-year-old female with metastatic liver lesions from a pancreatic primary. A: The diffusion weighted imaging at b = 500 shows two hyperintense nodules in the liver, in keeping with solid lesions; B, C: The late arterial phase (B) shows hypervascular masses that washout on the excretory phase (C) of contrast administration; D: The hepatocyte phase shows low signal lesions in the right lobe of the liver, corresponding to liver metastases.

3 cm that are complicated by intralesional hemorrhage, necrosis and fibrotic tissue formation. On the delayed images, most hypervascular metastases demonstrate incomplete enhancement due to poor central vascularity with simultaneous peripheral washout. The peripheral washout observed on the delayed images is considered specific for liver malignancies that include metastases and HCC (Figure 8). Hepatocyte contrast agent provides increased conspicuity on the 20 min hepatocyte phase images, while liver metastases do not take up contrast (Figure 8)[30]. In some series, there are reports of increased lesion detection that affected decision making and the clinical approach to the patient.

Hypovascular liver metastases

Metastases that are considered hypovascular are most commonly from colon carcinoma. Other less common primary lesions include: bladder carcinoma, prostate carcinoma, and pulmonary carcinoma[40]. At MR imaging, hypovascular metastases have variable appearances on both T1WI and T2WI, which are commonly mild to moderately hypointense on T1WI and hyperintense on T2WI, with variability in signal intensity due to the presence of intralesional substances. At DCE MRI, hypovascular metastases generally demonstrate variable enhancement in the arterial phase with the most common pattern being peripheral complete ring enhancement (Figure 9). Hypovascular metastases generally demonstrate a lesser degree of enhancement relative to the surrounding liver parenchyma. Occasionally, transient perilesional circumferential or wedge-shaped enhancements are seen in the arterial phase, most commonly with colorectal metastases[3,27,40]. Hypovascular metastases are conspicuous on the portal venous phase as hypointense lesions relative to the liver[27]. On the excretory phase, peripheral washout is commonly observed (Figure 9)[40]. The hepatocyte agents provide high CNR and sensitivity for liver metastasis at 20 min[30]. In this phase, these masses will appear hypointense to liver.

Arterially enhancing nodules

Liver lesions are typically classified as hypervascular and hypovascular based on their enhancement pattern on the arterial phase of DCE-MRI. The arterial phase is highly sensitive in detecting hypervascular lesions but may have a low specificity in lesion characterization. The arterial enhancing nodule (AEN) can be true masses with mass effect and rounded/lobulated shapes. These are seen only during the arterial phase of contrast administration. AEN can also be pseudolesions that mimic masses without a mass effect. To confidently distinguish between benign and malignant processes and possibly arrive at a correct diagnosis, the AEN enhancement characteristics should be evaluated in conjunction with other MRI imaging features[41].

Differential diagnoses of benign AEN include hepatocellular adenoma, FNH, hemangiomas, transient hepatic intensity differences, and arteriovenous shunts/perfusion anomalies. The differential diagnosis includes malignant processes such as HCC and hypervascular me-

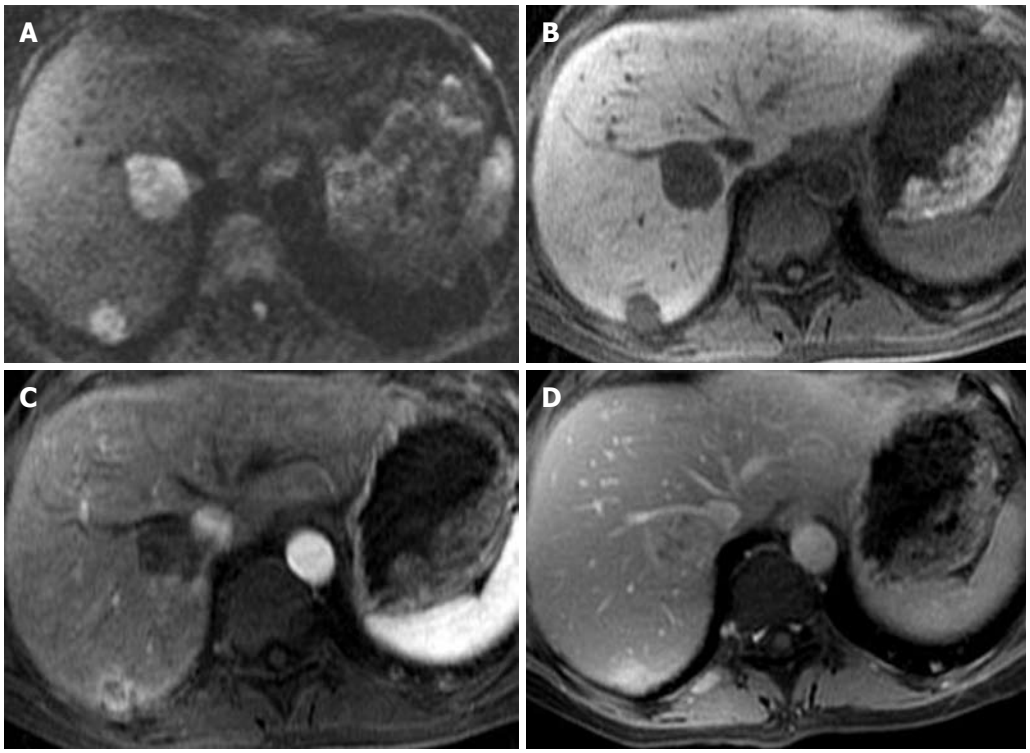

Figure 9 A 64-year-old with liver metastases from a primary sarcoma. A: The diffusion weighted imaging at b = 500 shows two solid lesions in the right lobe of the liver; B-D: The pre-contrast (B), late arterial (C), and delayed phase (D) show late enhancement. The enhancement pattern is similar to intrahepatic cholangiocarcinoma.

tastasis[42]. Even in the setting of a cirrhotic liver, these lesions are more likely to be benign in nature[10,41-43]. Imaging features that suggest a malignant process include hyperintense signal on the T2WI and washout on the delayed phase of contrast administration. A smaller lesion (< 5 mm) should be monitored at least at 6 mo intervals, whereas a larger lesion (> 1 cm) should be monitored every 3 mo for interval size change or signal changes on the T2WI.

DIFFUSE LIVER DISEASE

Fatty liver disease

In the United States, fatty liver disease (FLD) is the leading cause of chronic liver disease in the adult and pediatric populations[44]. Two conditions commonly associated with FLD are alcoholic abuse and non alcoholic FLD (NAFLD)[45]. NAFLD is expected to surpass chronic hepatitis C as the number one indication for liver transplantation[25]. NAFLD is closely linked to metabolic syndromes that encompass constellations of metabolic abnormalities that include type II diabetes mellitus, obesity, hyperlipidemia, and insulin resistance[6,25]. Other conditions that can result in NAFLD include drug toxicity (such as amiodarone, tamoxifen and antiretrovirals), viral hepatitis, radiation therapy, and storage disease such as glycogen storage disorder. Patterns of fatty deposition in FLD is commonly diffuse deposition, and less commonly focal fat deposition in normal liver and diffuse fat deposition with focal sparing. NAFLD comprises a spectrum of liver pathologies that range from simple steatosis to nonalcoholic steatohepatitis that may further progress to fibrosis and cirrhosis with resultant increased risk for HCC development and liver failure[25,46]. Histopathologic hallmarks of simple steatosis that represents 80%-90% of NAFLD cases is fat accumulation within the liver cells. The current standard of reference for detection and disease severity of FLD assessment is liver biopsy, which is invasive, costly and is associated with complications and high sampling error due to heterogeneous fat distribution that can be seen with FLD. Noninvasive repeat evaluation of fatty liver for monitoring of treatment response is often desired.

At MR imaging, areas of fat deposition in the liver appear isointense or hyperintense to the liver on the IP T1WI. On the opposed-phase T1WI, these areas demonstrate signal loss (Figure 10). Diffuse liver steatosis will demonstrate diffuse heterogeneous, or more commonly homogenous signal loss, on the opposed phase. Wedged shaped, geographic or nodular morphology of focal FLD allows for distinction from fat containing tumors, such as HCC, adenoma, angiomyolipoma or lipoma. At DCE MRI, focal FLD will not demonstrate a mass effect on adjacent vessels or biliary tract, or changes in CNR relative to liver[47]. Patchy enhancement of the liver parenchyma, sometimes seen on the arterial phase, that becomes isointense to surrounding liver parenchyma at delayed imaging are considered indicators of areas with necro-inflammatory activity[48]. It is important to note that accumulation of iron (patients with hemochromatosis) or glycogen (patients with glycogen storage disease) in the liver cells can alter signal intensity or signal loss of fatty liver in patients with concomitant FLD[44].

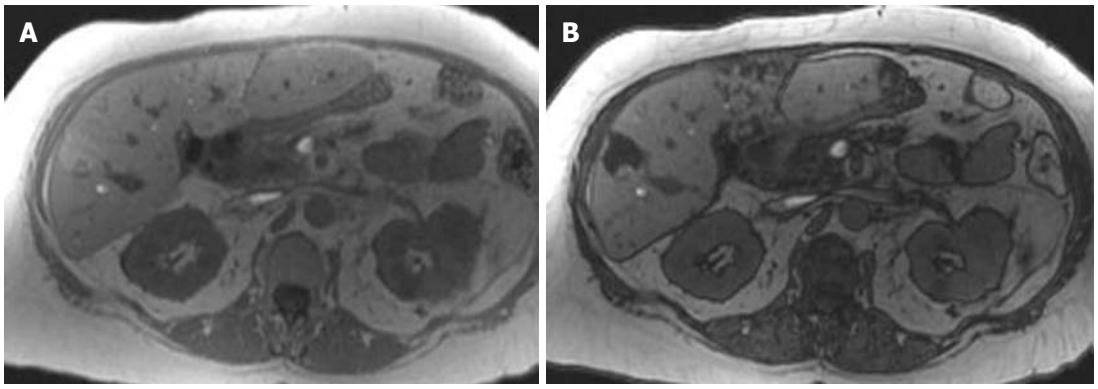

Figure 10 A 57-year-old female with breast cancer with focal fat deposition in the liver. The in-phase (A) and out-of-phase (B) images show a signal drop of the area in segment Ⅴ of the liver.

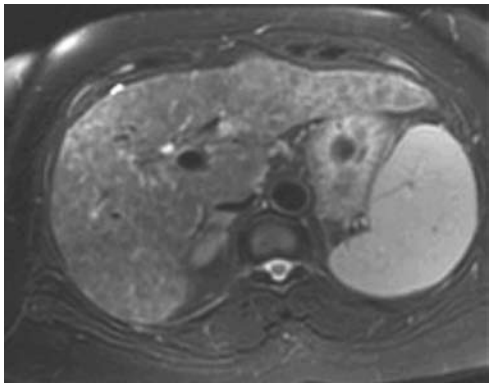

Figure 11 A 57-year-old female with hepatocellular carcinoma and liver cirrhosis. The T2 weighted imaging shows enlargement of the lateral segment of the left lobe of the liver and caudate lobe. There is a nodular contour of the liver. All these findings are in keeping with cirrhosis. The spleen is enlarged in keeping with portal hypertension.

Cirrhosis

Hepatic fibrosis is a dynamic process that is usually induced by a nonspecific inflammatory response of hepatocytes to hepatocellular injury (hepatitis) due to numerous etiologies such as hepatitis viruses (B and C), alcohol abuse, autoimmune disease, drug toxicity, radiation therapy and metabolic disorders such as NAFLD and hemochromatosis[19,49-52]. Cirrhosis progresses from chronic hepatitis to early cirrhosis to advanced cirrhosis, which are initially compensated, and later progresses to decompensated cirrhosis to finally end-stage cirrhosis.

The morphological changes seen on imaging in a patient with cirrhosis include a nodular liver and enlargement of the left lobe and caudate lobe (Figure 11). A right hepatic notch and enlarged gallbladder fossa have been described in patients with cirrhosis[19,49-52].

Extrahepatic findings associated with decompensated cirrhosis are mainly features associated with portal hypertension that include splenomegaly (Figure 11), ascites, portosystemic collateral vessels and nonspecific periportal and portocaval lymphadenopathy (greater than 1 cm in the short axis). Findings related to hepatocellular dysfunction with resultant metabolic abnormality, causing small bowel edema and gallbladder wall thickening, are also observed. Spleen size greater than 13 cm in cephalocaudal indicates splenomegaly. The presences of 3-8 mm hemosiderin containing nodules called Gamna-Gandy are indirect signs of portal hypertension. These nodules result from hypertensive bleeding in the splenic follicles[10,48].

The current standard of reference for the diagnosis of cirrhosis is liver biopsy, which has its inherent limitations due to sampling error and post procedural complications. MRI has emerged as a relatively safer, inexpensive and comprehensive alternative method for the detection and evaluation of cirrhosis[53]. At MRI, liver fibrosis demonstrates imaging patterns that range from an absent distinct pattern, reticular, confluent or both reticular and confluent patterns[48]. The fibrous septa and bridges in cirrhosis appear as hypointense on T1WI and hyperintense on T2W1. These signal characteristics are due to inflammatory changes, vascular dilation and and/or development of pseudobile ducts. The RN typically appear intermediate to hyperintense on T1WI and intermediate to hypointense on T2WI. Some of these RNs accumulate iron (called siderotic nodules) and will appear strikingly hypointense on T2- and T2WI. There also RNs that accumulate fat (called steatotic nodules) and tend to show signal loss on the OP images. It is worth noting that the fibrous septa and bridges lack iron or fat in either the patients with iron or fat deposition because both diseases are an intracellular deposition phenomenon[38,40,49]. At DCE-MRI with nonspecific GBCA, liver fibrosis demonstrates no significant enhancement in the arterial and early venous phases. Delayed progressive enhancement with peaks in the late venous and equilibrium phases is typically observed. This delayed enhancement pattern can be explained by the characteristic accumulation of nonspecific GDBA in the extracellular spaces that are abundant in the fibrous tissues. In contrast to reticular fibrosis that is linear reticulations surrounding RNs, confluent fibrosis is thicker fibrotic scars up to several centimeters thick with masslike configurations. Confluent fibrosis has signal intensity and an enhancement pattern similar to reticular type liver fibrosis. Occasionally, arterial enhancement is seen with confluent and reticular type fibrosis that can be differentiated from other

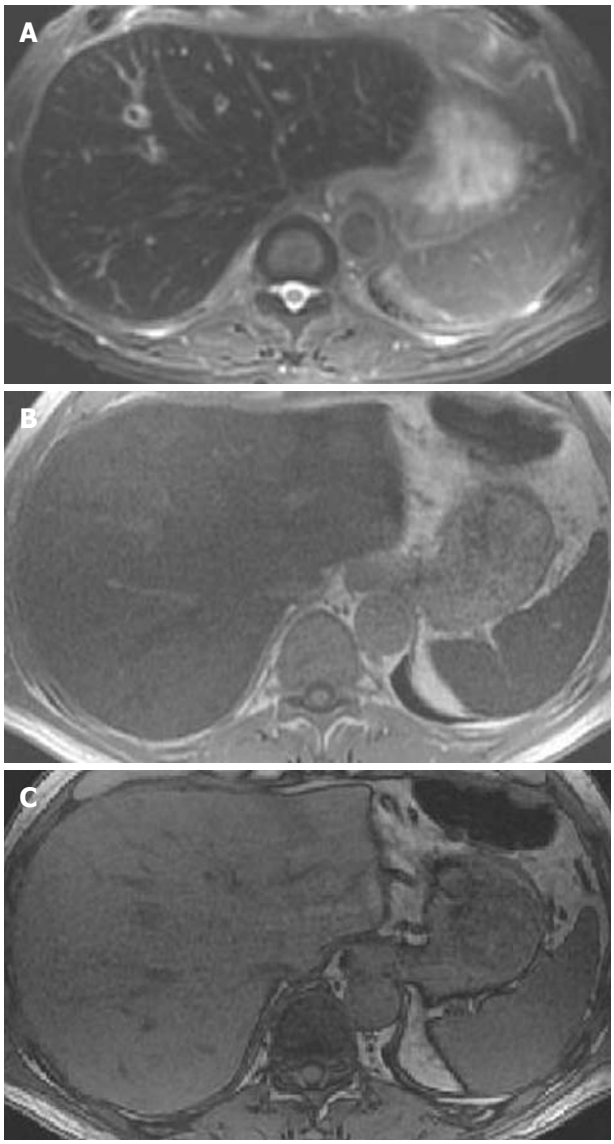

Figure 12 A 64-year-old male with a pancreatic mass and iron deposition in the liver. A: Respiratory triggered fast spin echo T2 weighted imaging image of the liver shows a darker liver relative to the muscles; B, C: In phase (B) and out-of-phase (C) T1 weighted imaging shows a signal drop on the former in keeping with iron deposition.

focal liver tumors based on the characteristic morphology and persistent enhancement on subsequent phases. At the hepatocyte phase, liver fibrosis has no contrast uptake and therefore will appear hypointense[48,49].

Hemochromatosis

Hemochromatosis can be categorized into primary or secondary disorders based on the causes. This disease results in increased intestinal iron absorption with normal dietary iron intake. The excess iron in primary hemochromatosis is deposited in parenchymal cells in organs such as liver, pancreas, heart, pituitary gland, thyroid and synovium[54]. Non genetic causes classified as secondary hemochromatosis include ineffective erythropoiesis disorders such as thalassemia, myelodysplastic syndrome, anemia due to chronic disease, cirrhosis related iron deposition and exogenous increase by multiple transfusions. In the liver, excessive iron deposition results in cellular damage that can lead to cirrhosis and its complication, such as portal hypertension and the development of HCC. In secondary hemochromatosis, excess iron is deposited in the reticuloendothelial system, such as spleen, bone marrow, and liver with minimal cellular damage. Hence, hemochromatosis can also be categorized into parenchymal and reticuloendothelial forms based of the distribution of the iron deposition. In general, hemochromatosis is a clinically silent disease. The laboratory values used to diagnosis this disease have low sensitivity and specificity. Liver biopsy is the standard of reference for diagnosis that comes with its inherent sampling error and complications. MRI is a good noninvasive alternative method for the detection, diagnosis and monitoring of treatment response[54].

Utilizing a core MR-protocol with the axial T1 weighted SPGR IP and OP imaging, liver parenchyma with excess intracellular iron deposition shows signal loss on the IP images with longer echo times. This signal loss due to susceptibility effects of iron are more pronounced at longer echo times (Figure 12). A caveat of this technique is that, in patients with both diffuse steatosis and hemochromatosis diseases, theoretically no signal loss will be detected on the IP and OP images[55]. The distribution of iron deposition based on signal loss observed on the IP images can help distinguish primary and secondary hemochromatosis. In primary hemochromatosis, both the liver and pancreas will show signal loss, while signal intensity in the spleen and bone marrow will be unchanged. In secondary hemochromatosis, signal loss will be seen in the liver, spleen and bone marrow, while the signal intensity of the pancreas will preserved[54]. If there is a clinical suspicion of hemochromatosis, multiple TEs can be obtained on GRE sequences and the degree of iron overload can be calculated from the rate of signal loss as a function of TE[56].

CONCLUSION

Liver MRI is rapidly becoming the first image modality of choice for the clinician in the evaluation of liver masses and diffused liver disease. We have presented a core imaging protocol with a combination of T1, including in-and out-of phase imaging, T2, DWI EPI and dynamic post-Gd images with and without hepatocyte agents to evaluate the liver. Utilizing this basic protocol, most of the benign and malignant liver lesions can be characterized and, in addition, underlying liver disease can be identified. In the coming months, new innovative techniques will used more expansively, such as elastography, and will improve the role of MRI in liver imaging.

REFERENCES

1 **Martin DR**, Semelka RC. Magnetic resonance imaging of the liver: review of techniques and approach to common diseases. *Semin Ultrasound CT MR* 2005; **26**: 116-131

2 **Honal M**, Bauer S, Ludwig U, Leupold J. Increasing efficiency of parallel imaging for 2D multislice acquisitions. *Magn*

Reson Med 2009; **61**: 1459-1470
3 **Low RN**. Abdominal MRI advances in the detection of liver tumours and characterisation. *Lancet Oncol* 2007; **8**: 525-535
4 **Zech CJ**, Grazioli L, Breuer J, Reiser MF, Schoenberg SO. Diagnostic performance and description of morphological features of focal nodular hyperplasia in Gd-EOB-DTPA-enhanced liver magnetic resonance imaging: results of a multicenter trial. *Invest Radiol* 2008; **43**: 504-511
5 **Larkman DJ**, Nunes RG. Parallel magnetic resonance imaging. *Phys Med Biol* 2007; **52**: R15-R55
6 **Hines CD**, Yu H, Shimakawa A, McKenzie CA, Warner TF, Brittain JH, Reeder SB. Quantification of hepatic steatosis with 3-T MR imaging: validation in ob/ob mice. *Radiology* 2010; **254**: 119-128
7 **Li T**, Mirowitz SA. Fast T2-weighted MR imaging: impact of variation in pulse sequence parameters on image quality and artifacts. *Magn Reson Imaging* 2003; **21**: 745-753
8 **Bayramoglu S**, Kilickesmez O, Cimilli T, Kayhan A, Yirik G, Islim F, Alibek S. T2-weighted MRI of the upper abdomen: comparison of four fat-suppressed T2-weighted sequences including PROPELLER (BLADE) technique. *Acad Radiol* 2010; **17**: 368-374
9 **Akin O**, Schwartz LH, Welber A, Maier CF, Decorato DR, Panicek DM. Evaluation of focal liver lesions: fast-recovery fast spin echo T2-weighted MR imaging. *Clin Imaging* 2006; **30**: 322-325
10 **Mortelé KJ**, Ros PR. Cystic focal liver lesions in the adult: differential CT and MR imaging features. *Radiographics* 2001; **21**: 895-910
11 **Koh DM**, Collins DJ. Diffusion-weighted MRI in the body: applications and challenges in oncology. *AJR Am J Roentgenol* 2007; **188**: 1622-1635
12 **Koike N**, Cho A, Nasu K, Seto K, Nagaya S, Ohshima Y, Ohkohchi N. Role of diffusion-weighted magnetic resonance imaging in the differential diagnosis of focal hepatic lesions. *World J Gastroenterol* 2009; **15**: 5805-5812
13 **Sandrasegaran K**, Akisik FM, Lin C, Tahir B, Rajan J, Aisen AM. The value of diffusion-weighted imaging in characterizing focal liver masses. *Acad Radiol* 2009; **16**: 1208-1214
14 **Blaimer M**, Breuer F, Mueller M, Heidemann RM, Griswold MA, Jakob PM. SMASH, SENSE, PILS, GRAPPA: how to choose the optimal method. *Top Magn Reson Imaging* 2004; **15**: 223-236
15 **Brau AC**, Beatty PJ, Skare S, Bammer R. Comparison of reconstruction accuracy and efficiency among autocalibrating data-driven parallel imaging methods. *Magn Reson Med* 2008; **59**: 382-395
16 **Margolis DJ**, Bammer R, Chow LC. Parallel imaging of the abdomen. *Top Magn Reson Imaging* 2004; **15**: 197-206
17 **Yoshioka H**, Takahashi N, Yamaguchi M, Lou D, Saida Y, Itai Y. Double arterial phase dynamic MRI with sensitivity encoding (SENSE) for hypervascular hepatocellular carcinomas. *J Magn Reson Imaging* 2002; **16**: 259-266
18 **Kanematsu M**, Goshima S, Kondo H, Yokoyama R, Kajita K, Hoshi H, Onozuka M, Nozaki A, Hirano M, Shiratori Y, Moriyama N. Double hepatic arterial phase MRI of the liver with switching of reversed centric and centric K-space reordering. *AJR Am J Roentgenol* 2006; **187**: 464-472
19 **Sharma P**, Kitajima HD, Kalb B, Martin DR. Gadolinium-enhanced imaging of liver tumors and manifestations of hepatitis: pharmacodynamic and technical considerations. *Top Magn Reson Imaging* 2009; **20**: 71-78
20 **Motosugi U**, Ichikawa T, Tominaga L, Sou H, Sano K, Ichikawa S, Araki T. Delay before the hepatocyte phase of Gd-EOB-DTPA-enhanced MR imaging: is it possible to shorten the examination time? *Eur Radiol* 2009; **19**: 2623-2629
21 **Reimer P**, Schneider G, Schima W. Hepatobiliary contrast agents for contrast-enhanced MRI of the liver: properties, clinical development and applications. *Eur Radiol* 2004; **14**: 559-578
22 **Seale MK**, Catalano OA, Saini S, Hahn PF, Sahani DV. Hepatobiliary-specific MR contrast agents: role in imaging the liver and biliary tree. *Radiographics* 2009; **29**: 1725-1748
23 **Tanimoto A**, Lee JM, Murakami T, Huppertz A, Kudo M, Grazioli L. Consensus report of the 2nd International Forum for Liver MRI. *Eur Radiol* 2009; **19** Suppl 5: S975-S989
24 **Tamada T**, Ito K, Sone T, Yamamoto A, Yoshida K, Kakuba K, Tanimoto D, Higashi H, Yamashita T. Dynamic contrast-enhanced magnetic resonance imaging of abdominal solid organ and major vessel: comparison of enhancement effect between Gd-EOB-DTPA and Gd-DTPA. *J Magn Reson Imaging* 2009; **29**: 636-640
25 **Taouli B**, Ehman RL, Reeder SB. Advanced MRI methods for assessment of chronic liver disease. *AJR Am J Roentgenol* 2009; **193**: 14-27
26 **Taouli B**, Vilgrain V, Dumont E, Daire JL, Fan B, Menu Y. Evaluation of liver diffusion isotropy and characterization of focal hepatic lesions with two single-shot echo-planar MR imaging sequences: prospective study in 66 patients. *Radiology* 2003; **226**: 71-78
27 **Silva AC**, Evans JM, McCullough AE, Jatoi MA, Vargas HE, Hara AK. MR imaging of hypervascular liver masses: a review of current techniques. *Radiographics* 2009; **29**: 385-402
28 **Kamaya A**, Maturen KE, Tye GA, Liu YI, Parti NN, Desser TS. Hypervascular liver lesions. *Semin Ultrasound CT MR* 2009; **30**: 387-407
29 **Hardie AD**, Naik M, Hecht EM, Chandarana H, Mannelli L, Babb JS, Taouli B. Diagnosis of liver metastases: value of diffusion-weighted MRI compared with gadolinium-enhanced MRI. *Eur Radiol* 2010; **20**: 1431-1441
30 **Ba-Ssalamah A**, Uffmann M, Saini S, Bastati N, Herold C, Schima W. Clinical value of MRI liver-specific contrast agents: a tailored examination for a confident non-invasive diagnosis of focal liver lesions. *Eur Radiol* 2009; **19**: 342-357
31 **Forner A**, Vilana R, Ayuso C, Bianchi L, Solé M, Ayuso JR, Boix L, Sala M, Varela M, Llovet JM, Brú C, Bruix J. Diagnosis of hepatic nodules 20 mm or smaller in cirrhosis: Prospective validation of the noninvasive diagnostic criteria for hepatocellular carcinoma. *Hepatology* 2008; **47**: 97-104
32 **Krinsky G**. Imaging of dysplastic nodules and small hepatocellular carcinomas: experience with explanted livers. *Intervirology* 2004; **47**: 191-198
33 **Roncalli M**, Borzio M, Di Tommaso L. Hepatocellular dysplastic nodules. *Hepatol Res* 2007; **37** Suppl 2: S125-S134
34 **Choi BI**, Lee JM. Advancement in HCC imaging: diagnosis, staging and treatment efficacy assessments : Imaging diagnosis and staging of hepatocellular carcinoma. *J Hepatobiliary Pancreat Sci* 2010; **17**: 369-373
35 **Frericks BB**, Loddenkemper C, Huppertz A, Valdeig S, Stroux A, Seja M, Wolf KJ, Albrecht T. Qualitative and quantitative evaluation of hepatocellular carcinoma and cirrhotic liver enhancement using Gd-EOB-DTPA. *AJR Am J Roentgenol* 2009; **193**: 1053-1060
36 **Jang HJ**, Yu H, Kim TK. Imaging of focal liver lesions. *Semin Roentgenol* 2009; **44**: 266-282
37 **Kelekis NL**, Semelka RC, Woosley JT. Malignant lesions of the liver with high signal intensity on T1-weighted MR images. *J Magn Reson Imaging* 1996; **6**: 291-294
38 **Parikh T**, Drew SJ, Lee VS, Wong S, Hecht EM, Babb JS, Taouli B. Focal liver lesion detection and characterization with diffusion-weighted MR imaging: comparison with standard breath-hold T2-weighted imaging. *Radiology* 2008; **246**: 812-822
39 **Taouli B**, Koh DM. Diffusion-weighted MR imaging of the liver. *Radiology* 2010; **254**: 47-66
40 **Danet IM**, Semelka RC, Leonardou P, Braga L, Vaidean G, Woosley JT, Kanematsu M. Spectrum of MRI appearances of untreated metastases of the liver. *AJR Am J Roentgenol* 2003; **181**: 809-817
41 **Brancatelli G**, Federle MP, Baron RL, Lagalla R, Midiri M,

Vilgrain V. Arterially enhancing liver lesions: significance of sustained enhancement on hepatic venous and delayed phase with magnetic resonance imaging. *J Comput Assist Tomogr* 2007; **31**: 116-124
42 **Iannaccone R**, Federle MP, Brancatelli G, Matsui O, Fishman EK, Narra VR, Grazioli L, McCarthy SM, Piacentini F, Maruzzelli L, Passariello R, Vilgrain V. Peliosis hepatis: spectrum of imaging findings. *AJR Am J Roentgenol* 2006; **187**: W43-W52
43 **Mortele KJ**, Ros PR. MR imaging in chronic hepatitis and cirrhosis. *Semin Ultrasound CT MR* 2002; **23**: 79-100
44 **Zhong L**, Chen JJ, Chen J, Li L, Lin ZQ, Wang WJ, Xu JR. Nonalcoholic fatty liver disease: quantitative assessment of liver fat content by computed tomography, magnetic resonance imaging and proton magnetic resonance spectroscopy. *J Dig Dis* 2009; **10**: 315-320
45 **Schwenzer NF**, Machann J, Martirosian P, Stefan N, Schraml C, Fritsche A, Claussen CD, Schick F. Quantification of pancreatic lipomatosis and liver steatosis by MRI: comparison of in/opposed-phase and spectral-spatial excitation techniques. *Invest Radiol* 2008; **43**: 330-337
46 **Reeder SB**, Robson PM, Yu H, Shimakawa A, Hines CD, McKenzie CA, Brittain JH. Quantification of hepatic steatosis with MRI: the effects of accurate fat spectral modeling. *J Magn Reson Imaging* 2009; **29**: 1332-1339
47 **Basaran C**, Karcaaltincaba M, Akata D, Karabulut N, Akinci D, Ozmen M, Akhan O. Fat-containing lesions of the liver: cross-sectional imaging findings with emphasis on MRI. *AJR Am J Roentgenol* 2005; **184**: 1103-1110
48 **Elias J Jr**, Altun E, Zacks S, Armao DM, Woosley JT, Semelka RC. MRI findings in nonalcoholic steatohepatitis: correlation with histopathology and clinical staging. *Magn Reson Imaging* 2009; **27**: 976-987
49 **Faria SC**, Ganesan K, Mwangi I, Shiehmorteza M, Viamonte B, Mazhar S, Peterson M, Kono Y, Santillan C, Casola G, Sirlin CB. MR imaging of liver fibrosis: current state of the art. *Radiographics* 2009; **29**: 1615-1635
50 **Ito K**, Mitchell DG. Hepatic morphologic changes in cirrhosis: MR imaging findings. *Abdom Imaging* 2000; **25**: 456-461
51 **Ito K**, Mitchell DG. Imaging diagnosis of cirrhosis and chronic hepatitis. *Intervirology* 2004; **47**: 134-143
52 **Ito K**, Mitchell DG, Siegelman ES. Cirrhosis: MR imaging features. *Magn Reson Imaging Clin N Am* 2002; **10**: 75-92, vi
53 **Mortelé KJ**, Praet M, Van Vlierberghe H, de Hemptinne B, Zou K, Ros PR. Focal nodular hyperplasia of the liver: detection and characterization with plain and dynamic-enhanced MRI. *Abdom Imaging* 2002; **27**: 700-707
54 **Queiroz-Andrade M**, Blasbalg R, Ortega CD, Rodstein MA, Baroni RH, Rocha MS, Cerri GG. MR imaging findings of iron overload. *Radiographics* 2009; **29**: 1575-1589
55 **Merkle EM**, Nelson RC. Dual gradient-echo in-phase and opposed-phase hepatic MR imaging: a useful tool for evaluating more than fatty infiltration or fatty sparing. *Radiographics* 2006; **26**: 1409-1418
56 **Alexopoulou E**, Stripeli F, Baras P, Seimenis I, Kattamis A, Ladis V, Efstathopoulos E, Brountzos EN, Kelekis AD, Kelekis NL. R2 relaxometry with MRI for the quantification of tissue iron overload in beta-thalassemic patients. *J Magn Reson Imaging* 2006; **23**: 163-170

S- Editor Cheng JX **L- Editor** Lutze M **E- Editor** Zheng XM

World Journal of Radiology

Online Submissions: http://www.wjgnet.com/1949-8470office
wjr@wjgnet.com
doi:10.4329/wjr.v2.i8.323

World J Radiol 2010 August 28; 2(8): 323-328
ISSN 1949-8470 (online)

REVIEW

Interventional management of tracheobronchial strictures

Ji Hoon Shin

Ji Hoon Shin, Department of Radiology and Research Institute of Radiology, University of Ulsan College of Medicine, Asan Medical Center 388-1, Pungnap-2dong, Songpa-gu, Seoul 138-736, South Korea
Author contributions: Shin JH was the sole author of this manuscript.
Correspondence to: Ji Hoon Shin, MD, Department of Radiology and Research Institute of Radiology, University of Ulsan College of Medicine, Asan Medical Center 388-1, Pungnap-2dong, Songpa-gu, Seoul 138-736, South Korea. jhshin@amc.seoul.kr
Telephone: +82-2-30104380 Fax: +82-2-4760090
Received: May 21, 2010 Revised: June 7, 2010
Accepted: June 14, 2010
Published online: August 28, 2010

Abstract

Tracheobronchial balloon dilation and stent placement have been well used in the treatment of patients with benign and/or malignant diseases. Balloon dilation is the first option in the treatment of benign airway stenosis. Although balloon dilation is simple and fast, recurrence rate is high. Stent placement promptly relieves acute airway distress from malignant extraluminal and intraluminal airway obstruction. Temporary stent placement may be an alternative for benign airway strictures refractory to balloon dilation. This article reviews the indications, pre-procedure evaluation, technique, outcomes and complications of balloon dilation and stent placement with regard to benign and malignant tracheobronchial stenoses.

Key words: Stent placement; Tracheobronchial balloon dilation; Tracheobronchial strictures

Peer reviewer: James Chow, PhD, Radiation Physicist, Radiation Medicine Program, Princess Margaret Hospital, 610 University Avenue, Toronto, ON, M5G 2M9, Canada

Shin JH. Interventional management of tracheobronchial strictures. *World J Radiol* 2010; 2(8): 323-328 Available from: URL: http://www.wjgnet.com/1949-8470/full/v2/i8/323.htm DOI: http://dx.doi.org/10.4329/wjr.v2.i8.323

INTRODUCTION

Tracheobronchial obstructions arising from either benign or malignant diseases result in dyspnea, stridor, and obstructive pneumonia, and can occasionally be life-threatening due to suffocation. Even in the absence of parenchymal lung disease, ventilatory failure frequently occurs if the obstruction is not relieved. Tracheobronchial obstructions are challenging to manage, particularly in patients unsuitable for curative surgery, with endobronchial intervention having an increasing role in their management[1]. Endobronchial intervention can be performed under local anesthesia by fluoroscopic guidance and/or fiberoptic bronchoscopy, or under general anesthesia using rigid bronchoscopy. Although aggressive endobronchial interventions for tissue destruction (Nd YAG laser, argon plasma coagulation, cryotherapy, or electrocautery) can be performed using rigid bronchoscopy, balloon dilation and stent placement can be performed using fluoroscopic guidance and/or flexible bronchoscopy.

TRACHEOBRONCHIAL BALLOON DILATION

Bronchoscopically or fluoroscopically guided balloon dilation is an accepted initial therapy for patients with benign bronchial strictures, primarily because balloon dilation is associated with lower morbidity and mortality rates than corrective surgery. The balloon dilates the stenotic trachea or bronchus by stretching and expanding the bronchial wall, making balloon dilation appropriate for the treatment of cicatric annular strictures. Balloon dilation has been extended to the treatment of tracheobronchial stenoses due to, for example, post-intubation tracheal stenosis, postoperative anastomotic stenosis, granulomatous steno-

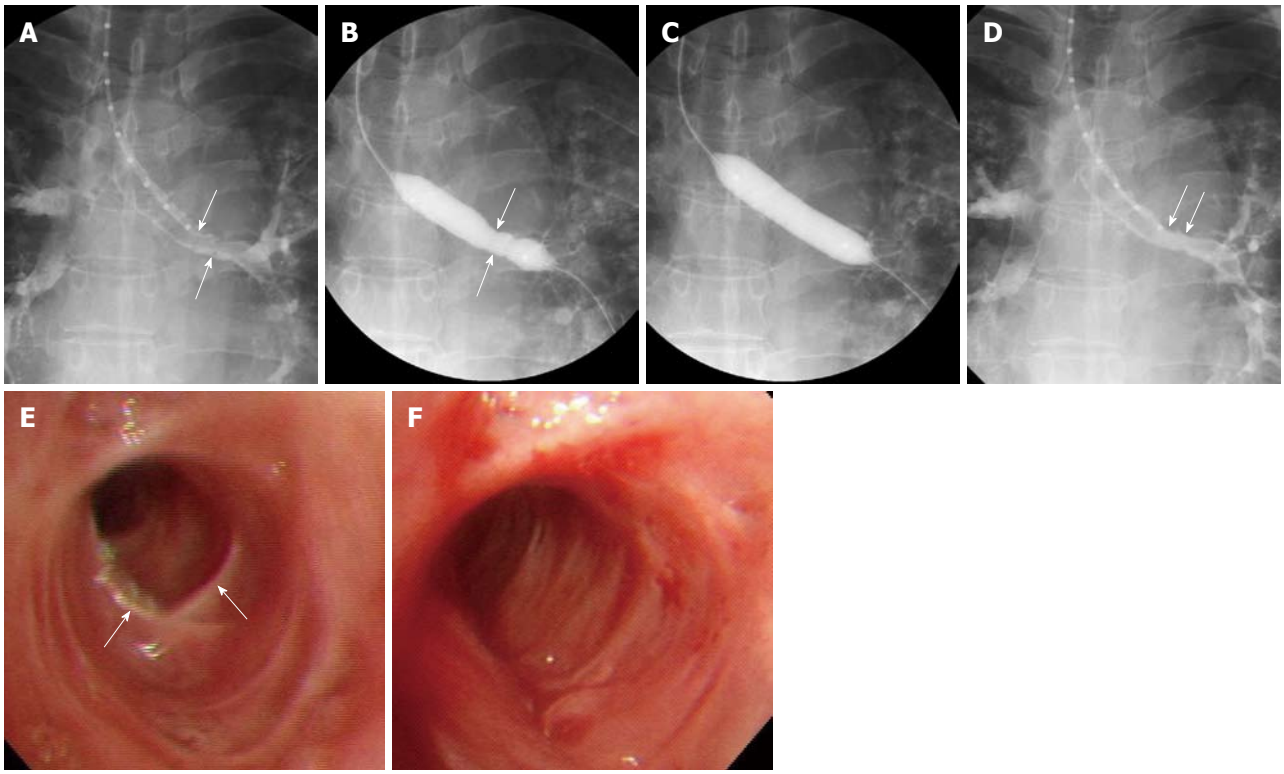

Figure 1 A 43-year-old woman with left main bronchial stricture caused by tuberculosis. A: Radiograph shows irregular narrowing (arrows) of the left main bronchus; B, C: Radiographs show waist formation (arrows in B) of the inflated balloon and subsequent full inflation; D: Radiograph shows marked improvement in stricture (arrows); E, F: Bronchoscopic images before (E) and after (F) balloon dilation show substantial improvement in the stricture (arrows in E).

sis (tuberculosis, histoplasmosis), radiation therapy, mediastinal fibrosis, congenital stenosis, bronchial trauma and bronchial artery embolization[2-5]. Before balloon dilation, the site, severity, proximal and distal extent, and characteristics of the stricture should be evaluated by conventional radiography, computed tomography scans including three-dimensional reconstructions, and/or bronchoscopy.

In our center, the pharynx and larynx are topically anesthetized using an aerosol spray 3-5 min before the procedure, followed by conscious sedation by intravenous administration of midazolam. A 0.035-inch angled exchange guide wire (Radifocus M; Terumo, Tokyo) is inserted through the bronchoscope and positioned across the stenosis. If a bronchoscope is not available, the guide wire can be inserted across the stenosis under fluoroscopic guidance. After removing the bronchoscope, the stricture is measured by passing a graduated sizing catheter over the guide wire to the distal part of the stricture. The degree and length of the stricture are evaluated in detail by selective tracheobronchography, by passing approximately 5 mL of water-soluble nonionic contrast medium mixed 1:1 with lidocaine through the sizing catheter (Figure 1). An angioplasty balloon catheter is then passed over the guide wire to dilate the stricture. In children, 6-mm diameter balloon catheters are used in the bronchi and tracheae, whereas in adults, 10-12-mm diameter balloon catheters are used in bronchi and 14-20-mm diameter balloon catheters are used in tracheae (Figure 1). If the stenosis is too narrow to allow passage of a balloon catheter > 10 mm in diameter, a 6-mm diameter balloon catheter is used first to provide a passage for the larger balloon catheter. Using diluted water-soluble nonionic contrast medium, the balloon is inflated at pressures up to 16 atm, as determined by a pressure-gauge monitor. After the procedure, selective tracheobronchography is performed to evaluate lumen dilation.

A review of several representative studies, each including 21-59 patients[2,3,5-7], found that the technical success rate was 100% and that all patients achieved initial symptomatic improvement. In some of these studies, however, up to 80% of patients required adjuvant treatment, including stent placement and laser therapy[2,3,5-7].

Complications associated with balloon dilation include chest pain during dilation, bronchospasm, atelectasis after dilation, superficial or deep mucosal laceration, pneumomediastinum, and massive bleeding have been reported[3,8-10]. In one large series, bronchial lacerations occurred during 64 of 124 (52%) tracheobronchial balloon dilation procedures, but none of these progressed to transmural laceration[10]. The median cumulative airway patency period was significantly longer in patients with than in those without lacerations (24 mo *vs* 4 mo), indicating that laceration secondary to balloon dilation may improve patency outcomes[10].

Recently, cutting balloon dilation has shown much better patency, approximately 60% at 2 years, for the treatment of benign bronchial strictures resistant to conventional balloon dilation[4]. Endobronchial brachytherapy

may be used to treat benign bronchial strictures resistant to conventional balloon dilation or as an adjuvant treatment to treat granulation tissue formation after airway restoration[5,11].

Tracheobronchial balloon dilation is a simple, rapid, and safe method of restoring airway lumen, providing immediate symptom relief. This simple procedure may be a first option in the treatment of benign airway stenosis. If restenosis occurs, however, adjuvant endobronchial therapy, consisting of stent placement or laser treatment, will be necessary.

TRACHEOBRONCHIAL STENT PLACEMENT

Up to 30% of patients with lung cancer have been reported to develop central airway obstruction secondary to endoluminal disease or external compression by a hilar tumor or bulky lymphadenopathy[12]. Recent technological advances have increased the popularity of tracheobronchial stents with interventional radiologists and chest physicians, particularly because stenting is effective for both extraluminal and intraluminal lesions and promptly relieves acute airway distress from airway obstruction. Expandable metallic stents are better tolerated than, and preferred to, non-expandable silicone stents because the former are more flexible and can be used in smaller delivery systems.

Indications for stent placement

Stent placement is indicated for patients with submucosal and extraluminal pathology or tracheobronchomalacia, as well as for patients with intraluminal pathology (Table 1 and Figure 2). Tracheobronchomalacia is a special entity denoting functional airway obstruction with destruction of the surrounding airway cartilage. In patients with malignancies, the most common indication for stent placement is bronchogenic carcinoma, which can present as extraluminal compression with or without an intraluminal lesion. Tracheobronchial stenting is the only immediate treatment for unresectable extraluminal compression, promptly stabilizing a threatened airway while the primary tumor is treated with radiation or chemotherapy.

The only definitive contraindication for placement of an airway stent is in patients with external compression of the airway by a vessel. Stent placement in these patients was associated with unacceptably high rates of erosion, hemorrhage, and death[12].

Types of stents

At present, two types of stents are available, silicone and metallic. The advantages of metallic stents include their favorable ratios of wall to inner diameter and their ability to be placed using flexible bronchoscopy and/or fluoroscopy. Metallic stents can be classified as balloon-expandable and covered and uncovered self-expandable metallic stents. Silicone stents have been associated with high rates of migration, resulting in reocclusion, adherence of secretions due to the impairment of mucociliary clearance, and unfavorable wall to inner diameter ratios. Among the advantages of silicone stents are their ability to be repositioned or removed as many times as needed, which is especially important for benign tracheobronchial stenoses and for slowly growing, frequently recurring stenoses[12]. General anesthesia and the use of a rigid bronchoscope are mandatory for the placement of silicone stents. Among the advantages of balloon-expandable stents, including Strecker and Palmaz stents, and of uncovered self-expandable metallic stents, including Gianturco Z, Ultraflex, and Polyflex stents, are their lower rates of migration and interference with mucociliary clearance. Among their disadvantages are difficult removal and the growth of tumors or granulation tissue through the stent meshes. Because balloon-expandable metallic stents require an additional step, balloon dilation, and sometimes require rigid bronchoscopes, they are less commonly used. Uncovered and covered self-expandable metallic stents have become increasingly popular due to their relative ease of placement. These stents can be compressed into a small delivery device, and once deployed, are embedded into the surrounding tissue *via* a radial force. Whereas uncovered self-expandable metallic stents cannot be removed or exchanged easily, covered self-expandable metallic stents, such as Ultraflex, Wall, and Alveolus stents, can be removed or exchanged relatively easily. Therefore, temporarily placed retrievable, covered self-expandable metallic stents can be used to treat benign airway strictures as well as to treat malignant airway strictures in combination with radiation therapy and/or chemotherapy (Figure 3)[13,14]. In addition, covered self-expandable metallic stents can

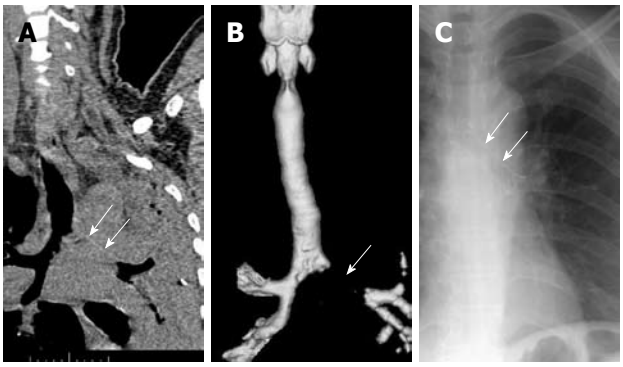

Figure 2 A 56-year-old woman with a left main bronchial obstruction caused by cervical cancer metastasis. A, B: Coronal reconstructed computed tomography (CT) scan (A) and 3D-reconstructed CT scan (B) showing complete obstruction (arrows) of the left main bronchus with left lung atelectasis; C: Radiograph taken 6 mo after left bronchial stent placement, showing good expansion of the stent (arrows) and good aeration of the left lung.

Table 1 Indications for tracheobronchial stent placement

Malignant intraluminal or extraluminal obstructive pathology
Benign inflammatory obstructive pathology such as tuberculosis
Benign post-intubation tracheal stenosis
Benign postoperative anastomotic stenosis
Tracheobronchomalacia
Compression by esophageal stents
Esophagorespiratory fistula

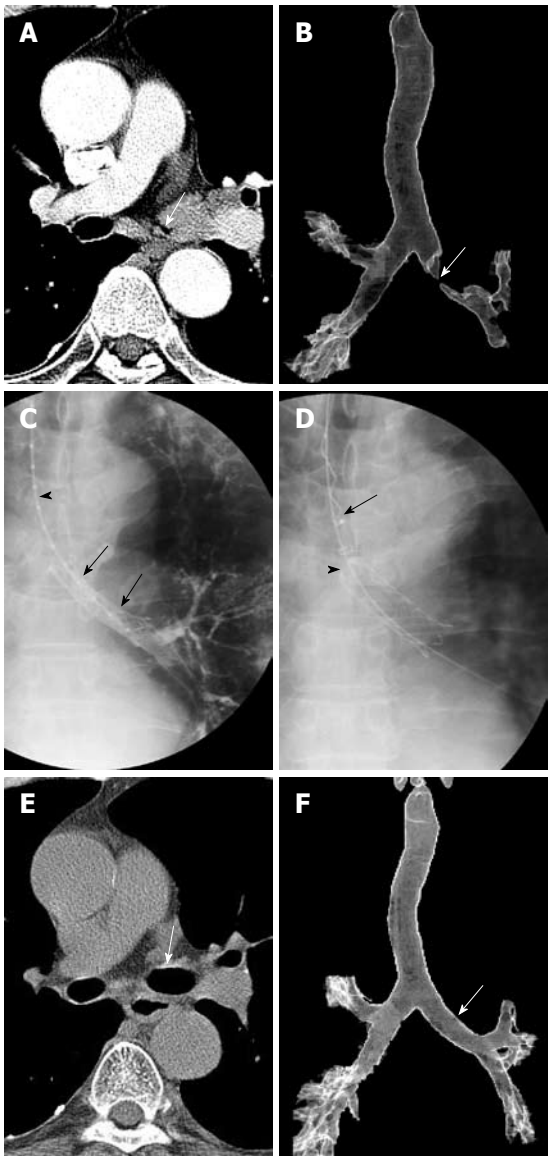

Figure 3 A 67-year-old man with a left main bronchial stricture caused by non-small-cell lung cancer. A, B: Axial computed tomography (CT) scan (A) and anteroposterior view (B) of 3D surface-rendered reconstruction CT scan performed 3 d before stent placement, showing a severe left main bronchial stricture (arrows); C: Radiograph showing retrievable covered stent (arrows) 12 mm in diameter and 4 cm in length placed at the stricture. A sizing catheter (arrowhead) is also shown; D: Radiograph showing the collapse of the proximal end (arrowhead) of the stent while the retrievable hookwire (arrow) was withdrawn into the sheath; E, F: Axial CT scan (E) and anteroposterior view (F) of 3D surface-rendered reconstruction CT obtained 6 mo after stent removal, showing marked improvement in the stricture (arrows).

be used to seal esophagorespiratory fistulae. Recently introduced barbed retrievable covered metallic stents have shown particularly low migration rates[15].

Technique

Expandable metallic stents can be inserted only under fluoroscopic guidance and only by radiologists with patients under topical anesthesia. Due to the importance of bronchoscopic evaluation immediately before and after stent placement, bronchoscopic assistance is valuable. Moreover, it is relatively easy to insert a guide wire across the stricture into the distal portion of the trachea or bronchus through the working channel of the bronchoscope.

The techniques for providing topical anesthesia, introducing the guide wire and catheter into the tracheobronchial tree, and obtaining selective tracheobronchography are the same as for balloon dilation. Subsequently, the location of the narrowed lumen can be marked on the patient's skin using radiopaque markers. With the patient in a supine position and with the neck fully extended, the delivery system, the proximal part of which is lubricated with jelly, is passed over the guide wire into the trachea and is advanced until the distal tip reaches beyond the stricture. When the stricture is severe (i.e. more than two-thirds of the lumen is narrowed), the stenotic portion is dilated with an angioplasty balloon catheter. The stent should be at least 10 mm longer than the stricture, so that the proximal and distal parts of the stent rest on the upper and lower margins of the stricture, respectively.

Following stent placement, its patency and location are evaluated by bronchoscopy. It is important to avoid inexact stent deployment that results in partial obstruction of a bronchial orifice or incomplete coverage of a tumor stenosis. If this occurs, the stent should be repositioned using bronchoscopic biopsy forceps or it should be removed and its placement reattempted.

Early investigators used forceps/rotation techniques to remove uncovered expandable metallic stents under general anesthesia[16,17]. In patients in whom the stent was tightly welded to the tracheobronchial wall, however, this removal procedure carried potential risks of mucosal bleeding and airway occlusion during the procedure. Our removal technique uses a hook-like device and has been reported to be safe and easy to perform because the stents (Song Airway Stent, S&G Biotech, Seongnam, Korea) are completely covered and designed for optimal removal[13-15,18]. To make the stent removable, a nylon loop is hooked inside each bend of its proximal end and two nylon threads are passed through each loop. To remove these stents, a hooked wire is introduced into the sheath and passed through it into the stent lumen. The sheath containing the hook is then pulled out of the stent so that the hook grasps the drawstring. When this occurs, the hook wire is withdrawn through the sheath, collapsing the proximal stent. The sheath, hook wire, and stent are then pulled out of the trachea.

Outcomes and complications

In benign tracheobronchial stenosis, technical success rates of 100% and clinical success rates of 88-100% have been reported in 46 patients across three representative studies using uncovered self-expandable stents[19-21]. The most common causes of stenosis in these patients were post-lung transplantation strictures and tuberculosis. Stent fracture was the most commonly observed complication, occurring in seven patients (15%), followed by granulation tissue formation (7%) and stent migration (2%). Four patients (9%) required stent removal due to stent fracture or migration, but stent removal was difficult because the wire mesh was embedded in the airway walls. These find-

ings indicate that the placement of permanent stents may not be ideal due to the formation of granulation tissue. We have placed 30 covered retrievable expandable metallic stents into 24 patients[13], resulting in technical and short-term clinical success rates of 100%. All stents were successfully removed electively, either 2 (n = 12) or 6 (n = 12) months after placement or when complications occurred (n = 6). The 6-mo stenting group showed a lower recurrence rate (41.7% *vs* 83.3%, P = 0.045) and a better mean maintained patency (39.7 ± 7.8 mo *vs* 9.4 ± 5.4 mo, P = 0.001) than the 2-mo stenting group. Although stent migration and tissue hyperplasia at either end of the stent was observed in 13% and 37% of these patients, respectively, stent removal was easy and safe.

Four representative studies of stent placement, two using uncovered[22,23] and two using covered[18,24] stents, in 133 patients with malignant tracheobronchial stenosis showed technical success rates of 98%-100% and clinical success rates of 82%-92%. Covered metallic stents were associated with much higher rates of stent migration (12%-17%) and sputum retention (20%-38%) than uncovered metallic stents (0% and 9%, respectively). In contrast, tumor ingrowth into the stent lumen occurred more often with uncovered (21%-23%) than with covered (0%) metallic stents because the former do not contain covering material between the wire mesh. In patients with malignant bronchial obstructions, involvement of the lower-lobe segmental bronchus has been associated with lower rates of radiologic and clinical improvement following stent placement[25].

In patients with benign disease, stent migration is more likely when there is no substantial extrinsic compression maintaining the stents in place and when short stents are placed in conical stenoses. In patients with malignancies, migration can be expected after tumor shrinkage from radiation or chemotherapy. Granulation tissue is more likely to form at the proximal and distal ends of the stent, and excessive granulation tissue can lead to obstruction of the airway. This occurs more commonly with metallic stents, especially uncovered stents (up to 7%), than with silicone stents because metal stents are more rigid and have multiple edges, therefore causing more irritation. The incidence of tumor overgrowth at the tip of the covered metallic stent depends on the follow-up period and extent of the malignancy at the time of stent placement and has been reported to occur in 6%-28% of patients[18,24]. Because airway obstruction by tumor ingrowth/overgrowth can be life-threatening, patients with new symptoms or radiographic findings should undergo further diagnostic evaluation. Sputum retention is more likely to occur after placement of silicone and covered expandable metallic stents than after placement of uncovered expandable metallic stents due to impaired mucociliary clearance in the former. Lack of mucociliary clearance can lead to obstruction and infection.

CONCLUSION

In summary, balloon dilation is an accepted initial therapy for benign airway stricture. It is easy to perform, but is plagued by a high recurrence rate. While, stent placement can improve life quality by dramatic resolution of dyspnea in malignant airway stricture. For benign airway strictures refractory to balloon dilation, temporary placement of airway stent could be considered.

REFERENCES

1 **Ranu H**, Madden BP. Endobronchial stenting in the management of large airway pathology. *Postgrad Med J* 2009; **85**: 682-687
2 **Shitrit D**, Kuchuk M, Zismanov V, Rahman NA, Amital A, Kramer MR. Bronchoscopic balloon dilatation of tracheobronchial stenosis: long-term follow-up. *Eur J Cardiothorac Surg* 2010; **38**: 198-202
3 **Lee KH**, Ko GY, Song HY, Shim TS, Kim WS. Benign tracheobronchial stenoses: long-term clinical experience with balloon dilation. *J Vasc Interv Radiol* 2002; **13**: 909-914
4 **Kim JH**, Shin JH, Song HY, Ko GY, Gwon DI, Yoon HK, Sung KB. Cutting balloon treatment for resistant benign bronchial strictures: report of eleven patients. *J Vasc Interv Radiol* 2010; **21**: 748-752
5 **Rahman NA**, Fruchter O, Shitrit D, Fox BD, Kramer MR. Flexible bronchoscopic management of benign tracheal stenosis: long term follow-up of 115 patients. *J Cardiothorac Surg* 2010; **5**: 2
6 **Low SY**, Hsu A, Eng P. Interventional bronchoscopy for tuberculous tracheobronchial stenosis. *Eur Respir J* 2004; **24**: 345-347
7 **Mayse ML**, Greenheck J, Friedman M, Kovitz KL. Successful bronchoscopic balloon dilation of nonmalignant tracheobronchial obstruction without fluoroscopy. *Chest* 2004; **126**: 634-637
8 **Ferretti G**, Jouvan FB, Thony F, Pison C, Coulomb M. Benign noninflammatory bronchial stenosis: treatment with balloon dilation. *Radiology* 1995; **196**: 831-834
9 **Kato R**, Kakizaki T, Hangai N, Sawafuji M, Yamamoto T, Kobayashi T, Watanabe M, Nakayama M, Kawamura M, Kikuchi K. Bronchoplastic procedures for tuberculous bronchial stenosis. *J Thorac Cardiovasc Surg* 1993; **106**: 1118-1121
10 **Kim JH**, Shin JH, Song HY, Shim TS, Ko GY, Yoon HK, Sung KB. Tracheobronchial laceration after balloon dilation for benign strictures: incidence and clinical significance. *Chest* 2007; **131**: 1114-1117
11 **Kim JH**, Shin JH, Song HY, Shim TS, Oh YM, Oh SJ, Moon DH. Liquid (188)Re-filled balloon dilation for the treatment of refractory benign airway strictures: preliminary experience. *J Vasc Interv Radiol* 2008; **19**: 406-411
12 **Chin CS**, Litle V, Yun J, Weiser T, Swanson SJ. Airway stents. *Ann Thorac Surg* 2008; **85**: S792-S796
13 **Kim JH**, Shin JH, Song HY, Shim TS, Yoon CJ, Ko GY. Benign tracheobronchial strictures: long-term results and factors affecting airway patency after temporary stent placement. *AJR Am J Roentgenol* 2007; **188**: 1033-1038
14 **Kim JH**, Shin JH, Song HY, Ohm JY, Lee JM, Lee DH, Kim SW. Palliative treatment of inoperable malignant tracheobronchial obstruction: temporary stenting combined with radiation therapy and/or chemotherapy. *AJR Am J Roentgenol* 2009; **193**: W38-W42
15 **Kim YH**, Shin JH, Song HY, Kim JH. Tracheal stricture and fistula: management with a barbed silicone-covered retrievable expandable nitinol stent. *AJR Am J Roentgenol* 2010; **194**: W232-W237
16 **Filler RM**, Forte V, Chait P. Tracheobronchial stenting for the treatment of airway obstruction. *J Pediatr Surg* 1998; **33**: 304-311
17 **Nicolai T**, Huber RM, Reiter K, Merkenschlager A, Haut-

mann H, Mantel K. Metal airway stent implantation in children: follow-up of seven children. *Pediatr Pulmonol* 2001; **31**: 289-296
18 **Shin JH**, Kim SW, Shim TS, Jung GS, Kim TH, Ko GY, Song HY. Malignant tracheobronchial strictures: palliation with covered retrievable expandable nitinol stent. *J Vasc Interv Radiol* 2003; **14**: 1525-1534
19 **Eisner MD**, Gordon RL, Webb WR, Gold WM, Hilal SE, Edinburgh K, Golden JA. Pulmonary function improves after expandable metal stent placement for benign airway obstruction. *Chest* 1999; **115**: 1006-1011
20 **Orons PD**, Amesur NB, Dauber JH, Zajko AB, Keenan RJ, Iacono AT. Balloon dilation and endobronchial stent placement for bronchial strictures after lung transplantation. *J Vasc Interv Radiol* 2000; **11**: 89-99
21 **Choi YW**, Kim YS, Jeon SC, Hahm CK, Choi CS. Treatment of tracheobronchial stenosis with a self-expandable metallic stents. *J Korean Radiol Soc* 1994; **31**: 35-41
22 **Miyazawa T**, Yamakido M, Ikeda S, Furukawa K, Takiguchi Y, Tada H, Shirakusa T. Implantation of ultraflex nitinol stents in malignant tracheobronchial stenoses. *Chest* 2000; **118**: 959-965
23 **Sawada S**, Tanigawa N, Kobayashi M, Furui S, Ohta Y. Malignant tracheobronchial obstructive lesions: treatment with Gianturco expandable metallic stents. *Radiology* 1993; **188**: 205-208
24 **Monnier P**, Mudry A, Stanzel F, Haeussinger K, Heitz M, Probst R, Bolliger CT. The use of the covered Wallstent for the palliative treatment of inoperable tracheobronchial cancers. A prospective, multicenter study. *Chest* 1996; **110**: 1161-1168
25 **Shin JH**, Song HY, Kim KR, Kim JH, Kim SW, Lee DH, Hong SB. Radiologic and clinical outcomes with special reference to tumor involvement pattern after stent placement for malignant bronchial obstructions. *Acta Radiol* 2009; **50**: 1011-1018

S- Editor Cheng JX **L- Editor** Webster JR **E- Editor** Zheng XM

World Journal of Radiology

Online Submissions: http://www.wjgnet.com/1949-8470office
wjr@wjgnet.com
doi:10.4329/wjr.v2.i8.329

World J Radiol 2010 August 28; 2(8): 329-333
ISSN 1949-8470 (online)

CASE REPORT

Chemoradiation as definitive treatment for primary squamous cell cancer of the rectum

Eva Iannacone, Francesco Dionisi, Daniela Musio, Rossella Caiazzo, Nicola Raffetto, Enzo Banelli

Eva Iannacone, Daniela Musio, Rossella Caiazzo, Nicola Raffetto, Enzo Banelli, Department of Radiation Oncology, "University Sapienza", 00161, Rome, Italy
Francesco Dionisi, Radiotherapy Unit, Niguarda Cà Granda Hospital, 20162, Milan, Italy
Author contributions: Iannacone E, Dionisi F and Musio D designed the study; Musio D and Caiazzo R analyzed the data of the literature cited in the text; Raffetto N and Banelli E approved the final version of the manuscript; Dionisi F and Iannacone E wrote the paper.
Correspondence to: Francesco Dionisi, MD, Radiotherapy Unit, Niguarda Cà Granda Hospital, Piazza dell'Ospedale Maggiore, 20162 Milan, Italy. francesco.dionisi@ospedaleniguarda.it
Telephone: +39-2-64442233 Fax: +39-2-64442834
Received: June 7, 2010 Revised: June 29, 2010
Accepted: July 6, 2010
Published online: August 28, 2010

Abstract

In this report, we present a case of advanced squamous cell cancer located in the rectum of a 78-year-old woman treated with chemoradiation with curative intent. The patient showed a complete clinical response to chemoradiation; multiple biopsies were performed at the site of the previous mass 5 mo after the end of treatment and histological examination showed no residual tumour in the specimens. Surgical intervention was avoided and the patient was free of disease 12 mo after the diagnosis of cancer. Primary chemoradiation should be considered as the treatment of choice for this rare malignancy.

Key words: Squamous cell carcinoma; Chemoradiation; Non operative management

Peer reviewers: Thomas J George, Jr., MD, FACP, Assistant Professor, Director, GI Oncology Program, Associate Director, HemOnc Fellowship Program, University of Florida, Division of Hematology and Oncology, 1600 SW Archer Road, PO Box 100277, Gainesville, FL 32610, United States; Heriberto Medina-Franco, MD, National Institute of Medical Sciences and Nutrition "Salvador Zubiran", Vasco de Quiroga 15 Colonia Seccion XVI, Mexico City ZIP 14000, Mexico

Iannacone E, Dionisi F, Musio D, Caiazzo R, Raffetto N, Banelli E. Chemoradiation as definitive treatment for primary squamous cell cancer of the rectum. *World J Radiol* 2010; 2(8): 329-333 Available from: URL: http://www.wjgnet.com/1949-8470/full/v2/i8/329.htm DOI: http://dx.doi.org/10.4329/wjr.v2.i8.329

INTRODUCTION

Colorectal cancer is the second most common cancer in the Western world[1]. Adenocarcinoma represents more than 90% of all colorectal cancers while other histological subtypes, such as squamous cell carcinomas (SCC), adenosquamous, carcinoid or lymphoid, are identified only occasionally. SCC of the rectum is an extremely rare malignancy with an incidence of less than 1/10000 of all colorectal cancers[2]. It was described for the first time by Raiford[3] in 1933.

Diagnosis of a primary SCC of the rectum is neither immediate nor simple. According to Williams *et al*[4], the following criteria must be satisfied: (1) absence of metastases from other sites (such as SCC of the lung); (2) absence of fistulas between the rectum and adjacent affected organs, which could be the source of SCCs; and (3) absence of a SCC of the anus with cranial extension into the lower rectum.

The natural history and therapeutic options for such a rare tumour have not yet been clearly defined. Surgery is still considered the gold standard of treatment, however, several authors consider the association of radiotherapy and chemotherapy as an effective alternative to resection[5]. The scientific literature on SCC consists mainly of case reports. Since 1933, only 73 cases of SCC have been reported, with the largest series on 12 patients being re-

ported by Nahas *et al*[6]. In this paper, we present a case of primary SCC of the rectum treated with chemoradiation alone with curative intent.

CASE REPORT

In May 2009 an obese, non-smoking, 78-year-old woman, with an ECOG performance status of 1, was referred to the Department of Radiotherapy, University "Sapienza" for a neoplasm located in the rectum. The first symptom of the disease was rectal bleeding and, therefore, the patient underwent digital rectal examination (DRE), which revealed the presence of a round and irregular mass located in the anterior rectal wall. Subsequently, a colonoscopy was performed. The exam registered a round and hard consistent mass protruding into the lumen, located entirely in the lower rectum at a distance of 5 cm from the anal verge. Histological examination of the specimen revealed a SCC of the large intestine. A total body computed tomography (CT) scan was performed, which confirmed the presence of a round neoplasm with irregular margins of 30 mm × 20 mm × 21 mm (Figure 1A). The cranial limit of the mass was located approximately 25 mm from the anorectal junction along the anterior rectal wall. A small lymph node was visible in the mesorectum 2 cm above the lesion (Figure 1B). The perirectal fat was not involved and neither were the elevator muscles of the anus.

The presence of metastatic disease was excluded. The therapeutic strategy for such a case was discussed with our surgery team. Operative risk was considered high due to the patient's age and comorbidities, and surgery was excluded. The patient was referred for chemoradiation as a curative treatment. An endorectal ultrasound (ERUS) was also performed, which confirmed localization of the lesion in the anterior wall of the rectum with no extension in the anal canal (Figure 2). The exam revealed the presence of 2 round, 8 mm diameter, possibly involved lymph nodes located in the mesorectum 8 cm and 7 cm from the anal margin.

Given the squamous nature of the neoplasm and the choice of treatment, the disease was staged as clinical T2N1M0 (stage ⅢA) according to the TNM classification system for squamous cell cancer of the anus (AJCC Sixth Edition).

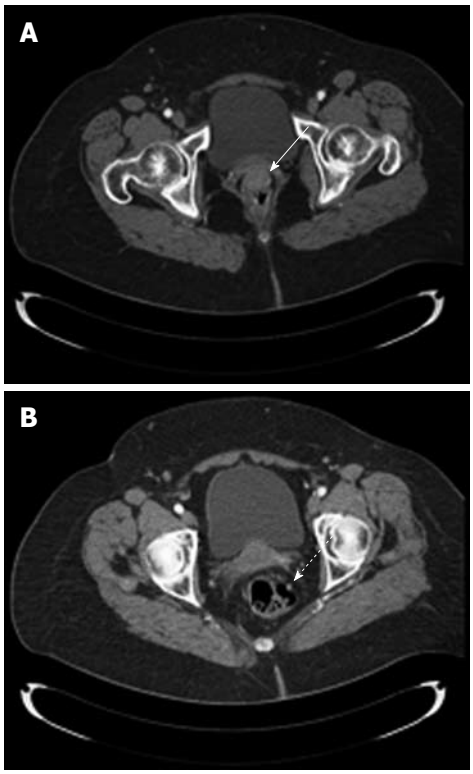

Figure 1 Pre-treatment computed tomography scans. A: The tumour mass (white arrow) occupying the anterior rectal wall; B: A small, possibly involved node on the left rectal wall (white dashed arrow).

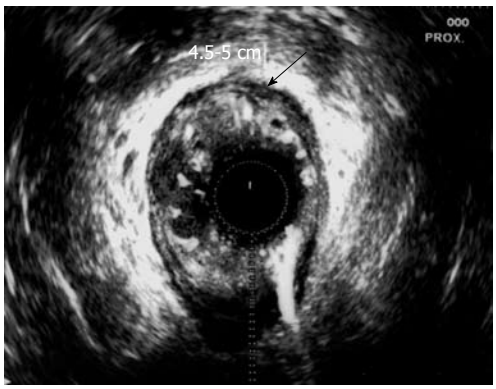

Figure 2 Pre-treatment endorectal ultrasound scan showing the inferior aspect of the mass located 4.5-5 cm from the anal margin (black arrow).

Treatment

Chemotherapy: A medical and physical exam, with complete laboratory tests, was performed before each cycle of chemotherapy. Chemotherapy consisted of continuous infusion of 5-FU 750 mg/mq die, days 1-4 and days 36-40, plus 10 mg/mq mitomycin days 1 and 36.

Radiotherapy: Radiotherapy was delivered using a linear accelerator with energy of 6-15 MV using a 3D conformal technique. The planning target volume 2 (PTV2) included the site of disease and pelvic nodal stations (internal iliac, external iliac, obturator, mesorectal, presacral and inguinal nodes).

The PTV1 encompassed the site of disease with an isotropic margin of 2 cm. The PTV2 received 45 Gy in 25 daily fractions of 1.8 Gy each. PTV1 was boosted to 59.4 Gy with the addition of 8 fractions using a multiple field technique. Toxicity was graded according the Common Terminology Criteria for Adverse Events version 3.0[7].

There was no haematological toxicity; gastrointestinal and skin toxicity adverse events were ⩽ G2. As expected, skin toxicity, grade 2, occurred bilaterally in the inguinal area and was controlled with proper topical treatment.

Results

The patient was revaluated 7 wk after the end of chemo-

Figure 3 Computed tomography scan performed after chemoradiation treatment. A: The anterior rectal wall appeared free of disease; B: The previously detected node appeared greatly reduced in size (white arrow).

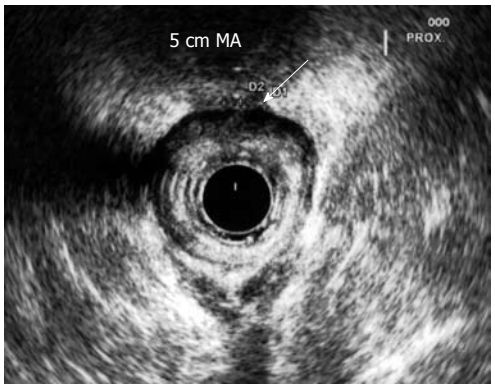

Figure 4 Endorectal ultrasound performed 12 wk after the end of chemoradiation. The tumour mass appeared reduced in size and hard to identify (white arrow). MA: Margin from anal verge.

radiation by DRE and ERUS. The anterior wall of the rectum appeared at DRE to be completely smooth with difficult identification of the treated lesion. Transanal ultrasound registered the presence of a hypoechoic scar located anteriorly in the rectum with a craniocaudal extension of 1 cm. A total body CT scan was performed 10 wk after the end of treatment. The lesion appeared greatly reduced in size and identifiable with difficulty, as was the small lymph node detected at the first CT scan (Figure 3).

Three months after the end of chemoradiation, a new ultrasound examination confirmed the reduction of the lesion with no pathological nodes identified in the meso-

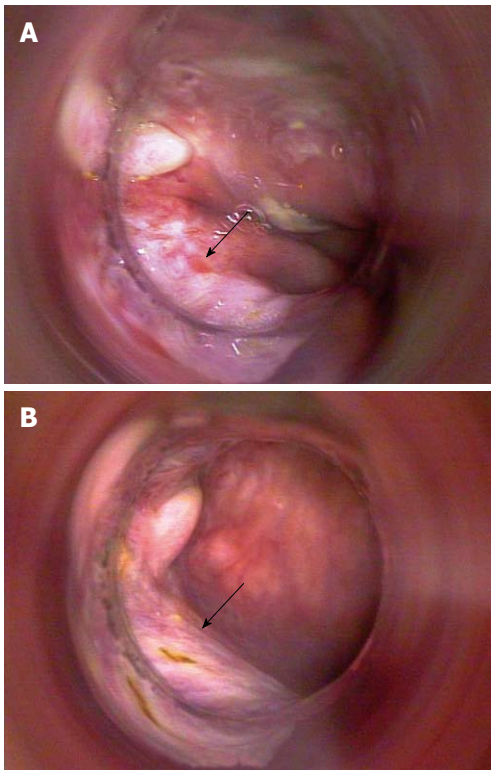

Figure 5 Images of proctoscopy (A, B) conducted 4 mo after the end of chemoradiation, which revealed the presence of a plain white scar at the site of previous disease (black arrows).

rectum (Figure 4). Given the initial desirable clinical outcome, a proctoscopy with possible biopsy was scheduled 4 mo after the end of treatment. Meanwhile, the patient underwent anal brushing to search for sequences of papillomavirus by means of PCR. The sample was negative for the presence of HPV6, HPV11, HPV16 and HPV18.

In December 2009, the patient underwent a first proctoscopy, which showed no lesions protruding into the intestinal lumen, but showed only the presence of a plain-white area at the site of the previous injury and no biopsies were performed (Figure 5A and B). One month later (5 mo after the end of treatment) a proctoscopy was executed and multiple biopsies were performed up to 8 cm from the anal margin. No residual cancer cells were found at the histological examination of specimens. A total body CT scan was also performed, which confirmed that the patient was free of disease 12 mo after the diagnosis of cancer.

DISCUSSION

Squamous cell cancer of the rectum is an extremely rare malignancy. It represents 0.1%-0.2% of all colorectal cancers. It seems to occur more frequently in women[8]. The review of Frizelle *et al*[9], conducted at the Mayo Clinic on all cases of adenosquamous carcinoma of the colon and rectum from 1907 to 1992, identified only 11 cases of pure SCC.

The etiology of SCC of the rectum is uncertain. Briefly, several theories have been proposed: (1) proliferation

of stem cells capable of multidirectional differentiation[10]; (2) differentiation of basal undifferentiated cells in squamous cells with subsequent malignant transformation[11]; (3) chronic irritation caused by conditions such as ulcerative colitis[12], radiation exposure[13], and HPV infection that can result in squamous metaplasia and subsequent tumor development; and (4) squamous differentiation of adenoma and adenocarcinoma[14]. Given the extreme rarity of this cancer, its natural history is not well known. Consequently, therapeutic strategy cannot be easily standardized. Traditionally, surgery is considered the most appropriate curative treatment. The surgical procedure depends on localization of the tumour mass and on TNM classification of the disease. In the case of advanced tumour, a conservative approach is not recommended. Total mesorectal excision, performed by anterior resection of the rectum or by abdominoperineal amputation with a definitive stoma, must be considered the preferred surgical option. Each type of surgery, however, is associated with a significant risk of morbidity (13%-46%) and mortality (1%-7%)[15].

Several authors suggested that chemoradiation could play a role in the treatment of squamous cell cancer of the rectum. Some researchers[16] investigated the effectiveness of chemoradiation as a postoperative treatment of this type of tumour, reporting a low profile of toxicity. Multimodal treatment did not show any advantage in terms of overall survival compared to surgery alone.

Other authors went even further, reporting their experience with chemoradiation as a definitive treatment for squamous cell cancer of the rectum. The series of Clark *et al*[17] included 7 patients treated by primary chemoradiation. Radiotherapy was administered at a dose of 30.6 Gy delivered to the primary tumour and the regional nodes. The tumour mass with a 2 cm margin was boosted to a total dose of a 50.4 Gy. The multimodal treatment was feasible; only one patient experienced severe anal soreness and had a 7 d break in the radiotherapy treatment.

Results of treatment were excellent; all patients but one showed a complete clinical response to chemoradiation. This patient, with a partial radiological response to treatment, decided to undergo surgery and no residual tumour was found at histological examination of the surgical specimen.

These findings demonstrate that definitive chemoradiation should be considered as a feasible and effective alternative to surgery. Acute toxicity of chemoradiation is low and long term toxicity, with symptomatic rectal stricture due to the non operative approach, is possible but its incidence is rarely reported in the literature[18]. A prospective comparison between the two therapeutic options is impossible, due to the rarity of this tumour. Nevertheless, some considerations are offered. First of all, the historical standard treatment for SCC of the anus was demolitive surgery by means of abdominoperineal amputation (Miles' intervention). It was only after the revolutionary work of Nigro[19], dated 1974, when chemoradiation was shown as effective as a primary treatment of epidermoid anal cancer. Currently, the latest update of the results of the ACT I trial[20], which compared chemoradiation to radiotherapy alone in the treatment of squamous anal cancer, showed that the superiority of chemoradiation is present even 12 years after treatment, confirming the association of radiotherapy and chemotherapy as the gold standard for anal cancer treatment.

In the case of rectal cancer, a different therapeutic strategy is required. Adenocarcinoma represents more than 90% of all rectal tumors and surgery, i.e. total mesorectal excision[21], must be considered as the milestone of a multimodal treatment, including radiotherapy and chemotherapy. Neoadjuvant chemoradiation has been demonstrated to reduce the rate of local recurrence compared to postoperative chemoradiation[22] The use of standard, 5-FU based preoperative chemoradiation in the case of adenocarcinoma of the rectum leads to a percentage of pathological complete response (pCR), which varies from 5% to 16%[23] in randomized phase Ⅲ studies. Several phase Ⅱ studies of intensified neoadjuvant treatment reported rates of pCR up to 30%[24]. The work of Habr-Gama *et al*[25] represents the first, successful, non operative approach to rectal cancer. This paper reported similar curves of survival between patients who avoided surgery and showed a clinical complete response, and operated patients registering a pathological complete response at histological examination.

In summary, non operative management represents the standard approach for anal cancer. In the case of squamous cell cancer of the rectum, a complete response to chemoradiation can be expected in the majority of patients, and surgery should be reserved for cases of treatment failure. The assessment of response to conservative therapy should be done 4-6 mo after the end of chemoradiation treatment.

In our paper, we described the case of a 78-year-old woman affected by squamous cell cancer of the rectum, successfully managed by chemoradiation as a definitive treatment. Chemoradiation was feasible, with a low profile of toxicity. It must be noted that, unlike other reports, in our case, radiotherapy was delivered with the use of 3D conformal technique, which permitted delivering high doses of radiation both to PTV2 and PTV1 (45 and 59.4 Gy, respectively) without exceeding nearby normal tissue tolerance. A further evolution of radiotherapy could be represented by the use of more sophisticated techniques, such as helical tomotherapy and intensity modulated radiation therapy, whose first experiences in the treatment of anal cancer were extremely promising in terms of local control and toxicity[26,27]. Squamous rectal cancer could also benefit from new radiotherapy techniques associated with well established protocols of chemotherapy, with the goal of making chemoradiation with radical intent the treatment of choice for this rare malignancy.

REFERENCES

1 **Dyson T**, Draganov PV. Squamous cell cancer of the rectum. *World J Gastroenterol* 2009; **15**: 4380-4386

2 **Anagnostopoulos G**, Sakorafas GH, Kostopoulos P, Grigoria-

dis K, Pavlakis G, Margantinis G, Vugiouklakis D, Arvanitidis D. Squamous cell carcinoma of the rectum: a case report and review of the literature. *Eur J Cancer Care* (Engl) 2005; **14**: 70-74
3 **Raiford TS**. Epitheliomata of the lower rectum and anus. *Surg Gynecol Obstet* 1933; **57**: 21-35
4 **Williams GT**, Blackshaw AJ, Morson BC. Squamous carcinoma of the colorectum and its genesis. *J Pathol* 1979; **129**: 139-147
5 **Rasheed S**, Yap T, Zia A, McDonald PJ, Glynne-Jones R. Chemo-radiotherapy: an alternative to surgery for squamous cell carcinoma of the rectum--report of six patients and literature review. *Colorectal Dis* 2009; **11**: 191-197
6 **Nahas CS**, Shia J, Joseph R, Schrag D, Minsky BD, Weiser MR, Guillem JG, Paty PB, Klimstra DS, Tang LH, Wong WD, Temple LK. Squamous-cell carcinoma of the rectum: a rare but curable tumor. *Dis Colon Rectum* 2007; **50**: 1393-1400
7 Cancer Therapy Evaluation Program: Common Terminology Criteria for Adverse Events, Version 3.0, Publish Date: August 9, 2006. Available from: URL: http://ctep.cancer.gov
8 **Lafreniere R**, Ketcham AS. Primary squamous carcinoma of the rectum. Report of a case and review of the literature. *Dis Colon Rectum* 1985; **28**: 967-972
9 **Frizelle FA**, Hobday KS, Batts KP, Nelson H. Adenosquamous and squamous carcinoma of the colon and upper rectum: a clinical and histopathologic study. *Dis Colon Rectum* 2001; **44**: 341-346
10 **Ouban A**, Nawab RA, Coppola D. Diagnostic and pathogenetic implications of colorectal carcinomas with multidirectional differentiation: a report of 4 cases. *Clin Colorectal Cancer* 2002; **1**: 243-248
11 **Michelassi F**, Mishlove LA, Stipa F, Block GE. Squamous-cell carcinoma of the colon. Experience at the University of Chicago, review of the literature, report of two cases. *Dis Colon Rectum* 1988; **31**: 228-235
12 **Michelassi F**, Montag AG, Block GE. Adenosquamous-cell carcinoma in ulcerative colitis. Report of a case. *Dis Colon Rectum* 1988; **31**: 323-326
13 **Yurdakul G**, de Reijke TM, Blank LE, Rauws EA. Rectal squamous cell carcinoma 11 years after brachytherapy for carcinoma of the prostate. *J Urol* 2003; **169**: 280
14 **Audeau A**, Han HW, Johnston MJ, Whitehead MW, Frizelle FA. Does human papilloma virus have a role in squamous cell carcinoma of the colon and upper rectum? *Eur J Surg Oncol* 2002; **28**: 657-660
15 **Martling AL**, Holm T, Rutqvist LE, Moran BJ, Heald RJ, Cedemark B. Effect of a surgical training programme on outcome of rectal cancer in the County of Stockholm. Stockholm Colorectal Cancer Study Group, Basingstoke Bowel Cancer Research Project. *Lancet* 2000; **356**: 93-96
16 **Schneider TA 2nd**, Birkett DH, Vernava AM 3rd. Primary adenosquamous and squamous cell carcinoma of the colon and rectum. *Int J Colorectal Dis* 1992; **7**: 144-147
17 **Clark J**, Cleator S, Goldin R, Lowdell C, Darzi A, Ziprin P. Treatment of primary rectal squamous cell carcinoma by primary chemoradiotherapy: should surgery still be considered a standard of care? *Eur J Cancer* 2008; **44**: 2340-2343
18 **Brammer RD**, Taniere P, Radley S. Metachronous squamous-cell carcinoma of the colon and treatment of rectal squamous carcinoma with chemoradiotherapy. *Colorectal Dis* 2009; **11**: 219-220
19 **Nigro ND**, Vaitkevicius VK, Considine B Jr. Combined therapy for cancer of the anal canal: a preliminary report. *Dis Colon Rectum* 1974; **17**: 354-356
20 **Northover J**, Glynne-Jones R, Sebag-Montefiore D, James R, Meadows H, Wan S, Jitlal M, Ledermann J. Chemoradiation for the treatment of epidermoid anal cancer: 13-year follow-up of the first randomised UKCCCR Anal Cancer Trial (ACT I). *Br J Cancer* 2010; **102**: 1123-1128
21 **Heald RJ**, Ryall RD. Recurrence and survival after total mesorectal excision for rectal cancer. *Lancet* 1986; **1**: 1479-1482
22 **Glynne-Jones R**, Mawdsley S, Pearce T, Buyse M. Alternative clinical end points in rectal cancer--are we getting closer? *Ann Oncol* 2006; **17**: 1239-1248
23 **Sauer R**, Becker H, Hohenberger W, Rödel C, Wittekind C, Fietkau R, Martus P, Tschmelitsch J, Hager E, Hess CF, Karstens JH, Liersch T, Schmidberger H, Raab R. Preoperative versus postoperative chemoradiotherapy for rectal cancer. *N Engl J Med* 2004; **351**: 1731-1740
24 **Gambacorta MA**, Valentini V, Coco C, Morganti AG, Smaniotto D, Miccichè F, Mantini G, Barbaro B, Garcia-Vargas JE, Magistrelli P, Picciocchi A, Cellini N. Chemoradiation with raltitrexed and oxaliplatin in preoperative treatment of stage II-III resectable rectal cancer: Phase I and II studies. *Int J Radiat Oncol Biol Phys* 2004; **60**: 139-148
25 **Habr-Gama A**, Perez RO, Nadalin W, Sabbaga J, Ribeiro U Jr, Silva e Sousa AH Jr, Campos FG, Kiss DR, Gama-Rodrigues J. Operative versus nonoperative treatment for stage 0 distal rectal cancer following chemoradiation therapy: long-term results. Ann Surg 2004; 240: 711-717; discussion 717-718
26 **Pepek JM**, Willett CG, Wu QJ, Yoo S, Clough RW, Czito BG. Intensity-Modulated Radiation Therapy for Anal Malignancies: A Preliminary Toxicity and Disease Outcomes Analysis. *Int J Radiat Oncol Biol Phys* 2010; Epub ahead of print
27 **Joseph KJ**, Syme A, Small C, Warkentin H, Quon H, Ghosh S, Field C, Pervez N, Tankel K, Patel S, Usmani N, Severin D, Nijjar T, Fallone G, Pedersen J. A treatment planning study comparing helical tomotherapy with intensity-modulated radiotherapy for the treatment of anal cancer. *Radiother Oncol* 2010; **94**: 60-66

S- Editor Cheng JX **L- Editor** Lutze M **E- Editor** Zheng XM

World Journal of Radiology

Online Submissions: http://www.wjgnet.com/1949-8470office
wjr@wjgnet.com
doi:10.4329/wjr.v2.i8.334

World J Radiol 2010 August 28; 2(8): 334-338
ISSN 1949-8470 (online)

CASE REPORT

Primary esophageal lymphoma in immunocompetent patients: Two case reports and literature review

Prasanna Ghimire, Guang-Yao Wu, Ling Zhu

Prasanna Ghimire, Guang-Yao Wu, Ling Zhu, Department of Magnetic Resonance Imaging, Zhongnan Hospital, Wuhan University, Wuhan 430071, Hubei Province, China

Author contributions: Ghimire P served as the primary author, reviewed the literature and wrote the case report; Wu GY and Ling Z reviewed the manuscript.

Correspondence to: Guang-Yao Wu, MD, PhD, Department of Magnetic Resonance Imaging, Zhongnan Hospital, Wuhan University, 169 East Lake Road, Wuhan 430071, Hubei Province, China. wuguangy2002@yahoo.com.cn

Telephone: +86-27-67813187 Fax: +86-27-67813188
Received: May 4, 2010 Revised: May 27, 2010
Accepted: June 4, 2010
Published online: August 28, 2010

Abstract

Primary lymphoma that involves the esophagus is very rare, with fewer than 30 cases reported in the English-language literature. Non-Hodgkin lymphoma accounts for most of the cases. Esophageal lymphomas have varied radiological appearances, which poses diagnostic difficulty. We report two cases of histopathologically confirmed primary diffuse large B-cell esophageal lymphoma and describe their radiological features, and briefly review the literature.

Key words: Esophageal neoplasms; Non-Hodgkin lymphoma; Primary lymphoma; Esophagography; Computed tomography

Peer reviewer: Yasunori Minami, MD, PhD, Division of Gastroenterology and Hepatology, Department of Internal Medicine, 377-2, Ohno-higashi, Osaka-sayama 589-8511, Japan

Ghimire P, Wu GY, Zhu L. Primary esophageal lymphoma in immunocompetent patients: Two case reports and literature review. *World J Radiol* 2010; 2(8): 334-338 Available from: URL: http://www.wjgnet.com/1949-8470/full/v2/i8/334.htm DOI: http://dx.doi.org/10.4329/wjr.v2.i8.334

INTRODUCTION

The gastrointestinal (GI) tract is the most common extranodal site for involvement by non-Hodgkin lymphoma[1]. Esophageal lymphoma accounts for < 1% of all GI lymphomas, and usually results from metastasis from the cervical or mediastinal lymph nodes or extension of a gastric lymphoma[2]. Primary esophageal lymphoma in immunocompetent patient is very rare[3-5]. Furthermore, imaging findings of esophageal lymphoma are nonspecific, thus posing a diagnostic dilemma[6,7]. We report two histopathologically confirmed cases of diffuse large B-cell non-Hodgkin lymphomas, describe their radiological and endoscopic features, and briefly review the literature.

CASE REPORT

Case 1

A 41-year-old man came to our hospital in April 2009 for evaluation of progressive dysphagia that was present only with solid food ingestion over the previous 1 mo. He had no other complaint and no evidence of any immunosuppressive disease, and physical examination, laboratory findings, chest radiography, and abdominal ultrasonography were unremarkable. Barium esophagography revealed an irregular wavy outline as a filling defect, with evidence of significant short segment narrowing of the distal esophagus that involved mainly the right side posterolaterally (Figure 1). Esophagogastroduodenoscopy revealed an esophageal ulcer starting at 32 cm of incisor teeth which measured approximately 1.8 cm × 1.4 cm. The remaining esophagus was irregular and erythematous. The stomach and duodenum were normal in appearance. Biopsy specimens were taken from multiple sites of the esophagus,

Figure 1 Barium esophagogram shows irregular outline and multiple filling defects (arrow), with short segment narrowing of the distal segment of the esophagus involving right side posterolaterally.

and revealed fibrin necrotic exudates with no evidence of dysplasia or neoplastic cells. Computed tomography (CT) of the thorax demonstrated asymmetric circumferential thickening of the esophageal wall that extended from the level of the carina to the diaphragm, which resulted in narrowing of the esophageal lumen. The gastroesophageal junction appeared normal. The fat plane between the thickened esophageal wall and surrounding structures was well maintained (Figure 2). There was no cervical or mediastinal lymphadenopathy. CT of the abdomen and pelvis was normal. The patient underwent subtotal esophagectomy with gastric pull-up reconstruction, along with radical thoracic and abdominal lymphadenectomy. Histological examination of the biopsy specimen from the mass was suggestive of diffuse large B-cell lymphoma (Figure 3). An immunohistochemical study confirmed an LCA-positive B-cell phenotype that stained positively for B-cell markers CD20 and CD79, and negatively for T-cell markers CD3 and CD5. Bone marrow biopsy specimens from the iliac crest were negative for lymphoma cells. In accordance with the Ann Arbor classification system, this was a stage IEA lymphoma of the esophagus. The patient recovered well from surgery. Postoperatively, he was treated with six cycles of immunochemotherapy in the form of R-CHOP (anti-CD20 monoclonal antibody rituximab, with cyclophosphamide, doxorubicin, vincristine sulfate and prednisolone) followed by irradiation. The patient achieved complete remission. Follow-up investigations ruled out any relapse and he was disease free until this article was written.

Case 2

A 77-year-old man was referred from another hospital for further workup and management of his illness. He had complained of dysphagia for solid food with loss of appetite for the past 2 mo. His past medical history was unremarkable except for hypertension, for which he had been taking antihypertensive drugs. His physical examination was not significant and did not reveal any signs that were suggestive of immune suppression. Blood parameters and serum chemistry were all within normal limits. The investigations performed in the other hospital included barium esophagography that showed multiple filling defects in the distal segment of the esophagus. Esophagogastroduodenoscopy showed multiple solid, irregular and firm nodular lesions starting at 27-31 cm from the incisor teeth, and the rest of the esophagus, stomach and duodenum was normal. Endoscopic biopsy specimens from the lesion were inconclusive for a diagnosis. Chest CT demonstrated concentric thickening of the esophageal wall, with slight enlargement of the subcarinal lymph nodes. The remaining thoracic CT and abdominal and pelvic CT were normal. Repeat esophagogastroduodenoscopy performed in our institution also demonstrated similar endoscopic findings (Figure 4). Multiple endoscopic biopsies were required from the lesion before pathological evaluation revealed the diagnosis of diffuse large B-cell lymphoma, which was confirmed by immunohistochemistry. A bone marrow biopsy was done from the iliac crest, which did not show any evidence of malignancy. After disclosure of the diagnosis, the patient refused further investigation and declined treatment, and was discharged on request.

DISCUSSION

The GI tract is the most common extranodal site for non-Hodgkin lymphoma, and accounts for 5%-20% of all cases, whereas some autopsy studies have revealed almost 50% involvement[1]. The stomach is the most common of the GI sites to be involved (48%-50%), followed by small intestine (30%-37%), and ileocecal region (12%-13%). The esophagus is a distinctly rare site to be involved and accounts for < 1% of all GI lymphomas[2]. Esophageal involvement usually results from metastasis from cervical or mediastinal lymph nodes or extension from gastric lymphoma. Primary esophageal lymphoma is an extremely rare occurrence, with fewer than 30 cases reported in the literature, with the majority being diffuse large B-cell type non-Hodgkin lymphomas. The age of presentation of the disease is highly variable. The etiology of the disease is unknown, with the role of Epstein-Barr virus being controversial. It has been noticed that it is most common in immunocompromised patients, with HIV infection as a probable risk factor[3-5]. Radiological and endoscopic findings of esophageal lymphoma are very varied and are nonspecific, which poses diagnostic challenges when differentiating it from other benign and malignant lesions[6,7].

Ann Arbor (AA) staging with Cotswold modification is now universally adopted for Hodgkin's as well as non-Hodgkin lymphoma. However, this staging has a number of shortcomings that are related to the different pattern of disease presentation in non-Hodgkin lymphoma, its inability to incorporate the grade of the tumor, as well as disease prognosis. Many types of lymphoma, particularly the indolent B-cell non-Hodgkin' lymphoma have bone marrow involvement in most cases, thus characterizing them as stage Ⅳ by AA staging. As bone marrow involve-

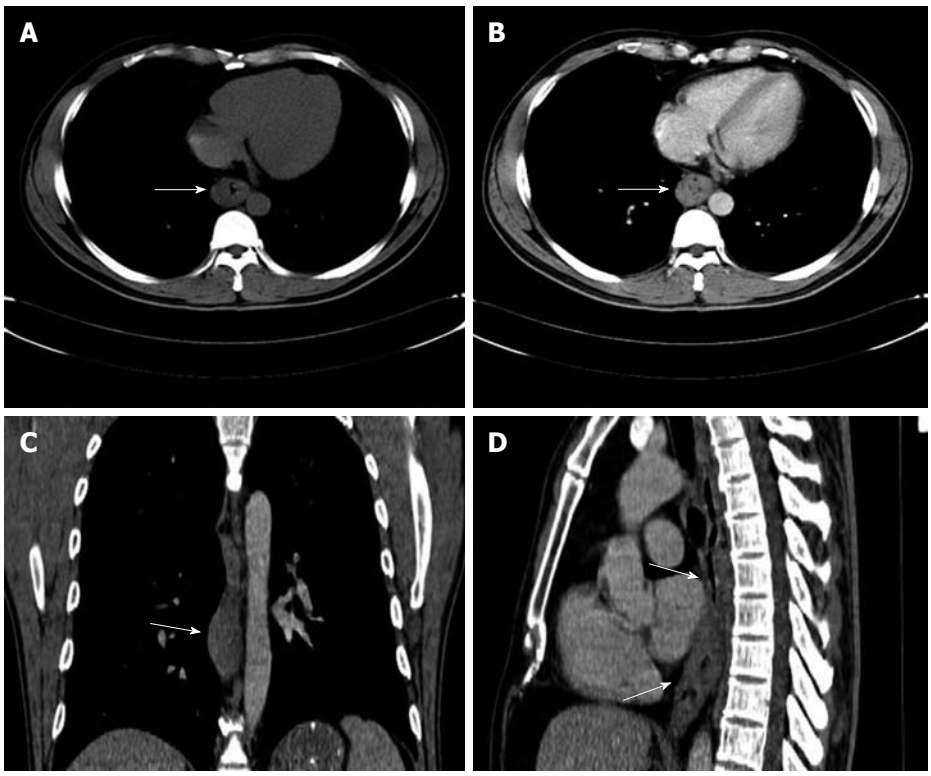

Figure 2 Computed tomography scan of the thorax. A: Plain computed tomography (CT) showing asymmetrical thickening of the esophageal wall (white arrow) with maintenance of the surrounding fat plane. No mediastinal lymphadenopathy is seen; B: Contrast-enhanced CT shows moderate enhancement of the lesion (white arrow); C: Coronal multiplanar reconstructed (MPR) CT image demonstrating the thickened esophagus (white arrow); D: Sagittal MPR CT image showing extension of the lesion (between two arrows).

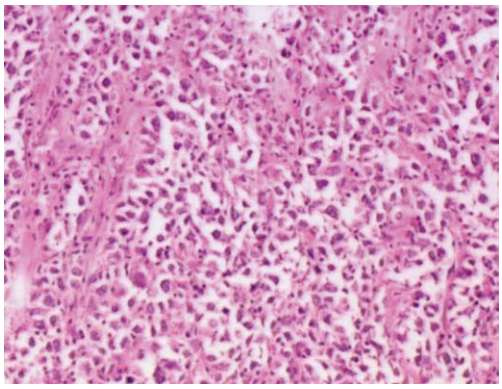

Figure 3 Photomicrograph of the biopsy specimen demonstrating large transformed lymphoid cells with vesicular nuclei and prominent nucleoli, which was suggestive of diffuse large B-cell lymphoma (hematoxylin and eosin, × 200).

ment does not independently confer a worse prognosis, this staging has a limited predictive value, thus warranting further workup[8].

The various radiographic patterns that have been described in the literature for esophageal lymphoma include stricture, ulcerated mass, multiple submucosal nodules, varicoid pattern, achalasia-like pattern, progressive aneurysmal dilatation, and tracheoesophageal fistula formation, with none being diagnostic[9-11]. Endoscopic ultrasound (EUS) has gained clinical acceptance for assessment of lymphoma and preoperative staging, because it can accurately depict the structural abnormalities and depth of invasion of the lesions. EUS appearance however is not pathognomonic, with presentation varying as anechoic, hypoechoic or even as hyperechoic masses[12,13]. CT findings of esophageal lymphoma are nonspecific and not diagnostic, with features such as thickening of the wall mimicking other common tumors, such as esophageal carcinoma. CT, however, is valuable for the evaluation of the extraluminal component of an esophageal mass, its mediastinal extension, any fistula formation, and status of lymph nodes, therefore, it has a role in disease staging, assisting in stratification of various available treatments, evaluating treatment responses, monitoring patient progress, as well as detection of any relapses. Recently, incorporation of positron emission tomography with CT (PET/CT) has emerged as an indispensable tool in the staging and follow-up of patients with extranodal involvement in Hodgkin's and non-Hodgkin lymphoma, with increased sensitivity and specificity. Diffuse large B-cell non-Hodgkin lymphoma of the esophagus has been shown to manifest as circumferential thickening of the wall, with diffuse increased fluorodeoxyglucose (FDG) uptake. However, intensity of FDG uptake in lymphoma is influenced by various intrinsic tumor factors such as histological features and grade, as well as various extrinsic factors. With proper correlation, FDG PET/CT has also significantly increased the detection of indolent lesions that were undetected by conventional cross-sectional imaging[14].

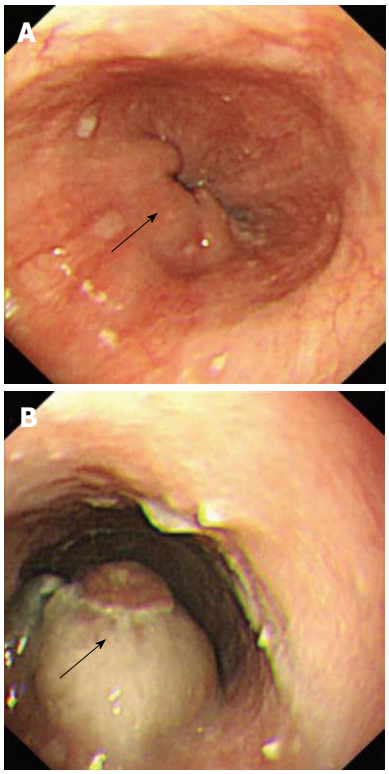

Figure 4 Esophagogastroduodenoscopy (A and B) showing multiple solid, firm nodular lesions in the lower esophagus. Overlying mucosa appearing relatively normal (black arrows).

In our first patient, the radiological findings were nonspecific to lymphoma. The presence of asymmetric circumferential thickening of esophageal wall is also evident in other malignant lesions such as carcinoma or metastases, or even in some benign lesions[6,7]. Preservation of the fat plane despite the size of the lesion and extent of infiltration was supportive of the diagnosis of lymphoma. Endoscopic features of the lesion preferentially suggested a diagnosis of carcinoma rather than lymphoma. Besides, repeated endoscopic biopsies of the lesion also did not yield a definite diagnosis. This posed a diagnostic difficulty that required further investigation. As management of the case depended on accurate diagnosis, further workup was mandatory to rule out the various possibilities. The definite diagnosis of lymphoma was made by histopathology and immunohistochemistry of the surgically removed specimen. Our patient fulfilled all of Dawson's criteria for making a retrospective clinical diagnosis of primary lymphoma, which include lesions that are localized to the GI tract with or without regional lymphadenopathy, and the absence of: (1) peripheral lymphadenopathy; (2) mediastinal adenopathy; (3) liver or spleen involvement; and (4) normal peripheral blood counts[15].

In the second patient, radiological findings were too inconclusive for the diagnosis of esophageal lymphoma. The finding of a non-ulcerative submucosal mass by esophagogastroduodenoscopy prompted suspicion of lymphoma, although this feature is also nonspecific and can even be seen in carcinoma as well as other benign submucosal lesions such as leiomyoma. Repeated endoscopic biopsies were required for the final pathological diagnosis, thus emphasizing the difficulty in diagnosis of primary esophageal lymphoma. It has been questioned whether the application of Dawson's criteria for the diagnosis of primary GI lymphoma holds true for the esophagus. Modifications as exclusion of mediastinal lymphadenopathy in the criteria for primary esophageal lymphoma have been suggested[16]. Of particular interest in our second patient was the finding of a mildly enlarged subcarinal lymph node. We believe that Dawson's criteria is not appropriate for diagnosis of esophageal lymphoma, because the esophagus is mostly a mediastinal structure that has an extensive lymphatic network with rich mucosal and submucosal lymphatics in the wall, which results in wide lymph node basins. Therefore, based on the predominant lesion in the esophagus of the patient with no involvement of liver, spleen, peripheral lymph nodes and with normal blood parameters we did not consider absence of mediastinal lymphadenopathy as a strict criterion of primary esophageal lymphoma.

To conclude, we have presented two cases of primary esophageal lymphoma in immunocompetent patients highlighting the difficulty in the accurate diagnosis radiologically requiring a tissue diagnosis. Even in immunocompetent patients with dysphagia, in whom radiological findings are equivocal, a high index of suspicion for lymphoma should also be borne in mind, because accurate diagnosis is pivotal to prognosis and deciding on treatment. We also briefly reviewed the literature, with an emphasis on the radiological spectrum of disease presentation.

REFERENCES

1 **Freeman C**, Berg JW, Cutler SJ. Occurrence and prognosis of extranodal lymphomas. *Cancer* 1972; **29**: 252-260
2 **Herrmann R**, Panahon AM, Barcos MP, Walsh D, Stutzman L. Gastrointestinal involvement in non-Hodgkin's lymphoma. *Cancer* 1980; **46**: 215-222
3 **Weeratunge CN**, Bolivar HH, Anstead GM, Lu DH. Primary esophageal lymphoma: a diagnostic challenge in acquired immunodeficiency syndrome--two case reports and review. *South Med J* 2004; **97**: 383-387
4 **Taal BG**, Van Heerde P, Somers R. Isolated primary oesophageal involvement by lymphoma: a rare cause of dysphagia: two case histories and a review of other published data. *Gut* 1993; **34**: 994-998
5 **Radin DR**. Primary esophageal lymphoma in AIDS. *Abdom Imaging* 1993; **18**: 223-224
6 **Wagner PL**, Tam W, Lau PY, Port JL, Paul S, Altorki NK, Lee PC. Primary esophageal large T-cell lymphoma mimicking esophageal carcinoma: a case report and literature review. *J Thorac Cardiovasc Surg* 2008; **135**: 957-958, 958.e1
7 **Kaplan KJ**. Primary esophageal lymphoma: a diagnostic challenge. *South Med J* 2004; **97**: 331-332
8 **Armitage JO**. Staging non-Hodgkin lymphoma. *CA Cancer J Clin* 2005; **55**: 368-376
9 **Carnovale RL**, Goldstein HM, Zornoza J, Dodd GD. Radiologic manifestations of esophageal lymphoma. *AJR Am J Roentgenol* 1977; **128**: 751-754
10 **Levine MS**, Sunshine AG, Reynolds JC, Saul SH. Diffuse nodularity in esophageal lymphoma. *AJR Am J Roentgenol*

1985; **145**: 1218-1220
11 **Coppens E**, El Nakadi I, Nagy N, Zalcman M. Primary Hodgkin's lymphoma of the esophagus. *AJR Am J Roentgenol* 2003; **180**: 1335-1337
12 **Kalogeropoulos IV**, Chalazonitis AN, Tsolaki S, Laspas F, Ptohis N, Neofytou I, Rontogianni D. A case of primary isolated non-Hodgkin's lymphoma of the esophagus in an immunocompetent patient. *World J Gastroenterol* 2009; **15**: 1901-1903
13 **Bolondi L**, De Giorgio R, Santi V, Paparo GF, Pileri S, Di Febo G, Caletti GC, Poggi S, Corinaldesi R, Barbara L. Primary non-Hodgkin's T-cell lymphoma of the esophagus. A case with peculiar endoscopic ultrasonographic pattern. *Dig Dis Sci* 1990; **35**: 1426-1430
14 **Paes FM**, Kalkanis DG, Sideras PA, Serafini AN. FDG PET/CT of extranodal involvement in non-Hodgkin lymphoma and Hodgkin disease. *Radiographics* 2010; **30**: 269-291
15 **Dawson IM**, Cornes JS, Morson BC. Primary malignant lymphoid tumours of the intestinal tract. Report of 37 cases with a study of factors influencing prognosis. *Br J Surg* 1961; **49**: 80-89
16 **Chadha KS**, Hernandez-Ilizaliturri FJ, Javle M. Primary esophageal lymphoma: case series and review of the literature. *Dig Dis Sci* 2006; **51**: 77-83

S- Editor Cheng JX **L- Editor** Kerr C **E- Editor** Zheng XM

World Journal of Radiology

Online Submissions: http://www.wjgnet.com/1949-8470office
wjr@wjgnet.com
www.wjgnet.com

World J Radiol 2010 August 28; 2(8): I
ISSN 1949-8470 (online)

Acknowledgments to reviewers of *World Journal of Radiology*

Many reviewers have contributed their expertise and time to the peer review, a critical process to ensure the quality of *World Journal of Radiology*. The editors and authors of the articles submitted to the journal are grateful to the following reviewers for evaluating the articles (including those published in this issue and those rejected for this issue) during the last editing time period.

Alain Chapel, PhD, Institut de Radioprotection et de S reté Nucléaire, DPHD, IRSN. B.P. no 17, F-92262 Fontenay-Aux-Roses, France

James Chow, PhD, Radiation Physicist, Radiation Medicine Program, Princess Margaret Hospital, 610 University Avenue, Toronto, ON, M5G 2M9, Canada

Kenneth Coenegrachts, MD, PhD, Department of Radiology, AZ St.-Jan AV, Ruddershove 10, B-8000 Bruges, Belgium

Thomas J George, Jr., MD, FACP, Assistant Professor, Director, GI Oncology Program, Associate Director, HemOnc Fellowship Program, University of Florida, Division of Hematology and Oncology, 1600 SW Archer Road, PO Box 100277, Gainesville, FL 32610, United States

Rajasvaran Logeswaran, PhD, Associate Professor, Faculty of Engineering, Multimedia University, 63100 Cyberjaya, Malaysia

Heriberto Medina-Franco, MD, National Institute of Medical Sciences and Nutrition "Salvador Zubiran", Vasco de Quiroga 15 Colonia Seccion XVI, Mexico City ZIP 14000, Mexico

Yasunori Minami, MD, PhD, Division of Gastroenterology and Hepatology, Department of Internal Medicine, 377-2, Ohno-higashi, Osaka-sayama 589-8511, Japan

Antonio Pinto, MD, PhD, Department of Radiology, Cardarelli Hospital, Via Posillipo 168/D, I-80123, Naples, Italy

Charikleia Triantopoulou, MD, PhD, Head of Radiology Department, Konstantopouleio general Hospital, 3-5, Agias Olgas street, 14233 N. Ionia, Athens, Greece

WJR World Journal of Radiology

Online Submissions: http://www.wjgnet.com/1949-8470office
wjr@wjgnet.com
www.wjgnet.com

World J Radiol 2010 August 28; 2(8): I
ISSN 1949-8470 (online)

Meetings

Events Calendar 2010

January 4-8
Beaver Creek, Colorado, United States
18th Annual Winter Diagnostic Imaging Update

January 7-9
Leuven, Belgium
4th Leuven Course on Ear Imaging

January 16-17
Hollywood, Florida, United States
The Symposium on Clinical Interventional Oncology

January 17-21
Hollywood, Florida, United States
The International Symposium on Endovascular Therapy

January 21-22
Cairo, Egypt
BGICC Breast Gyne International Cancer Conference

January 21-24
Phoenix, AZ, United States
13th Society for Cardiovascular Magnetic Resonance (SCMR) Annual Scientific Sessions

January 23-23
Atlanta, GA, United States
Emory Winship Cancer Institute: Breast Cancer 2010: Advances in Science, Emerging Data, and Novel Therapeutics

January 25-29
Maui, HI, United States
Musculoskeletal & Neuroradiology MR Imaging Update in Maui

January 27-February 2
Albuquerque, NM, United States
2010 SNM Conjoint Mid-Winter Meetings

January 29-30
Barcelona, Spain
7th European Congress: Perspectives in Gynecologic Oncology

February 7-12
Vail, CO, United States
15th Annual Vail 2010: Multislice CT in Clinical Practice

February 11-13
Las Vegas, NV, United States
5th Annual Symposium on PET/CT and Molecular Imaging

February 16-19
Park City, UT, United States
6th Interventional/ Neurointerventional Conference

February 18-19
London, United Kingdom
Diagnostic and Interventional Radiology

February 18-21
Las Vegas, NV, United States
American Society of Spine Radiology Annual Symposium

February 20-20
Jacksonville, Florida, United States
Mayo Clinic Molecular Markers and Management of Breast Cancer

February 20-21
Bethesda, Maryland, United States
25th Anniversary Washington Neuroradiology Review

February 21-26
Orlando, FL, United States
The Abdominal Radiology Course

February 21-27
Snowmass, CO, United States
16th Annual Snowmass 2010: Clinical Ultrasound

February 22-26
Bethesda, MD, United States
48th Annual Dr. Kenneth M. Earle Memorial Neuropathology Review

February 24-27
Lake Buena Vista, FL, United States
ACRO 2010 American College of Radiation Oncology Symposium: Clinical Radiation Oncology Challenges

February 25-27
Chandler, AZ, United States
Multidisciplinary Head and Neck Cancer Symposium

February 26-27
Brussels, Belgium
10èmes Mises au Point en Imagerie Ostéo-Articulaire

February 27-March 1
Cairo, Egypt
7th Gastroenterology Hepatology & Endoscopy Symposium

February 28-March 4
Scottsdale, AZ, United States
International Congress XXIII on Endovascular Interventions

February 28-March 5
Breckenridge, CO, United States
5th Annual Breckenridge 2010: Musculoskeletal MRI

March 3-6
Las Vegas, Nevada, United States
11th Annual Advances in Breast Imaging and Interventions

March 4-8
Vienna, Austria
European Congress of Radiology (ECR 2010) Annual Meeting

March 5-7
Mt Tremblant, QC, Canada
Neuroimaging and Head & Neck Radiology Update in Mt Tremblant

March 7-11
San Diego, CA, United States
SCBT-MR Masters in Body Imaging: "What's New, What's Hot, What You May Not Have Known"

March 10-13
San Antonio, Texas, United States
Clinical Osteoporosis 2010: An ISCD-NOF Symposium

March 11-13
Barcelona, Spain
EORTC Group Meeting: EORTC Radiation Oncology Group

March 11-13
Hannover, Germany
40. Kongress der Deutschen Gesellschaft für Endoskopie und Bildgebende Verfahren e.V.

March 13-18
Tampa, FL, United states
Society of interventional radiology 35th Annual Scientific Meeting

March 14-17
Park City, UT, United States
14th Annual Park City 2010: MRI in Clinical Practice

March 22-26
Beaver Creek, CO, United States
NYU Radiology Spring Skiing Symposium in Beaver Creek

March 22-26
Maui, HI, United States
18th Annual Spring Diagnostic Imaging Update

March 24-27
San Diego, California, United States
2010 American institute of ultrasound in Medicine Annual Convention Preliminary Program

March 24-27
Barcelona, Spain
7th European Breast Cancer Conference

April 8-12
Shanghai, China
The 26th International Congress of Radiology

September 8-12
Guangzhou, China
Chinese Society of Interventional Radiology, 2010 CSIR

November 28-December 03
Chicago, United States
Radiological Society of North America: 2010 Annual Meeting

World Journal of Radiology

Online Submissions: http://www.wjgnet.com/1949-8470office
wjr@wjgnet.com
www.wjgnet.com

World J Radiol 2010 August 28; 2(8): I-V
ISSN 1949-8470 (online)

Instructions to authors

GENERAL INFORMATION

World Journal of Radiology (*World J Radiol*, *WJR*, online ISSN 1949-8470, DOI: 10.4329), is a monthly, open-access (OA), peer-reviewed journal supported by an editorial board of 319 experts in Radiology from 40 countries.

The biggest advantage of the OA model is that it provides free, full-text articles in PDF and other formats for experts and the public without registration, which eliminates the obstacle that traditional journals possess and usually delays the speed of the propagation and communication of scientific research results. The open access model has been proven to be a true approach that may achieve the ultimate goal of the journals, i.e. the maximization of the value to the readers, authors and society.

Maximization of personal benefits

The role of academic journals is to exhibit the scientific levels of a country, a university, a center, a department, and even a scientist, and build an important bridge for communication between scientists and the public. As we all know, the significance of the publication of scientific articles lies not only in disseminating and communicating innovative scientific achievements and academic views, as well as promoting the application of scientific achievements, but also in formally recognizing the "priority" and "copyright" of innovative achievements published, as well as evaluating research performance and academic levels. So, to realize these desired attributes of *WJR* and create a well-recognized journal, the following four types of personal benefits should be maximized. The maximization of personal benefits refers to the pursuit of the maximum personal benefits in a well-considered optimal manner without violation of the laws, ethical rules and the benefits of others. (1) Maximization of the benefits of editorial board members: The primary task of editorial board members is to give a peer review of an unpublished scientific article via online office system to evaluate its innovativeness, scientific and practical values and determine whether it should be published or not. During peer review, editorial board members can also obtain cutting-edge information in that field at first hand. As leaders in their field, they have priority to be invited to write articles and publish commentary articles. We will put peer reviewers' names and affiliations along with the article they reviewed in the journal to acknowledge their contribution; (2) Maximization of the benefits of authors: Since *WJR* is an open-access journal, readers around the world can immediately download and read, free of charge, high-quality, peer-reviewed articles from *WJR* official website, thereby realizing the goals and significance of the communication between authors and peers as well as public reading; (3) Maximization of the benefits of readers: Readers can read or use, free of charge, high-quality peer-reviewed articles without any limits, and cite the arguments, viewpoints, concepts, theories, methods, results, conclusion or facts and data of pertinent literature so as to validate the innovativeness, scientific and practical values of their own research achievements, thus ensuring that their articles have novel arguments or viewpoints, solid evidence and correct conclusion; and (4) Maximization of the benefits of employees: It is an iron law that a first-class journal is unable to exist without first-class editors, and only first-class editors can create a first-class academic journal. We insist on strengthening our team cultivation and construction so that every employee, in an open, fair and transparent environment, could contribute their wisdom to edit and publish high-quality articles, thereby realizing the maximization of the personal benefits of editorial board members, authors and readers, and yielding the greatest social and economic benefits.

Aims and scope

The major task of *WJR* is to rapidly report the most recent improvement in the research of medical imaging and radiation therapy by the radiologists. *WJR* accepts papers on the following aspects related to radiology: Abdominal radiology, women health radiology, cardiovascular radiology, chest radiology, genitourinary radiology, neuroradiology, head and neck radiology, interventional radiology, musculoskeletal radiology, molecular imaging, pediatric radiology, experimental radiology, radiological technology, nuclear medicine, PACS and radiology informatics, and ultrasound. We also encourage papers that cover all other areas of radiology as well as basic research.

Columns

The columns in the issues of *WJR* will include: (1) Editorial: To introduce and comment on major advances and developments in the field; (2) Frontier: To review representative achievements, comment on the state of current research, and propose directions for future research; (3) Topic Highlight: This column consists of three formats, including (A) 10 invited review articles on a hot topic, (B) a commentary on common issues of this hot topic, and (C) a commentary on the 10 individual articles; (4) Observation: To update the development of old and new questions, highlight unsolved problems, and provide strategies on how to solve the questions; (5) Guidelines for Basic Research: To provide guidelines for basic research; (6) Guidelines for Clinical Practice: To provide guidelines for clinical diagnosis and treatment; (7) Review: To review systemically progress and unresolved problems in the field, comment on the state of current research, and make suggestions for future work; (8) Original Articles: To report innovative and original findings in radiology; (9) Brief Articles: To briefly report the novel and innovative findings in radiology; (10) Case Report: To report a rare or typical case; (11) Letters to the Editor: To discuss and make reply to the contributions published in *WJR*, or to introduce and comment on a controversial issue of general interest; (12) Book Reviews: To introduce and comment on quality monographs of radiology; and (13) Guidelines: To introduce consensuses and guidelines reached by international and national academic authorities worldwide on the research in radiology.

Name of journal

World Journal of Radiology

CSSN

ISSN 1949-8470 (online)

Indexed and Abstracted in

PubMed Central

Published by

Baishideng Publishing Group Co., Limited

SPECIAL STATEMENT

All articles published in this journal represent the viewpoints of the authors except where indicated otherwise.

Biostatistical editing

Statisital review is performed after peer review. We invite an expert in Biomedical Statistics from to evaluate the statistical method used in the paper, including *t*-test (group or paired comparisons), chi-

squared test, Ridit, probit, logit, regression (linear, curvilinear, or stepwise), correlation, analysis of variance, analysis of covariance, *etc*. The reviewing points include: (1) Statistical methods should be described when they are used to verify the results; (2) Whether the statistical techniques are suitable or correct; (3) Only homogeneous data can be averaged. Standard deviations are preferred to standard errors. Give the number of observations and subjects (*n*). Losses in observations, such as drop-outs from the study should be reported; (4) Values such as ED50, LD50, IC50 should have their 95% confidence limits calculated and compared by weighted probit analysis (Bliss and Finney); and (5) The word 'significantly' should be replaced by its synonyms (if it indicates extent) or the *P* value (if it indicates statistical significance).

Conflict-of-interest statement

In the interests of transparency and to help reviewers assess any potential bias, *WJR* requires authors of all papers to declare any competing commercial, personal, political, intellectual, or religious interests in relation to the submitted work. Referees are also asked to indicate any potential conflict they might have reviewing a particular paper. Before submitting, authors are suggested to read "Uniform Requirements for Manuscripts Submitted to Biomedical Journals: Ethical Considerations in the Conduct and Reporting of Research: Conflicts of Interest" from International Committee of Medical Journal Editors (ICMJE), which is available at: http://www.icmje.org/ethical_4conflicts.html.

Sample wording: [Name of individual] has received fees for serving as a speaker, a consultant and an advisory board member for [names of organizations], and has received research funding from [names of organization]. [Name of individual] is an employee of [name of organization]. [Name of individual] owns stocks and shares in [name of organization]. [Name of individual] owns patent [patent identification and brief description].

Statement of informed consent

Manuscripts should contain a statement to the effect that all human studies have been reviewed by the appropriate ethics committee or it should be stated clearly in the text that all persons gave their informed consent prior to their inclusion in the study. Details that might disclose the identity of the subjects under study should be omitted. Authors should also draw attention to the Code of Ethics of the World Medical Association (Declaration of Helsinki, 1964, as revised in 2004).

Statement of human and animal rights

When reporting the results from experiments, authors should follow the highest standards and the trial should comform to Good Clinical Practice (for example, US Food and Drug Administration Good Clinical Practice in FDA-Regulated Clinical Trials; UK Medicines Research Council Guidelines for Good Clinical Practice in Clinical Trials) and/or the World Medical Association Declaration of Helsinki. Generally, we suggest authors follow the lead investigator's national standard. If doubt exists whether the research was conducted in accordance with the above standards, the authors must explain the rationale for their approach and demonstrate that the institutional review body explicitly approved the doubtful aspects of the study.

Before submitting, authors should make their study approved by the relevant research ethics committee or institutional review board. If human participants were involved, manuscripts must be accompanied by a statement that the experiments were undertaken with the understanding and appropriate informed consent of each. Any personal item or information will not be published without explicit consents from the involved patients. If experimental animals were used, the materials and methods (experimental procedures) section must clearly indicate that appropriate measures were taken to minimize pain or discomfort, and details of animal care should be provided.

SUBMISSION OF MANUSCRIPTS

Manuscripts should be typed in 1.5 line spacing and 12 pt. Book Antiqua with ample margins. Number all pages consecutively, and start each of the following sections on a new page: Title Page, Abstract, Introduction, Materials and Methods, Results, Discussion, Acknowledgements, References, Tables, Figures, and Figure Legends. Neither the editors nor the publisher are responsible for the opinions expressed by contributors. Manuscripts formally accepted for publication become the permanent property of Baishideng Publishing Group Co., Limited, and may not be reproduced by any means, in whole or in part, without the written permission of both the authors and the publisher. We reserve the right to copy-edit and put onto our website accepted manuscripts. Authors should follow the relevant guidelines for the care and use of laboratory animals of their institution or national animal welfare committee. For the sake of transparency in regard to the performance and reporting of clinical trials, we endorse the policy of the ICMJE to refuse to publish papers on clinical trial results if the trial was not recorded in a publicly-accessible registry at its outset. The only register now available, to our knowledge, is http://www.clinicaltrials.gov sponsored by the United States National Library of Medicine and we encourage all potential contributors to register with it. However, in the case that other registers become available you will be duly notified. A letter of recommendation from each author's organization should be provided with the contributed article to ensure the privacy and secrecy of research is protected.

Authors should retain one copy of the text, tables, photographs and illustrations because rejected manuscripts will not be returned to the author(s) and the editors will not be responsible for loss or damage to photographs and illustrations sustained during mailing.

Online submissions

Manuscripts should be submitted through the Online Submission System at: http://www.wjgnet.com/1949-8470office. Authors are highly recommended to consult the ONLINE INSTRUCTIONS TO AUTHORS (http://www.wjgnet.com/1949-8470/g_info_20100316162358.htm) before attempting to submit online. For assistance, authors encountering problems with the Online Submission System may send an email describing the problem to wjr@wjgnet.com, or by telephone: +86-10-85381892. If you submit your manuscript online, do not make a postal contribution. Repeated online submission for the same manuscript is strictly prohibited.

MANUSCRIPT PREPARATION

All contributions should be written in English. All articles must be submitted using word-processing software. All submissions must be typed in 1.5 line spacing and 12 pt. Book Antiqua with ample margins. Style should conform to our house format. Required information for each of the manuscript sections is as follows:

Title page

Title: Title should be less than 12 words.

Running title: A short running title of less than 6 words should be provided.

Authorship: Authorship credit should be in accordance with the standard proposed by International Committee of Medical Journal Editors, based on (1) substantial contributions to conception and design, acquisition of data, or analysis and interpretation of data; (2) drafting the article or revising it critically for important intellectual content; and (3) final approval of the version to be published. Authors should meet conditions 1, 2, and 3.

Institution: Author names should be given first, then the complete name of institution, city, province and postcode. For example, Xu-Chen Zhang, Li-Xin Mei, Department of Pathology, Chengde Medical College, Chengde 067000, Hebei Province, China. One author may be represented from two institutions, for example, George Sgourakis, Department of General, Visceral, and Transplantation Surgery, Essen 45122, Germany; George Sgourakis, 2nd Surgical

Department, Korgialenio-Benakio Red Cross Hospital, Athens 15451, Greece

Author contributions: The format of this section should be: Author contributions: Wang CL and Liang L contributed equally to this work; Wang CL, Liang L, Fu JF, Zou CC, Hong F and Wu XM designed the research; Wang CL, Zou CC, Hong F and Wu XM performed the research; Xue JZ and Lu JR contributed new reagents/analytic tools; Wang CL, Liang L and Fu JF analyzed the data; and Wang CL, Liang L and Fu JF wrote the paper.

Supportive foundations: The complete name and number of supportive foundations should be provided, e.g., Supported by National Natural Science Foundation of China, No. 30224801

Correspondence to: Only one corresponding address should be provided. Author names should be given first, then author title, affiliation, the complete name of institution, city, postcode, province, country, and email. All the letters in the email should be in lower case. A space interval should be inserted between country name and email address. For example, Montgomery Bissell, MD, Professor of Medicine, Chief, Liver Center, Gastroenterology Division, University of California, Box 0538, San Francisco, CA 94143, United States. montgomery.bissell@ucsf.edu

Telephone and fax: Telephone and fax should consist of +, country number, district number and telephone or fax number, e.g., Telephone: +86-10-85381892 Fax: +86-10-85381893

Peer reviewers: All articles received are subject to peer review. Normally, three experts are invited for each article. Decision for acceptance is made only when at least two experts recommend an article for publication. Reviewers for accepted manuscripts are acknowledged in each manuscript, and reviewers of articles which were not accepted will be acknowledged at the end of each issue. To ensure the quality of the articles published in *WJR*, reviewers of accepted manuscripts will be announced by publishing the name, title/position and institution of the reviewer in the footnote accompanying the printed article. For example, reviewers: Professor Jing-Yuan Fang, Shanghai Institute of Digestive Disease, Shanghai, Affiliated Renji Hospital, Medical Faculty, Shanghai Jiaotong University, Shanghai, China; Professor Xin-Wei Han, Department of Radiology, The First Affiliated Hospital, Zhengzhou University, Zhengzhou, Henan Province, China; and Professor Anren Kuang, Department of Nuclear Medicine, Huaxi Hospital, Sichuan University, Chengdu, Sichuan Province, China.

Abstract

There are unstructured abstracts (no more than 256 words) and structured abstracts (no more than 480). The specific requirements for structured abstracts are as follows:

An informative, structured abstracts of no more than 480 words should accompany each manuscript. Abstracts for original contributions should be structured into the following sections. AIM (no more than 20 words): Only the purpose should be included. Please write the aim as the form of "To investigate/study/…; MATERIALS AND METHODS (no more than 140 words); RESULTS (no more than 294 words): You should present *P* values where appropriate and must provide relevant data to illustrate how they were obtained, e.g. 6.92 ± 3.86 *vs* 3.61 ± 1.67, $P < 0.001$; CONCLUSION (no more than 26 words).

Key words

Please list 5-10 key words, selected mainly from *Index Medicus*, which reflect the content of the study.

Text

For articles of these sections, original articles and brief articles, the main text should be structured into the following sections: INTRODUCTION, MATERIALS AND METHODS, RESULTS and DISCUSSION, and should include appropriate Figures and Tables. Data should be presented in the main text or in Figures and Tables, but not in both. The main text format of these sections, editorial, topic highlight, case report, letters to the editors, can be found at: http://www.wjgnet.com/1949-8470/g_info_20100313183720.htm.

Illustrations

Figures should be numbered as 1, 2, 3, *etc.*, and mentioned clearly in the main text. Provide a brief title for each figure on a separate page. Detailed legends should not be provided under the figures. This part should be added into the text where the figures are applicable. Figures should be either Photoshop or Illustrator files (in tiff, eps, jpeg formats) at high-resolution. Examples can be found at: http://www.wjgnet.com/1007-9327/13/4520.pdf; http://www.wjgnet.com/1007-9327/13/4554.pdf; http://www.wjgnet.com/1007-9327/13/4891.pdf; http://www.wjgnet.com/1007-9327/13/4986.pdf; http://www.wjgnet.com/1007-9327/13/4498.pdf. Keeping all elements compiled is necessary in line-art image. Scale bars should be used rather than magnification factors, with the length of the bar defined in the legend rather than on the bar itself. File names should identify the figure and panel. Avoid layering type directly over shaded or textured areas. Please use uniform legends for the same subjects. For example: Figure 1 Pathological changes in atrophic gastritis after treatment. A: ...; B: ...; C: ...; D: ...; E: ...; F: ...; G: …*etc.* It is our principle to publish high resolution-figures for the printed and E-versions.

Tables

Three-line tables should be numbered 1, 2, 3, *etc.*, and mentioned clearly in the main text. Provide a brief title for each table. Detailed legends should not be included under tables, but rather added into the text where applicable. The information should complement, but not duplicate the text. Use one horizontal line under the title, a second under column heads, and a third below the Table, above any footnotes. Vertical and italic lines should be omitted.

Notes in tables and illustrations

Data that are not statistically significant should not be noted. $^{a}P < 0.05$, $^{b}P < 0.01$ should be noted ($P > 0.05$ should not be noted). If there are other series of *P* values, $^{c}P < 0.05$ and $^{d}P < 0.01$ are used. A third series of *P* values can be expressed as $^{e}P < 0.05$ and $^{f}P < 0.01$. Other notes in tables or under illustrations should be expressed as ^{1}F, ^{2}F, ^{3}F; or sometimes as other symbols with a superscript (Arabic numerals) in the upper left corner. In a multi-curve illustration, each curve should be labeled with ●, ○, ■, □, ▲, △, *etc.*, in a certain sequence.

Acknowledgments

Brief acknowledgments of persons who have made genuine contributions to the manuscript and who endorse the data and conclusions should be included. Authors are responsible for obtaining written permission to use any copyrighted text and/or illustrations.

REFERENCES

Coding system

The author should number the references in Arabic numerals according to the citation order in the text. Put reference numbers in square brackets in superscript at the end of citation content or after the cited author's name. For citation content which is part of the narration, the coding number and square brackets should be typeset normally. For example, "Crohn's disease (CD) is associated with increased intestinal permeability[1,2]". If references are cited directly in the text, they should be put together within the text, for example, "From references[19,22-24], we know that..."

When the authors write the references, please ensure that the order in text is the same as in the references section, and also ensure the spelling accuracy of the first author's name. Do not list the same citation twice.

PMID and DOI

Pleased provide PubMed citation numbers to the reference list, e.g. PMID and DOI, which can be found at http://www.ncbi.nlm.nih.gov/sites/entrez?db=pubmed and http://www.crossref.org/SimpleTextQuery/, respectively. The numbers will be used in E-version of this journal.

Style for journal references

Authors: the name of the first author should be typed in bold-faced letters. The family name of all authors should be typed with the initial letter capitalized, followed by their abbreviated first and middle initials. (For example, Lian-Sheng Ma is abbreviated as Ma LS, Bo-Rong Pan as Pan BR). The title of the cited article and italicized journal title (journal title should be in its abbreviated form as shown in PubMed), publication date, volume number (in black), start page, and end page [PMID: 11819634 DOI: 10.3748/wjg.13.5396].

Style for book references

Authors: the name of the first author should be typed in bold-faced letters. The surname of all authors should be typed with the initial letter capitalized, followed by their abbreviated middle and first initials. (For example, Lian-Sheng Ma is abbreviated as Ma LS, Bo-Rong Pan as Pan BR) Book title. Publication number. Publication place: Publication press, Year: start page and end page.

Format

Journals

English journal article (list all authors and include the PMID where applicable)

1 **Jung EM**, Clevert DA, Schreyer AG, Schmitt S, Rennert J, Kubale R, Feuerbach S, Jung F. Evaluation of quantitative contrast harmonic imaging to assess malignancy of liver tumors: A prospective controlled two-center study. *World J Gastroenterol* 2007; **13**: 6356-6364 [PMID: 18081224 DOI: 10.3748/wjg.13.6356]

Chinese journal article (list all authors and include the PMID where applicable)

2 **Lin GZ**, Wang XZ, Wang P, Lin J, Yang FD. Immunologic effect of Jianpi Yishen decoction in treatment of Pixu-diarrhoea. *Shijie Huaren Xiaohua Zazhi* 1999; **7**: 285-287

In press

3 **Tian D**, Araki H, Stahl E, Bergelson J, Kreitman M. Signature of balancing selection in Arabidopsis. *Proc Natl Acad Sci USA* 2006; In press

Organization as author

4 **Diabetes Prevention Program Research Group**. Hypertension, insulin, and proinsulin in participants with impaired glucose tolerance. *Hypertension* 2002; **40**: 679-686 [PMID: 12411462 PMCID:2516377 DOI:10.1161/01.HYP.0000035706.28494.09]

Both personal authors and an organization as author

5 **Vallancien G**, Emberton M, Harving N, van Moorselaar RJ; Alf-One Study Group. Sexual dysfunction in 1, 274 European men suffering from lower urinary tract symptoms. *J Urol* 2003; **169**: 2257-2261 [PMID: 12771764 DOI:10.1097/01.ju.0000067940.76090.73]

No author given

6 21st century heart solution may have a sting in the tail. *BMJ* 2002; **325**: 184 [PMID: 12142303 DOI:10.1136/bmj.325.7357.184]

Volume with supplement

7 **Geraud G**, Spierings EL, Keywood C. Tolerability and safety of frovatriptan with short- and long-term use for treatment of migraine and in comparison with sumatriptan. *Headache* 2002; **42** Suppl 2: S93-99 [PMID: 12028325 DOI:10.1046/j.1526-4610.42.s2.7.x]

Issue with no volume

8 **Banit DM**, Kaufer H, Hartford JM. Intraoperative frozen section analysis in revision total joint arthroplasty. *Clin Orthop Relat Res* 2002; (**401**): 230-238 [PMID: 12151900 DOI:10.1097/00003086-200208000-00026]

No volume or issue

9 Outreach: Bringing HIV-positive individuals into care. *HRSA Careaction* 2002; 1-6 [PMID: 12154804]

Books

Personal author(s)

10 **Sherlock S**, Dooley J. Diseases of the liver and billiary system. 9th ed. Oxford: Blackwell Sci Pub, 1993: 258-296

Chapter in a book (list all authors)

11 **Lam SK**. Academic investigator's perspectives of medical treatment for peptic ulcer. In: Swabb EA, Azabo S. Ulcer disease: investigation and basis for therapy. New York: Marcel Dekker, 1991: 431-450

Author(s) and editor(s)

12 **Breedlove GK**, Schorfheide AM. Adolescent pregnancy. 2nd ed. Wieczorek RR, editor. White Plains (NY): March of Dimes Education Services, 2001: 20-34

Conference proceedings

13 **Harnden P**, Joffe JK, Jones WG, editors. Germ cell tumours V. Proceedings of the 5th Germ cell tumours Conference; 2001 Sep 13-15; Leeds, UK. New York: Springer, 2002: 30-56

Conference paper

14 **Christensen S**, Oppacher F. An analysis of Koza's computational effort statistic for genetic programming. In: Foster JA, Lutton E, Miller J, Ryan C, Tettamanzi AG, editors. Genetic programming. EuroGP 2002: Proceedings of the 5th European Conference on Genetic Programming; 2002 Apr 3-5; Kinsdale, Ireland. Berlin: Springer, 2002: 182-191

Electronic journal (list all authors)

15 Morse SS. Factors in the emergence of infectious diseases. Emerg Infect Dis serial online, 1995-01-03, cited 1996-06-05; 1(1): 24 screens. Available from: URL: http://www.cdc.gov/ncidod/eid/index.htm

Patent (list all authors)

16 **Pagedas AC**, inventor; Ancel Surgical R&D Inc., assignee. Flexible endoscopic grasping and cutting device and positioning tool assembly. United States patent US 20020103498. 2002 Aug 1

Statistical data

Write as mean ± SD or mean ± SE.

Statistical expression

Express *t* test as *t* (in italics), *F* test as *F* (in italics), chi square test as χ^2 (in Greek), related coefficient as *r* (in italics), degree of freedom as υ (in Greek), sample number as *n* (in italics), and probability as *P* (in italics).

Units

Use SI units. For example: body mass, m (B) = 78 kg; blood pressure, p (B) = 16.2/12.3 kPa; incubation time, t (incubation) = 96 h, blood glucose concentration, c (glucose) 6.4 ± 2.1 mmol/L; blood CEA mass concentration, p (CEA) = 8.6 24.5 μg/L; CO_2 volume fraction, 50 mL/L CO_2, not 5% CO_2; likewise for 40 g/L formaldehyde, not 10% formalin; and mass fraction, 8 ng/g, *etc.* Arabic numerals such as 23, 243, 641 should be read 23 243 641.

The format for how to accurately write common units and quantums can be found at: http://www.wjgnet.com/1949-8470/g_info_20100313185816.htm.

Abbreviations

Standard abbreviations should be defined in the abstract and on first mention in the text. In general, terms should not be abbreviated unless they are used repeatedly and the abbreviation is helpful to the reader. Permissible abbreviations are listed in Units, Symbols and Abbreviations: A Guide for Biological and Medical Editors and Authors (Ed. Baron DN, 1988) published by The Royal Society of Medicine, London. Certain commonly used abbreviations, such as DNA, RNA, HIV, LD50, PCR, HBV, ECG, WBC, RBC, CT, ESR, CSF, IgG, ELISA, PBS, ATP, EDTA, mAb, can be used directly without further explanation.

Italics
Quantities: *t* time or temperature, *c* concentration, *A* area, *l* length, *m* mass, *V* volume.
Genotypes: *gyrA*, *arg* 1, *c myc*, *c fos*, *etc.*
Restriction enzymes: *Eco*RI, *Hin*dI, *Bam*HI, *Kbo* I, *Kpn* I, *etc.*
Biology: *H. pylori*, *E coli*, *etc.*

Examples for paper writing
Editorial: http://www.wjgnet.com/1949-8470/g_info_20100313182341.htm

Frontier: http://www.wjgnet.com/1949-8470/g_info_20100313182448.htm

Topic highlight: http://www.wjgnet.com/1949-8470/g_info_20100313182639.htm

Observation: http://www.wjgnet.com/1949-8470/g_info_20100313182834.htm

Guidelines for basic research: http://www.wjgnet.com/1949-8470/g_info_20100313183057.htm

Guidelines for clinical practice: http://www.wjgnet.com/1949-8470/g_info_20100313183238.htm

Review: http://www.wjgnet.com/1949-8470/g_info_20100313183433.htm

Original articles: http://www.wjgnet.com/1949-8470/g_info_20100313183720.htm

Brief articles: http://www.wjgnet.com/1949-8470/g_info_20100313184005.htm

Case report: http://www.wjgnet.com/1949-8470/g_info_20100313184149.htm

Letters to the editor: http://www.wjgnet.com/1949-8470/g_info_20100313184410.htm

Book reviews: http://www.wjgnet.com/1949-8470/g_info_20100313184803.htm

Guidelines: http://www.wjgnet.com/1949-8470/g_info_20100313185047.htm

SUBMISSION OF THE REVISED MANUSCRIPTS AFTER ACCEPTED

Please revise your article according to the revision policies of *WJR*. The revised version including manuscript and high-resolution image figures (if any) should be re-submitted or uploaded online. The author should send copyright transfer letter, and responses to the reviewers and science news to us *via* email.

Editorial Office

World Journal of Radiology
Editorial Department: Room 903, Building D,
Ocean International Center,
No. 62 Dongsihuan Zhonglu,
Chaoyang District, Beijing 100025, China
E-mail: wjr@wjgnet.com
http://www.wjgnet.com
Telephone: +86-10-85381892
Fax: +86-10-85381893

Language evaluation
The language of a manuscript will be graded before it is sent for revision. (1) Grade A: priority publishing; (2) Grade B: minor language polishing; (3) Grade C: a great deal of language polishing needed; and (4) Grade D: rejected. Revised articles should reach Grade A or B.

Copyright assignment form
Please download a Copyright assignment form from http://www.wjgnet.com/1949-8470/g_info_20100313185522.htm.

Responses to reviewers
Please revise your article according to the comments/suggestions provided by the reviewers. The format for responses to the reviewers' comments can be found at: http://www.wjgnet.com/1949-8470/g_info_20100313185358.htm.

Proof of financial support
For paper supported by a foundation, authors should provide a copy of the document and serial number of the foundation.

Links to documents related to the manuscript
WJR will be initiating a platform to promote dynamic interactions between the editors, peer reviewers, readers and authors. After a manuscript is published online, links to the PDF version of the submitted manuscript, the peer-reviewers' report and the revised manuscript will be put on-line. Readers can make comments on the peer reviewer's report, authors' responses to peer reviewers, and the revised manuscript. We hope that authors will benefit from this feedback and be able to revise the manuscript accordingly in a timely manner.

Science news releases
Authors of accepted manuscripts are suggested to write a science news item to promote their articles. The news will be released rapidly at EurekAlert/AAAS (http://www.eurekalert.org). The title for news items should be less than 90 characters; the summary should be less than 75 words; and main body less than 500 words. Science news items should be lawful, ethical, and strictly based on your original content with an attractive title and interesting pictures.

Publication fee
Authors of accepted articles must pay a publication fee.
EDITORIAL, TOPIC HIGHLIGHTS, BOOK REVIEWS and LETTERS TO THE EDITOR are published free of charge.